NOTE TO USERS

This reproduction is the best copy available.

uOttawa

L'Université canadienne
Canada's university

FACULTÉ DES ÉTUDES SUPÉRIEURES ET POSTOCTORALES

uOttawa

L'Université canadienne
Canada's university

FACULTY OF GRADUATE AND POSDOCTORAL STUDIES

Christopher Hart
AUTEUR DE LA THÈSE / AUTHOR OF THESIS

M.Sc. (Chemistry)
GRADE / DEGREE

Department of Chemistry
FACULTÉ, ÉCOLE, DÉPARTEMENT / FACULTY, SCHOOL, DEPARTMENT

Functional and Structural Studies of the Anti-MincCD Domain of MinE
TITRE DE LA THÈSE / TITLE OF THESIS

N. Goto
DIRECTEUR (DIRECTRICE) DE LA THÈSE / THESIS SUPERVISOR

CO-DIRECTEUR (CO-DIRECTRICE) DE LA THÈSE / THESIS CO-SUPERVISOR

C. Boddy

Y. Aubin

Gary W. Slater
Le Doyen de la Faculté des études supérieures et postdoctorales / Dean of the Faculty of Graduate and Postdoctoral Studies

Functional and Structural Studies of the Anti- MinCD Domain of MinE

Christopher T. Hart

Thesis submitted to the
Faculty of Graduate and Postdoctoral Studies
University of Ottawa
In partial fulfillment of the requirements for the degree of

Master of Science in Chemistry

Ottawa-Carleton Chemistry Institute
University of Ottawa
Ottawa, Ontario
Canada K1N 6N5

Candidate

Christopher T. Hart

Supervisor

Dr. Natalie K. Goto

Your file Votre référence
ISBN: 978-0-494-69082-6
Our file Notre référence
ISBN: 978-0-494-69082-6

"To conceive, understand, and grasp the whole symmetry of the scientific edifice . . . is equivalent to tasting that enjoyment only conveyed by the highest forms of beauty and truth."

-Dmitri Mendeleev

"But gradually, by patience and hard work, we brought order out of chaos, just as will be true of any problem if we stick to it with patience and wisdom and earnest effort."

-Booker T. Washington

Abstract

The Min protein system, comprised of MinC, MinD and MinE, functions to ensure that the cytokinetic septum formed during bacterial binary fission is placed at midcell in gram negative bacteria. When bound to ATP, MinD binds to the cell membrane and recruits MinC, forming a complex which inhibits formation of the cell division septum. MinE plays a central role in the regulation of this process by opposing this inhibition through interactions with MinD that displace MinC and site-selectively permit formation of the cell division septum at midcell. However, the amino acid residues of MinE that are important for this interaction have yet to be delineated. In this thesis, I present data from an *in vitro* ATPase assay where I examined the ability of MinE mutant proteins from *Neisseria gonorrhoeae* (*N. gonorrhoeae)*, and synthetic peptides corresponding to the N-terminal amino acids of *N. gonorrhoeae*, to stimulate the ATPase activity of MinD from *N. gonorrhoeae*. The *in vitro* experimental data suggests that a sequence of five amino acids in the N-terminus of MinE plays a crucial role in MinE's ability to stimulate MinD ATPase activity and suggests that the N-terminal region of MinE is a functionally autonomous domain. To support the *in vitro* data, I also present preliminary data from an *in vivo* assay examining select MinE mutants. The preliminary *in vivo* experimental data supports the *in vitro* data, suggesting the importance of five amino acids in the N-terminus of MinE. Finally, I present spectroscopic data to complement my findings from both *in vivo* and *in vitro* assays. The results from this study have implications for all current theories regarding

the mechanism by which MinE ensures that cell division occurs exclusively at midcell in gram negative bacteria.

Table of Contents

Abstract ____ *iii*

Table of Contents ____ *v*

List of Figures ____ *vii*

List of Tables ____ *vii*

Acknowledgments ____ *viii*

Chapter 1: Introduction ____ *1*

1.1 Overview of the Role of Min Proteins in Bacterial Cell Division ____ **1**

1.2 Min Protein Interactions ____ **6**

1.3 Macromolecular Organization of MinE: the E-Ring ____ **7**

1.4 Probing the Interaction between MinE and MinD ____ **8**

1.5 MinE Structure ____ **10**

1.6 Thesis Rationale and Objectives ____ **13**

1.7 Chemical Foundations of the ATPase Assay ____ **14**

1.8 Enzyme Kinetics ____ **15**

Chapter 2: Materials and Methods ____ *17*

2.1 Bacterial Plasmids and Synthetic Peptides ____ **17**

2.2 Bacterial Growth Media ____ **18**

2.3 Competent Cell Preparation ____ **18**

2.4 Transformation of Bacterial Plasmid DNA into E. coli competent cells ____ **20**

2.5 Overexpression of Recombinant Gonococcal MinE and MinD ____ **20**

2.6 Site Directed Mutagenesis ____ **21**

2.7 Amplification and Isolation of $MinD_{Ng}$ and $MinE_{Ng}$ Plasmids ____ **24**

2.8 Purification of Min Proteins by Nickel Affinity Chromatography and Size Exclusion Chromatography ____ **24**

2.9 Optimization of Protein Solubility ____ **26**

2.10 ATPase Stimulation Assay ____ **27**

i) Preparation of Phospholipid Vesicles ____ 27

ii) Preparation of Malachite Green Working Reagent ____ 28

iii) ATPase Stimulation Assay Protocol ____ 28

2.11 Protein Concentration Determination 30
2.12 Sodium Dodecyl Sulphate – Polyacrylamide Gel Electrophoresis (SDS-PAGE) 32
2.13 Preparation and Examination of Microscopy Slides 33
2.14 NMR Spectroscopy 33
2.15 Circular Dichroism Spectroscopy 34
Chapter 3: Results *36*
3.1 Solubility Studies of WT $MinE_{Ng}$ 36
3.2 Site Directed Mutagenesis of WT $MinE_{Ng}$ 40
3.3 Development of ATPase Assay 41
3.4 Purification of WT and Mutant $MinE_{Ng}$ and $MinD_{Ng}$ 48
3.5 Identification of Critical MinE Residues Required for Stimulation of MinD Activity 50
3.6 Preliminary Results from In Vivo Assay of $MinE_{Ng}$ Function 55
3.7 Conformational Studies of $MinE_{Ng}$ L22D and R21A 57
3.8 Stimulation of $MinD_{Ng}$ ATPase Activity by $MinE_{Ng}$ Anti-MinCD Domain Peptides 60
3.9 Results Summary 63
Chapter 4: Discussion *65*
4.1 Specific Activity of MinD from N. gonorrhoeae 65
4.2 $MinE^{1-22}$ is Sufficient to Stimulate MinD ATPase Activity 68
4.3 Structural and Functional Impact of R21A and L22D 69
4.4 Preliminary In vivo Results Agree with In vitro Results 72
4.5 Implications for Theories Describing the MinE-MinD Interaction 73
i) Implications for the Soj/SpoOj Hypothesis 73
ii) Implications for the Arginine Finger Hypothesis 75
iii) Implications for the MinD Competition Hypothesis 76
iv) Implications for the Coiled-Coil Hypothesis 77
v) Implications for Dimerization of the anti-MinCD Domain 78
vi) Summary of Implications for Theories Describing the MinE-MinD Interaction 79
Claims to Original Research *81*
References *82*
Appendix *91*
A.1 Temperature Cycling Program Used in Eppendorf Mastercycler Personal 91
A.2 Buffer Conditions Used for Solubility Study of WT $MinE_{Ng}$ 92
A.3 Raw Data from ATPase Assay 95
i) ATPase Assay Examining $MinE_{Ng}$ Mutants (2.7uM MinD; 2.7uM MinE) 95
ii) ATPase Assay Examining $MinE_{Ng}$ Mutants (2.7uM MinD; 0.06uM MinE) 97
iii) ATPase Assay Examining Synthetic Peptides (2.7uM MinD; variable concentration MinE) 101

List of Figures

Figure 1.1: Oscillation of the MinCD Inhibitor and E-ring in Rod Shaped Cells. 3
Figure 1.2: MinE Protein Sequence Alignment. 5
Figure 1.3: Interactions Between Min Proteins. 7
Figure 1.4: Structures of the $MinE_{Ec}$ TSD and Full Length $MinE_{Ng}$ Proteins. 12
Figure 1.5: Malachite Green Reacts with Phosphomolybdate Complex. 14
Figure 3.1: Solubility Study of WT $MinE_{Ng}$. 38
Figure 3.2: WT $MinE_{Ng}$ Purification with CHAPS Buffer Results in Formation of Soluble Aggregates. 39
Figure 3.3: Inorganic Phosphate Standard Curve for the Malachite Green Method. 42
Figure 3.4: Initial Attempts at Malachite Green-Based ATPase Assay. 43
Figure 3.5: Size Exclusion and SDS PAGE of Nickel Affinity Chromatography Purified $MinE_{Ng}$ and $MinD_{Ng}$. 45
Figure 3.6: Sonication of E. coli Phospholipids Alters Level of Stimulation of $MinD_{Ng}$ ATPase Activity. 47
Figure 3.7: SDS-PAGE Gel Analysis of Fractions from Nickel Affinity Chromatography Purifications. 49
Figure 3.8: Size Exclusion Chromatography Profiles Illustrate Abnormalities in Elution Volume and Solubility. 50
Figure 3.9: ATPase Assay Indicates that $MinE_{Ng}$ L22D and $MinE_{Ng}$ A18D Have a Reduced Ability to Stimulate $MinD_{Ng}$ ATPase Activity. 51
Figure 3.10: Stimulation of $MinD_{Ng}$ Specific ATPase Activity Varies with WT $MinE_{Ng}$ Concentration. 53
Figure 3.11: $MinD_{Ng}$ ATPase Stimulation by WT and Mutant $MinE_{Ng}$ Under Non-Saturating Conditions. 54
Figure 3.12: Preliminary Results from in vivo Assay of $MinE_{Ng}$ Function. 56
Figure 3.13: Circular Dichroism Data Suggests that MinE R21A is Structurally Perturbed. 58
Figure 3.14: ^{1}H-^{15}N HSQC spectrum of $MinE_{Ng}$ TSD (red) superimposed on the L22D spectrum (black). 60
Figure 3.15: Stimulation of $MinD_{Ng}$ ATPase Activity by Anti-MinCD Domain Peptides. 62
Figure 4.1: Comparison of the Walker A Motif with the Deviant Walker A Motif found in MinD. 74

List of Tables

Table 2.1: Plasmid names, mutagenesis primers used to introduce these mutations, and annealing temperatures used during temperature cycling. 23

Acknowledgments

Thank you Dr. Natalie Goto for taking a chance on me –for permitting me to pursue research in an area in which I had limited practical experience, and for accepting me at such a late point in the application cycle. I hope that I have repaid your generosity with the effort I have invested into your laboratory.

Thank you Roxanne for supporting me throughout the time I have spent in the Goto laboratory. Without you the world would be a much lonelier place.

Thank you Ali Al-Baldawi and Danya Al-Baldawi for being wonderful undergraduate students to direct –your assistance with all things Min was an invaluable contribution to this thesis.

Thank you Asma Abedin, Houman Ghasriani, Allison Melhuish, and Tabussom Qureshi for the many moments we have shared in Natalie's laboratory during the past two years. Because of your multifarious abilities, I am now able to determine the correct literary status of celebrities, create conspiracy theories without much effort, understand that boy band T-shirts are not appropriate attire for a man, and proficiently wager upon the outcome of other individuals' academic accomplishments.

Thank you Mom, Dad, and Catherine, for supporting my sudden return to science from law. Those who suffer from aimlessness never benefit by having that aimlessness pointed out to them. Though you *did* point my aimlessness out, you always did so in a manner that never made me feel like I was especially aimless. At some point I'll find my way. Or maybe I won't.

Chapter 1: Introduction

1.1 Overview of the Role of Min Proteins in Bacterial Cell Division

Normal bacterial cells reproduce symmetrically through the process of binary fission, whereby following cell growth, DNA replication, and polar segregation of DNA, the cell wall invaginates at midcell, resulting in two daughter cells with equal amounts of genetic material (*1*). It has also been observed that bacterial cells may divide asymmetrically, where invagination of the cell wall occurs at a non-midcell division site, resulting in a minicell lacking genetic material and a large cell containing extra genetic material (*2*). To reconcile these distinct patterns of bacterial cell division, research has focused upon elucidation of the mechanism by which bacterial cells exert positional control over the placement of the septal ring, the multi-protein polymer responsible for invagination (*3-5*). The research presented in this thesis contributes to the understanding of this complex mechanism by providing new data concerning a prominent protein, MinE, involved in the symmetric cell division of gram negative bacteria.

Positional control of the septal ring in gram negative bacteria is achieved through two independent systems: the nucleoid occlusion system (*6-10*), and the Min system (*11-13*). Of the two control mechanisms, the Min system appears to be of greater importance, as its removal results in asymmetric cell division (*14*). In contrast, anucleate cells possess only a slightly misplaced septal ring (*15*). The Min system is

composed of three proteins, MinC, MinD, and MinE, that work concertedly to ensure that the septal ring is placed at the midcell location (*16*). MinC, when bound to MinD, forms the general division inhibitor complex (MinCD), which antagonizes septal ring assembly (*17;18*). In the absence of MinE, this MinCD inhibitor lines the membrane of the cell, preventing septation at all points, resulting in non-septate filamentous cells (*19*). MinE counters this inhibitory action by inducing the oscillation of MinD and MinC from pole to pole (*20;21*).

This oscillation (Figure 1.1) begins with the formation of a zone of high local concentration of MinD at the membrane of one of the cell poles. Over time this MinD zone expands towards midcell, then disassembles back towards the cell pole from where it originated. Meanwhile, a new MinD polar zone appears in the opposite cell pole, expanding towards midcell. Once the new growing MinD polar zone reaches midcell, disassembly is initiated, and the cycle begins anew at the original cell pole. MinC is observed to undergo an identical spatio-temporal pattern of oscillation as MinD; however, MinC may only oscillate when in the presence of both MinD and MinE, indicating that MinD and MinC most probably oscillate as a complex (*22;23*). It is believed that this MinCD oscillation results in a higher time-averaged concentration of the MinCD inhibitor at the cell poles than the cell midpoint, permitting septal ring formation at the cell midpoint (*24*).

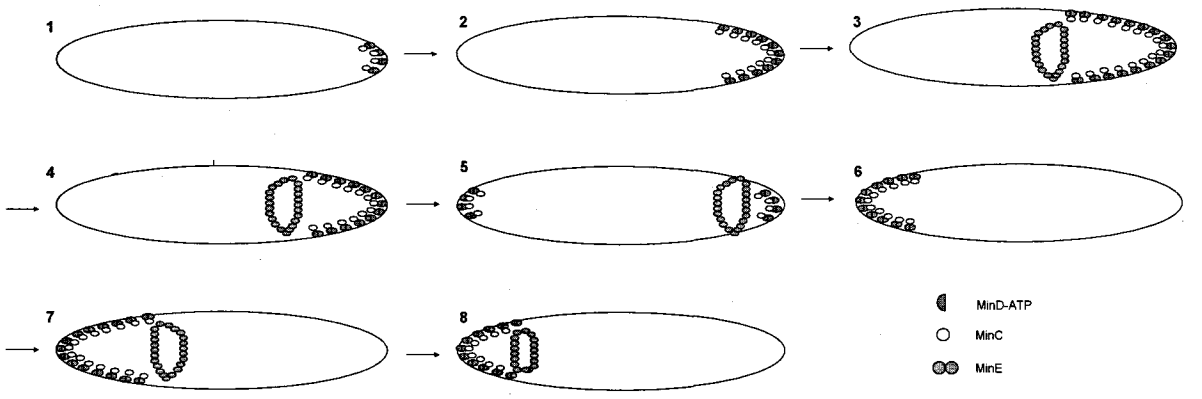

Figure 1.1: Oscillation of the MinCD Inhibitor and E-ring in Rod Shaped Cells.
A zone of high local concentration of MinD (blue)/MinC (beige) expands towards midcell, then retracts towards the pole from where it originated. Meanwhile, a new MinD polar zone forms in the opposite pole and expands towards midcell. Once at midcell, this new MinD polar zone retracts towards the cell pole, and the cycle begins anew. An annular accumulation of MinE, termed the E-ring (green), also undergoes oscillation: when the expanding MinD polar zone reaches midcell, the E-ring appears and follows the MinD polar zone as it retracts back towards the cell pole from where it originated.

According to the model described above, MinE plays the crucial role of inducing pole-to-pole oscillation of the MinCD complex, and hence the regulation of septal ring placement. Without MinE, the MinCD complex is associated with the membrane around the entire cell periphery, causing a total cell division block which results in a filamentous cell morphology (*25*). Oscillation of the MinCD complex is dependent upon an interaction between MinE and MinD whereby MinE imparts topological specificity to the MinCD inhibitor (*26*). However, the method by which MinE is able to interact with MinD and impart topological specificity is incompletely understood.

Research in the Goto laboratory seeks to elucidate the molecular details of the interactions between Min proteins. Toward this goal, my research has focused on the identification of critical amino acid residues in the *N. gonorrrhoeae* MinE protein ($MinE_{Ng}$) that are important its interaction with the *N. gonorrhoeae* MinD protein ($MinD_{Ng}$).

It should be noted that although a great deal of Min protein research has concerned the *E. coli* version of MinE ($MinE_{Ec}$), which operates in the rod-shaped *E. coli* cell, the *Neisseria* homologues operate in a round cell with no discernible poles. Regardless of this distinction in cell morphology, the Min system appears to operate similarly in round and rod shaped bacteria (*27*), with $MinE_{Ng}$ possessing the capability of serving as a functional replacement for $MinE_{Ec}$ *in vivo* (*28-30*). This is unsurprising, given that the two proteins share 42% sequence identity (Figure 1.2). It also suggests that $MinE_{Ec}$ and $MinE_{Ng}$ bear a significant structural and functional resemblance.

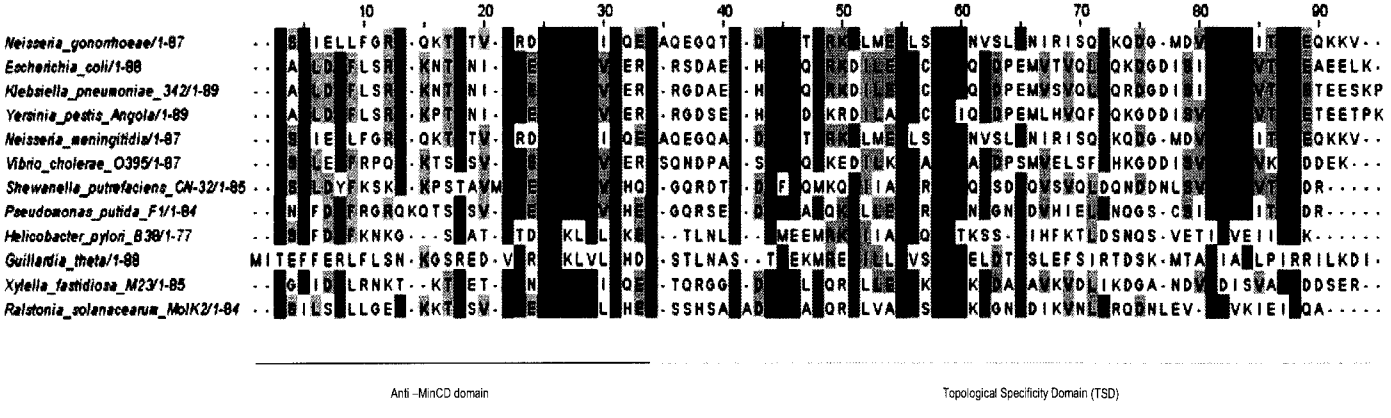

Figure 1.2: MinE Protein Sequence Alignment. *Sequence alignment was generated through the use of COBALT (Constraint Based Multiple Alignment Tool)(31) from the NCBI, with the alignment presented using JALVIEW (32). Blue regions correspond to residues which are conserved, where dark blue regions indicate more conservation, and light blue regions indicate less conservation.*

1.2 Min Protein Interactions

MinE activity involves interactions with MinD, a peripheral membrane ATPase, in a functional cycle outlined in Figure 1.3 (*33-38*). ADP bound MinD is in a monomeric form that does not interact with the membrane; however, upon nucleotide exchange with ATP, it undergoes self-interaction to form a dimer which binds to the bacterial inner membrane. MinE is able to bind to this membrane-associated dimeric MinD complex, where it stimulates MinD ATPase activity, thereby inducing dissociation of MinD from the membrane and regenerating the monomeric ADP-bound cytoplasmic MinD. When MinC is bound to the membrane-associated MinD, this process is coupled with displacement of MinC from the complex, which may be explained because MinC and MinE appear to bind to the same site on MinD (*39*), with MinE being the preferred binding partner.

The cycle of interactions between MinE and MinD gives rise to four primary effects: 1) targeting MinE to the membrane; 2) stimulating MinD ATPase activity; 3) releasing MinD from the membrane; and 4) disrupting the binding interaction between MinC and MinD. These functions appear to be associated with a common binding surface on MinD (*40*), indicating that examination of any one of these four functions could provide insight into the general MinE-MinD interaction. In this thesis I have used the ability of $MinE_{Ng}$ to stimulate $MinD_{Ng}$'s ATPase activity to identify the $MinE_{Ng}$ residues necessary for interaction with $MinD_{Ng}$, as this was a straightforward function to assay in a quantitative manner *in vitro*.

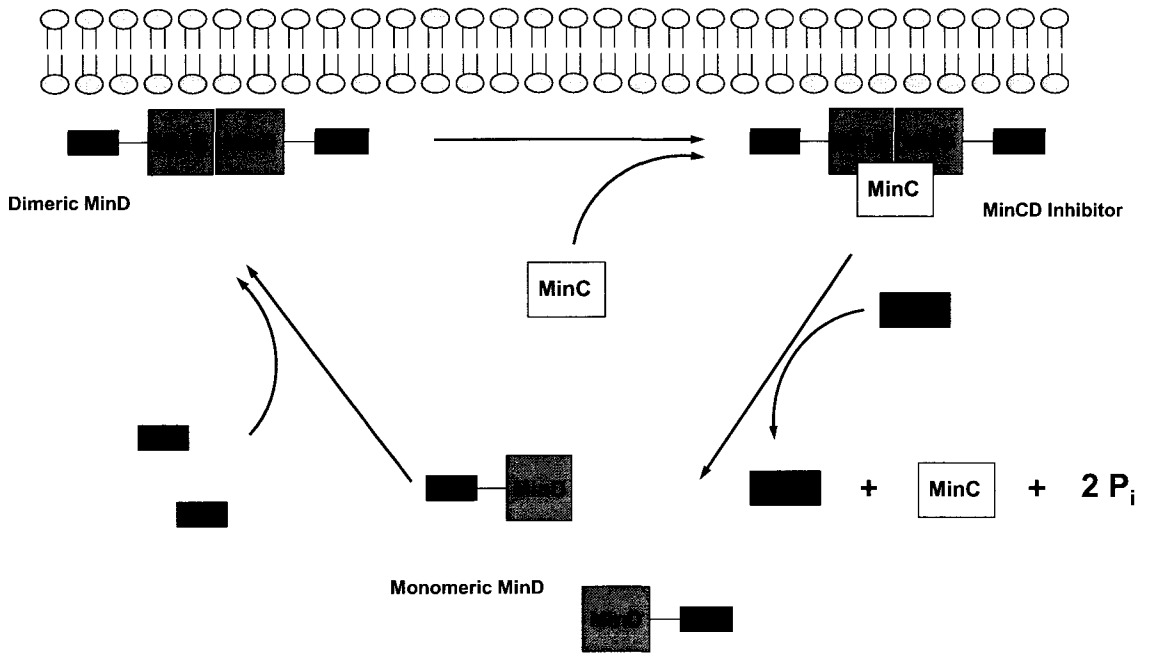

Figure 1.3: Interactions Between Min Proteins. *ADP bound monomeric MinD undergoes nucleotide exchange with ATP, resulting in dimerization and membrane binding. When MinC is present, it is bound to the membrane- bound dimeric MinD. MinE is targeted to the membrane by MinD, where MinE stimulates MinD ATPase activity, displaces MinC from MinD, and causes the release of MinD from the membrane.*

1.3 Macromolecular Organization of MinE: the E-Ring

In addition to the oscillation of MinD and MinC, it has been observed with GFP fusion proteins that MinE exhibits its own oscillatory behaviour which coincides temporally and spatially with the observed oscillation of MinD and MinC (*41-45*). As outlined in Figure 1.1, the arrival of the growing MinD polar zone at midcell triggers the appearance of an annular accumulation of MinE at midcell, called an E-ring. This E-ring remains situated at the rim of the MinD polar zone, moving in the direction of the retracting MinD polar zone, and dissipating at the cell pole. In addition, a smaller

amount of MinE seems to be present throughout the MinD polar zone, and appears to be an integral part of the MinD polymer that comprises this zone (*46*).

While the precise role of the E-ring remains unclear, it has been shown that mutations in $MinE_{Ec}$ which abrogate E-ring formation result in altered $MinD_{Ec}$ oscillation, where the $MinD_{Ec}$ polar zone extends past midcell during its assembly phase (*47*). *E. coli* containing these variants of $MinE_{Ec}$ were found to undergo asymmetric cell division, suggesting that E-ring formation was required for normal symmetric cell division to occur. However, the fact that oscillation did occur, but was irregular in length and occurrence indicates that the E-ring is not required for MinD oscillation, but may help regulate it. Whether this regulation of MinD oscillation requires interactions with the E-ring is not yet known. In this thesis I have tried to address this question by examining the effects of mutating a residue previously shown to be crucial for E-ring formation (E46) on the MinE-MinD interaction.

1.4 Probing the Interaction between MinE and MinD

Early attempts at examining the MinE-MinD interaction involved the overexpression of $MinE_{Ec}$ truncation mutants in *E. coli* minCDE knockout cells (*48;49*). Specifically, $MinE_{Ec}$1-22 (*50*) and $MinE_{Ec}^{1-32}$ (*51*) were able to correct the blockage of cell division arising when $MinC_{Ec}$ and $MinD_{Ec}$ were expressed in a min*CDE* knockout; the C-terminal portions ($MinE_{Ec}^{22-88}$ (*52*) and $MinE_{Ec}^{33-88}$ (*53*)) did not show any anti-MinCD activity. However, overexpression of the C-terminal portions of $MinE_{Ec}$ ($MinE_{Ec}^{22-88}$ and $MinE_{Ec}^{33-88}$) in bacteria expressing endogenous levels of

$MinE_{Ec}$ gave rise to a minicell phenotype, which suggested that these proteins interacted with endogenous Min proteins to disrupt regulation of symmetric cell division. As a consequence of these observations, it is believed that the portion of MinE which interacts with MinD is located in the N-terminal (the anti-MinCD domain), and the portion of MinE associated with the ability of MinE to impart topological specificity to the MinCD inhibitor is located in the C-terminal (the topological specificity domain (TSD)).

The discovery that $MinE_{Ec}$ stimulates $MinD_{Ec}$ ATPase activity *in vitro* provided another avenue through which the MinE-MinD interaction could be examined (*54*). Using a MinD ATPase assay to test the ability of certain $MinE_{Ec}$ mutants to stimulate $MinD_{Ec}$ ATPase activity, Leu22 and Ala18 were identified as critical residues for this activity. Lys19 was also identified as a functionally important MinE residue for stimulation of MinD ATPase activity, although mutations made at this site only led to partial reduction in anti-MinCD activity.

The MinE-MinD interaction has also been investigated through the use of two and three hybrid yeast assays, which confirmed the importance of the aforementioned three residues (Ala18, Lys19, Leu22), and also identified Ala15, Lys19, Ile25, Val26, and Arg30, as potential participants in the $MinE_{Ec}$-$MinD_{Ec}$ interaction (*55*). Accompanying cell morphology and localization studies using GFP-Min fusion proteins also showed that Ala18, Leu22, and Ile25 play a critical role for $MinE_{Ec}$ function *in vivo*, while Lys19 played an important, but not crucial role. Analysis of this data suggested that the $MinE_{Ec}$ residues identified as necessary for interaction with $MinD_{Ec}$ clustered upon one face of a hypothesized alpha helix formed from the first 35

residues of $MinE_{Ec}$, which in turn lead to the suggestion that the MinE-MinD interaction may involve the interaction of helices.

Complementary 2-hybrid studies have also examined the interaction between various truncation $MinE_{Ng}$ mutants and $MinD_{Ng}$, . These experiments showed that $MinE_{Ng}^{11-88}$ was capable of interaction with $MinD_{Ng}$, whereas $MinE_{Ng}^{26-88}$ was not, suggesting that the critical residues for the MinE-MinD interaction lay between residues 12-26 (*56*). $MinE_{Ng}$ L22D and A18D were also confirmed as non-functional mutants using *in vitro* ATPase and *in vivo* fluorescence localization studies. In addition, $MinE_{Ng}$ E67L was identified as a non-functional mutant, raising the possibility that residues in the TSD may also play a role in the MinE-MinD interaction.

1.5 MinE Structure

Current models of MinE structure assume that each functional domain is associated with a separate structural domain, since it was possible to solve the structure of the $MinE_{Ec}$ TSD isolated from the N-terminal anti-MinCD domain (*57*). As shown in Figure 1.4 A, the TSD forms an alpha/beta homodimeric sandwich structure, with residues important for topological specificity function localizing to a region in the helical dimeric interface. Based on this structure, and on NMR studies with a 22-residue peptide from the N-terminus of the *E. coli* MinE sequence (*58*), it was proposed that the anti-minCD domain forms a largely unstructured region that does not interact with this domain. However, recent work by the Goto laboratory suggests that alteration of this hypothesis may be necessary. Specifically, NMR spectra of $MinE_{Ng}$ proteins

with mutations in the anti-MinCD domain showed chemical shift perturbations in the TSD, indicating that the two domains are in close proximity to each other (*59*).

A high-resolution structure determination of a full-length $MinE_{Ng}$ sample has since been undertaken by Dr. Thierry Ducat and Dr. Houman Ghasriani in the Goto lab (personal communication), which provides confirmation of this new model. Most importantly, this structure shows that a portion of the anti-MinCD domain is actually buried in the center of the structure as a β-strand that forms part of the dimeric interface (Figure 1.4 B). Meanwhile, the part of the protein that has been assigned as the TSD adopts a structure that bears some similarity to that seen for the independently solved domain. However, some interactions between secondary structure elements appear to be altered in order to accommodate the additional β-strands in the β -sheet. Overall, this structure provides a different view of the functional domains of MinE, and suggests that previous models of MinE function need to be reconsidered.

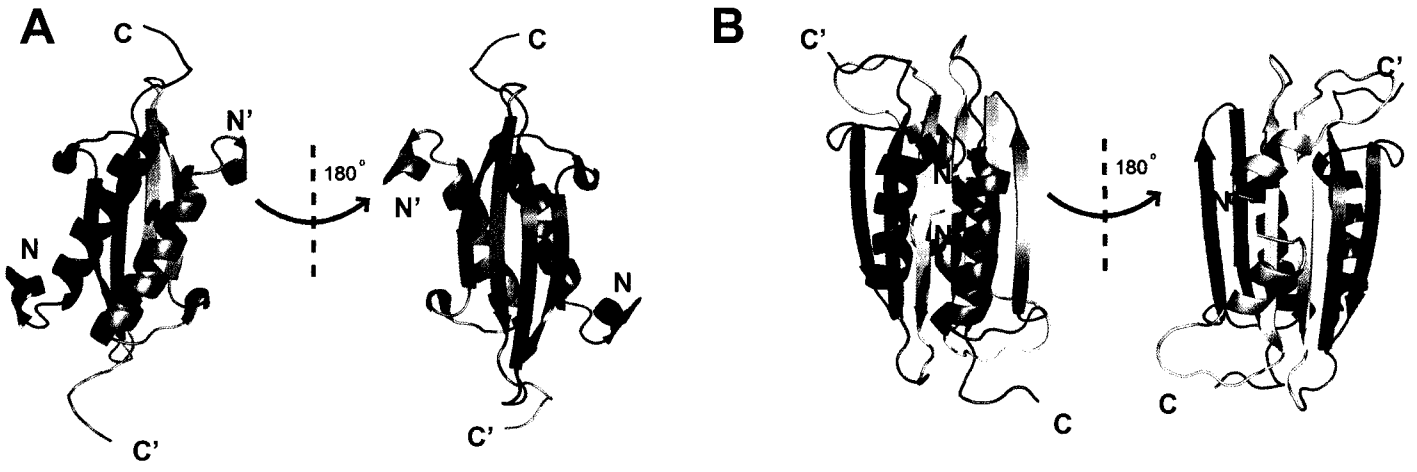

Figure 1.4: Structures of the $MinE_{Ec}$ TSD and Full Length $MinE_{Ng}$ Proteins. ***A)*** *The structure of the $MinD_{Ec}$ TSD is a novel alpha/beta homodimeric sandwich structure (60). The monomers forming the dimeric structure are indicated in blue and grey.* ***B)*** *The structure of the full length $MinE_{Ng}$ as determined by Dr.'s Thierry Ducat and Houman Ghasriani also indicates an alpha/beta homodimeric sandwich structure, but differs from the TSD structure significantly: portions of the anti-MinCD domain (yellow) previously identified by functional studies are located as beta strands at the dimeric interface, with the N-terminal residues forming an alpha helix secondary structure that interacts with the central β-sheet.*

1.6 Thesis Rationale and Objectives

Previous experiments performed to delineate the functional role of the N- and C-terminal portions of MinE presumed that the anti-MinCD domain was generally unstructured and therefore mutations in this region which abrogated function were directly involved in MinD interactions (*61-63*). However, the new structure determined in the Goto lab raises the possibility that these mutations severely impact the structure, suggesting that the residues believed to be important for anti-MinCD activity are not directly involved in MinD interactions. Specifically, residues 23-26 are in buried, structurally critical regions of the dimer, and would not be accessible for interactions with MinD. Meanwhile, there is a high level of sequence conservation within the first 22 residues of MinE (see Figure 1.2), including regions that have not been directly probed for participation in MinD interactions. For these reasons, this thesis has evaluated the functional role of residues 3 to 22 of $MinE_{Ng}$. The following objectives were pursued in this research:

- generation of an ATPase assay to probe $MinE_{Ng}$-$MinD_{Ng}$ interactions
- generation of various $MinE_{Ng}$ mutants
- examination of the capacity for each $MinE_{Ng}$ mutant to stimulate $MinD_{Ng}$ ATPase activity *in vitro*
- evaluation of the *in vivo* function of $MinE_{Ng}$ mutants
- characterization of the structural properties of functionally compromised $MinE_{Ng}$ mutants

1.7 Chemical Foundations of the ATPase Assay

The basis for the ATPase assay developed in this thesis rests upon the reaction between phosphate, molybdate, and a cationic dye, malachite green, and the consequent change in maximum absorbance (*64*) (see Figure 1.5). A solution containing malachite green and molybdate, with pH < 2, has a maximum absorbance in the 410-440nm range, thus appearing yellow. Addition of phosphate to this solution results in the formation of large phosphomolybdate complexes, which bind electrostatically to malachite green, resulting in a shift in maximum absorbance to 610-630nm (*65*). By assuring excess molybdate and appropriate pH, a linear relationship between phosphate and absorbance can be determined, thus allowing measurement of the rate of hydrolysis of ATP by MinD. .

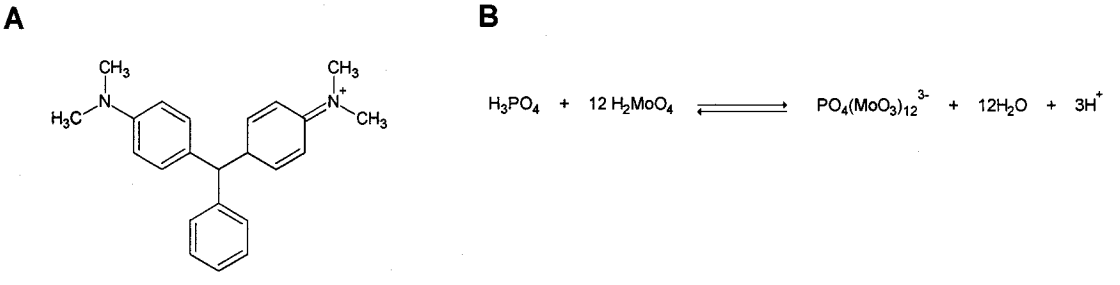

Figure 1.5: Malachite Green Reacts with Phosphomolybdate Complex. A) *The structure of malachite green at pH > 1.2.* ***B)*** *The reaction between phosphate and molybdate results in the formation of a large phosphomolybdate complex. This phosphomolybdate complex reacts with malachite green, causing a shift in the maximum absorbance of the solution.*

1.8 Enzyme Kinetics

Enzymes are biological catalysts which increase rates of chemical reactions by lowering the activation energy necessary for interconversion of substrates and products, which is equivalent to decreasing the time it takes for a chemical reaction to reach equilibrium. Impressively, they often cause rate enhancements orders of magnitude greater than the best chemical catalysts without the extreme conditions often associated with chemical catalysis. However, the basic catalytic mechanisms which underlie enzymatic catalysis do not differ from normal chemical catalysts; acid-base catalysis, covalent catalysis, electrostatic catalysis, and catalysis through preferential transition state binding are all employed in the enzyme's catalytic arsenal. The rate enhancement may instead be attributed to the specificity of each enzyme for a specific substrate, combined with an optimal arrangement of catalytic groups which promotes catalysis through orientation effects (*66*).

By examining the kinetics of chemical reactions catalyzed by enzymes, information concerning an enzyme's mechanism of action may be discovered. In this thesis, the rate of reaction of conversion of ATP to ADP and phosphate was used to probe the mechanism through which $MinE_{Ng}$ stimulates $MinD_{Ng}$. By measuring the amount of phosphate (in nanomoles) released per minute in a reaction vessel, and normalizing this value to the amount of MinD (in milligrams) in the reaction vessel, the specific activity (nmoles P_i/min/mg MinD) of MinD can be determined. Comparison of the specific activity of $MinD_{Ng}$ in the presence and absence of $MinE_{Ng}$ mutants should allow determination of the key residues necessary for $MinE_{Ng}$ stimulation of $MinD_{Ng}$.

A description of ligand binding to an enzyme may also be obtained by monitoring reaction rates as a function of substrate concentration. Assuming that there is no accumulation of an intermediate species, the rate of conversion of substrate to product may be represented by the Hill equation (extended Michaelis-Menten equation):

$$\frac{V}{V_{\max}} = \frac{[S]^h}{[S]^h + K_{0.5}^h}$$

Where V is the rate of appearance of the product; V_{max} is the maximum rate of appearance of the product; *[S]* is the substrate concentration; $K_{0.5}$ is the substrate concentration at 50% of the maximum rate of appearance of the product; and h is the Hill coefficient (*66*).

With the exception of the Hill coefficient, the aforementioned values may be estimated from a plot of the reaction rate versus substrate concentration. An appropriate Hill coefficient in combination with these estimated values may then be used to fit this data with the Hill equation. This method was used to examine the cooperativity of MinE binding to MinD, as the Hill coefficient indicates the level of cooperativity of ligand binding.

Chapter 2: Materials and Methods

2.1 Bacterial Plasmids and Synthetic Peptides

Plasmids for the overexpression of $MinD_{Ng}$, $MinE_{Ng}$, $MinE_{Ng}$ TSD (MinE residues 31-89), and $MinE_{Ng}$ mutant E46A, L22D, and A18D plasmids were provided by Dennis Ramos (*67*), and had been derived from the pet30a vector with kanamycin resistance. All other plasmids (see Table 2.1) were generated by site directed mutagenesis of the WT $MinE_{Ng}$ plasmid, using a protocol based on the methods employed by the Quikchange Site-Directed mutagenesis kit. All Min constructs expressed included a C-terminal sequence of eight additional residues (LEHHHHHH) to permit purification using nickel affinity chromatography.

The sequence of all DNA constructs was confirmed by sequencing at the Ontario Genomics Innovation Centre at the Ontario Health Research Institute, followed by comparison with the known sequence of WT $MinE_{Ng}$ using the Lalign program (http://www.ch.embnet.org/software/LALIGN_form.html).

Synthetic peptides were ordered from Genscript, with C-terminal amidation. The purity of all synthetic peptides was > 95%. Synthetic peptides were dissolved in peptide buffer (250 mM Tris; 250 mM NaCl; pH = 8.5) and stored at -20°C until use.

2.2 Bacterial Growth Media

Minimal medium (M9) or Luria-Bertani medium (LB) were both used to culture bacteria for protein expression (*68;69*). A 10-fold dilution of sterile 10xM9 solution (0.48 M Na_2HPO_4; 0.22 M KH_2PO_4; 0.085 M NaCl) with double distilled H_2O (ddH_2O), followed by addition of 1 mL of 1 M $MgSO_4$, 0.1 M $CaCl_2$, 50 mg/mL Kanamycin, 1 g/mL NH_4Cl, 0.2 g/mL D-glucose, and 10x Gibco MEM vitamin solution, gave M9 solution (1xM9 salts, 1 mM $MgSO_4$, 100 μM $CaCl_2$, 0.1% (w/v) NH_4Cl, 30% (w/v) D-glucose, 0.01% Gibco MEM vitamins, and 50 μg/mL Kanamycin). All solutions were filter sterilized and added under sterile conditions. To produce ^{15}N-labelled Min proteins, $^{15}NH_4Cl$ was used as the sole nitrogen source.

To make LB broth, 10 g of tryptone, 5 g of yeast extract, 5 g of NaCl, and 1 mL of 1 M NaOH were mixed in a large beaker, and the volume of the solution was brought to 1 L with ddH_2O. Following sterilization using an autoclave, and cooling, 1 mL of 50 mg/mL Kanamycin was added to 1 L LB solution. To make LB agar, 15 g agar was added before sterilization in addition to all other components of LB broth. The LB agar solution was allowed to cool before adding the appropriate antibiotic, after which the solution was transferred under sterile conditions into petri dishes.

2.3 Competent Cell Preparation

Stock solutions (200 μL) of *E. coli* BL21(DE3) competent cells were purchased from Novagen. 20 μL aliquots of thawed BL21(DE3) cells were transferred into sterile

cold microcentrifuge tubes (4°C) followed by flash freezing with liquid nitrogen to create working solutions. Each 20 µL aliquot was stored at -80°C.

E. coli DH5α competent cells were created using the $CaCl_2$ method (*70*). DH5α cells from a frozen glycerol stock were streaked onto non-selective LB agar plates and left overnight at 37°C. One colony was used to inoculate 50 mL LB medium, which was then grown overnight at 37°C with shaking at 220 rpm. 4 mL of the overnight culture was added to 400 mL LB medium in a sterile 2 L Fernbach flask or Erlenmeyer flask and allowed to grow at 37°C with 220 rpm shaking to an OD_{600} of ~0.4. At this point, the culture was transferred into eight 50 mL pre-chilled, sterile polypropylene centrifuge tubes from Corning (Falcon tubes), left on ice for five minutes and then centrifuged for 7 minutes at 1600 x g with a fixed angle BC C0650 rotor in a Beckman Coulter (BC) Spinchron 15R centrifuge pre-cooled to 4°C. Following centrifugation, the supernatant was decanted and each pellet was resuspended in 10 mL of ice cold sterile $CaCl_2$ solution (60 mM $CaCl_2$; 15% glycerol). Resuspended cells were centrifuged for 5 minutes at 1100 x g at 4°C, in the same centrifuge and rotor. Following the final centrifugation cycle, the supernatant was decanted and the bacterial pellet in each centrifuge tube was resuspended in 2 mL of $CaCl_2$ solution. Each 2 mL suspension was divided into forty 50 µL aliquots in pre-chilled microcentrifuge tubes and immediately frozen at -80°C.

2.4 Transformation of Bacterial Plasmid DNA into E. coli competent cells

Transformation of bacterial plasmids into *E. coli* competent cells was accomplished using the $CaCl_2$ method (*71*). Briefly, 1 μL of 10 ng/μL plasmid stock was added to 20 μL *E. coli* competent cells. The plasmid/competent cell mixture was placed on ice and allowed to rock for 30 minutes, after which the plasmid/competent cell mixture was heat shocked at 42°C for 2 minutes, then placed on ice for 1 minute. After incubation on ice, 200 μL of LB medium was added to the plasmid/competent cell mixture, and the mixture was placed in a shaker (220 rpm) for 1 hour at 37°C. Following this 1 hour incubation period, the competent cells were plated onto LB agar plates containing kanamycin and left to incubate overnight at 37°C.

The particular *E. coli* strain used in transformation depended upon the intended application. For amplification of bacterial DNA, *E. coli* DH5α competent cells were used, and for overexpression of protein, *E. coli* BL21(DE3) competent cells were used.

2.5 Overexpression of Recombinant Gonococcal MinE and MinD

Following transformation of *E. coli* BL21(DE3) competent cells with the desired plasmid, a single colony was transferred into 80 mL of M9 or LB medium and allowed to incubate for ~17 hours at 37°C while shaking at 220 rpm. Following the ~ 17 hour incubation period, 80 mL of M9 was added to 800 mL M9, or 25 mL LB was

added to 800 mL LB, the culture was grown to an OD_{600} of 0.5 – 0.7 at 37°C with 220 rpm shaking, and then induced with 1mM isopropyl-β-D-1-thiogalactopyranoside (IPTG) for 3 hours. Following IPTG induction, the bacterial cells were harvested by centrifugation at 4800 x g for 10 minutes at 4°C with a BC Avanti JE Centrifuge equipped with a BC JA 10.50 fixed angle rotor, and the supernatant was decanted. The cell pellets were divided and transferred to 50 mL Falcon tubes, such that each Falcon tube contained a bacterial pellet corresponding to a 400 mL culture. The cell pellets were stored at -20°C for future use.

2.6 Site Directed Mutagenesis

Eighteen of the $MinE_{Ng}$ mutant proteins examined in this study were created with a nearly identical protocol, where only the annealing temperature used during the temperature cycling portion of the amplification phase was different.

Generally, four separate reactions were performed for each $MinE_{Ng}$ mutant. In the first reaction, 18.25 µL ddH_2O, 0.75 µL DMSO (Sigma; >99.9% purity), 2.5 µL 10x Pfu Buffer (Stratagene), 1.0 µL 10mM dNTP mix (Stratagene or New England Biolabs), 1.0 µL of 125 ng/ µL sense primer, 1.0 µL of 125 ng/µL anti-sense primer, and 0.5 µL of 10 ng/µL WT $MinE_{Ng}$ plasmid was added in sequence to a 200 µL DNase and RNase free thin walled test tube (Thermo Scientific). The three other reactions contained identical reaction components, but different amounts of WT $MinE_{Ng}$ plasmid: reaction 2 used 1.0 µL, reaction 3 used 2.0 µL and reaction 4 used 5.0 µL of 10 ng/µL WT $MinE_{Ng}$ plasmid, with water volumes being adjusted to maintain a 25 µL volume.

Following careful mixing by pipetting, and centrifugation for 5 seconds using a VWR Galaxy mini tabletop centrifuge, 1.0 μL of 2.5 U/μL Pfu polymerase or Pfu Turbo polymerase (Stratagene) was added to each reaction mixture.

Each reaction mixture was next placed in an Eppendorf Mastercycler Personal, and subjected to temperature cycling. (Appendix A.1 presents the complete program). Briefly, the mutagenesis reaction was initially heated to 95°C for 2 minutes to ensure melting of the WT $MinE_{Ng}$ plasmid. The mutagenesis reaction was then heated to 95°C for 1 minute, lowered to a variable temperature to allow annealing for 1 minute (temperatures used for each primer is shown in Table 2.1), and then heated to 68°C, where this temperature was maintained for 12 minutes. This cycle was repeated 16 times, whereupon the temperature was maintained at 68°C for 10 minutes, before being lowered to 4°C. Following completion of temperature cycling, 1.0 μL of 20 U/μL DPN1 enzyme was added to each reaction mixture, and the mixtures were incubated at 37°C for 2 or more hours to allow digestion of non-mutated plasmids. Following digestion using DPN1, 1.5 μL of the mutagenesis reaction product was transformed into 50 μL of *E. coli* DH5α competent cells, where the plasmid was amplified and then isolated using plasmid midi-preps.

Plasmid Name	Primer Sequence	Annealing Temp. (°C)
$MinE_{Ng}$ E67L	Sense: GAC AAT ATC CGT ATT TCC CAA CTA AAG CAG GAT GGT ATG GAT GTG Anti-Sense: CAC ATC CAT ACC ATC CTG CTT TAG TTG GGA AAT ACG GAT ATT GTC	65
$MinE_{Ng}$ R21A	Sense: GCA ACC GTT GCC CGC GAC GCC CTT CAA ATC ATC ATT GCC Anti-Sense: GGC AAT GAT GAT TTG AAG GGC GTC GCG GGC AAC GGT TGC	64
$MinE_{Ng}$ D20A	Sense: ACG GCA ACC GTT GCC CGC GCC CGC CTT CAA ATC ATC ATT Anti-Sense: AAT GAT GAT TTG AAG GCG GGC GCG GGC AAC GGT TGC CGT	63
$MinE_{Ng}$ R19A	Sense: ACG GCA ACC GTT GCC GCC GAC CGC CTT CAA ATC Anti-Sense: GAT TTG AAG GCG GTC GGC GGC AAC GGT TGC CGT	63
$MinE_{Ng}$ V17A	Sense: CAG AAA ACG GCA ACC GCT GCC CGC GAC CGC CTT Anti-Sense: AAG GCG GTC GCG GGC AGC GGT TGC CGT TTT CTG	63
$MinE_{Ng}$ T16A	Sense: AGA AAG CAG AAA ACG GCA GCC GTT GCC CGC GAC CGC CTT Anti-Sense: AAG GCG GTC GCG GGC AAC GGC TGC CGT TTT CTG CTT TCT	65
$MinE_{Ng}$ A15D	Sense: AGA AAG CAG AAA ACG GAC ACC GTT GCC CGC GAC Anti-Sense: GTC GCG GGC AAC GGT GTC CGT TTT CTG CTT TCT	66
$MinE_{Ng}$ T14A	Sense: GGT AGA AAG CAG AAA GCG GCA ACC GTT GCC CGC Anti-Sense: GCG GGC AAC GGT TGC CGC TTT CTG CTT TCT ACC	65
$MinE_{Ng}$ K13A	Sense: TTC GGT AGA AAG CAG GCA ACG GCA ACC GTT GCC Anti-Sense: GGC AAC GGT TGC CGT TGC CTG CTT TCT ACC GAA	65
$MinE_{Ng}$ Q12A	Sense: CTT TTA TTC GGT AGA AAG GCG AAA ACG GCA ACC GTT GCC Anti-Sense: GGC AAC GGT TGC CGT TTT CGC CTT TCT ACC GAA TAA AAG	63
$MinE_{Ng}$ K11A	Sense: GAA CTT TTA TTC GGT AGA GCG CAG AAA ACG GCA ACC GTT Anti-Sense: AAC GGT TGC CGT TTT CTG CGC TCT ACC GAA TAA AAG TTC	64
$MinE_{Ng}$ R10A	Sense: TTG ATC GAA CTT TTA TTC GGT GCA AAG CAG AAA ACG GCA ACC GTT Anti-sense: AAC GGT TGC CGT TTT CTG CTT TGC ACC GAA TAA AAG TTC GAT CAA	63
$MinE_{Ng}$ F8A	Sense: ATG TCA TTG ATC GAA CTT TTA GCC GGT AGA AAG CAG AAA ACG GCA Anti-Sense: TGC CGT TTT CTG CTT TCT ACC GGC TAA AAG TTC GAT CAA TGA CAT	64
$MinE_{Ng}$ L7A	Sense: CAT ATG TCA TTG ATC GAA CTT GCA TTC GGT AGA AAG CAG AAA ACG Anti-Sense: CGT TTT CTG CTT TCT ACC GAA TGC AAG TTC GAT CAA TGA CAT ATG	65
$MinE_{Ng}$ L6A	Sense: CAT ATG TCA TTG ATC GAA GCT TTA TTC GGT AGA AAG CAG Anti-Sense: CTG CTT TCT ACC GAA TAA AGC TTC GAT CAA TGA CAT ATG	65
$MinE_{Ng}$ E5A	Sense: GAT ATA CAT ATG TCA TTG ATC GCA CTT TTA TTC GGT AGA AAG CAG Anti-Sense: CTG CTT TCT ACC GAA TAA AAG TGC GAT CAA TGA CAT ATG TAT ATC	63
$MinE_{Ng}$ I4A	Sense: GGA GAT ATA CAT ATG TCA TTG GCC GAA CTT TTA TTC GGT AGA AAG Anti-Sense: CTT TCT ACC GAA TAA AAG TTC GGC CAA TGA CAT ATG TAT ATC TCC	63
$MinE_{Ng}$ L3A	Sense: GAA GGA GAT ATA CAT ATG TCA GCG ATC GAA CTT TTA TTC GGT AGA Anti-Sense: TCT ACC GAA TAA AAG TTC GAT CGC TGA CAT ATG TAT ATC TCC TTC	66

Table 2.1: Plasmid names, mutagenesis primers used to introduce these mutations, and annealing temperatures used during temperature cycling.

2.7 Amplification and Isolation of $MinD_{Ng}$ and $MinE_{Ng}$ Plasmids

To amplify and isolate $MinD_{Ng}$, WT $MinE_{Ng}$, and $MinE_{Ng}$ mutant plasmids, a protocol from Qiagen based on alkaline lysis and purification using an anion-exchange column was adopted. Following transformation of competent *E. coli* DH5α cells, a single colony was transferred into 3-5 mL of LB containing 50 μg/mL Kanamycin and allowed to grow at 37°C for ~8 hours with 220 rpm shaking. Following the ~8 hour incubation period, 500 μL of the growing culture was added to 50 mL of sterile LB containing 50 μg/mL Kanamycin and allowed to grow overnight at 37°C with 220 rpm shaking. Following the overnight growth, the bacterial cells were harvested by centrifugation at 6000 x g for 15 minutes at 4°C, and the supernatant discarded.

Isolation of the plasmid from the bacterial pellet was accomplished using the Qiagen HiSpeed Plasmid Midi and Maxi Kit following the protocol as outlined in the November 2005 HiSpeed Plasmid Purification Handbook.

2.8 Purification of Min Proteins by Nickel Affinity Chromatography and Size Exclusion Chromatography

All Min proteins were purified identically, insofar as their particular solubility limitations permitted. Following overexpression, the bacterial pellet from a ~400 mL LB or M9 growth was resuspended in 17 mL of lysis buffer (50 mM Tris-HCl; 250 mM NaCl; 10 mM imidazole; pH = 8.5) with 15 mg of benzamidine (Bioshop) and allowed to rock on ice for 30 minutes. The cells were then lysed on ice using a Fisher Scientific 500 Sonic Dismembrator using a titanium alloy microprobe (Fisher) for three cycles of

sonication (45% amplitude; 50% duty cycle pulse sequence; 1 minute), where following each sonication cycle the lysed cell mixture was mixed. The lysed bacterial cells and insoluble material were harvested by centrifugation in polypropylene centrifuge tubes using a BC Avanti JE Centrifuge equipped with a BC JA 25.50 fixed angle rotor at 16,000 x g for 20 minutes at 4°C.

Following centrifugation, the supernatant was applied to 2.5 mL Ni-NTA resin in a 2.7 cm inner diameter column (Novagen) previously equilibrated with lysis buffer and allowed to flow through by gravity. To ensure binding of the Min protein, the flow-through was applied to the column three times. The resin was then washed with 50 mL of lysis buffer, followed by 50 mL of wash buffer (lysis buffer; 20 mM imidazole). The protein was eluted with 17.5 mL of lysis buffer containing 500 mM imidazole. 17.5 µL of 0.5 mg/mL EDTA (pH = 8.5) was added to the eluted protein solution to prevent proteolysis by metal proteases. Normally, the protein samples were subjected to size exclusion chromatography immediately following nickel affinity chromatography purification. However, on rare occasions, this was not possible. Consequently, the protein solution was stored at 4°C and subjected to size exclusion chromatography the next day. This one day lag period appeared to have no effect on the overall results.

In order to prepare the samples for size exclusion chromatography, the samples were concentrated using an Amicon Ultra 15 10,000 M.W.C.O concentrating device previously equilibrated with lysis buffer. 10 mL of the pooled elution fractions were concentrated in a BC Spinchron 15R centrifuge pre-cooled to 4°C and equipped with a BC S4180 hanging bucket rotor, at 3700 – 3900 x g for ~ 5 minutes. Following the first cycle of concentration, additional eluted protein was added to the concentrating device,

and concentration was repeated. This process was continued until the ~17.5 mL pooled protein fractions were concentrated to ~2 mL. The 2 mL concentrate was removed from the concentrating device and transferred to two microcentrifuge tubes, which were centrifuged at 16,000 x g for 2 minutes using an Eppendorf 5415 D tabletop centrifuge.

Following concentration, the supernatant from each tube was transferred into a single microcentrifuge tube, and 1500 µL of the supernatant was injected onto a GE Superdex 75 10/300 GL column (Superdex 75) which had previously been equilibrated with size exclusion buffer (50 mM Tris; 100 mM NaCl; 0.2 mM EDTA; pH = 8.5) using an AKTA FPLC. Equilibration of the Superdex 75 occurred by passing 2 column volumes (CVs) of ddH_2O at a flow rate of 1.0 mL/min, followed by two CVs of equilibration buffer. Following injection, the AKTA-FPLC was run at a flow rate of 0.85 mL/min – 1.0 mL/min, while monitoring elution at 280 nm. The dimeric form of $MinE_{Ng}$ WT normally eluted at ~ 12.0 mL; the monomeric form of $MinD_{Ng}$ eluted at ~11.7 mL, and 4-6 500 µL fractions of the eluted protein were collected. The protein fractions collected from FPLC were not pooled together, but were kept in separate microcentrifuge tubes.

2.9 Optimization of Protein Solubility

An incomplete factorial set of 81 extraction buffers (see Appendix A.2) was generated using the SamBa software (available at http://igs-server.cnrs-mrs.fr/samba) according to Ducat *et al.* (*72*). Four factors and 25 factor levels served as the basis set for the extraction buffer solutions: pH (4.5, 5, 5.5, 6, 6.5, 7, 7.5, 8, 8.5); nature of salt

(NaCl, Na_2SO_4, and KSCN); salt concentration (0 mM, 50 mM, 250 mM, 500 mM); and additives (1%, 5%, 10% glycerol; or 0.25 M, 0.5 M, 1 M sucrose; or 1 mM, 10 mM, 50 mM CHAPS). $MinE_{Ng}$ solubility in each of the 81 extraction buffers was tested using cell micro-lysis and detection by SDS-PAGE, according to Ducat *et al.* Briefly, one pellet from an 800 mL growth was resuspended in 100 mL of resuspension buffer (10 mM Tris; 100 mM NaCl; pH=7.5), and the resuspended cell solution was transferred into 90 separate microcentrifuge tubes (1 mL of cell suspension in each). The separate cell solutions were centrifuge at 16,000 x g for 5 minutes, the supernatant was removed, and each individual cell pellet was dissolved in one of the 81 extraction buffers. Each of the 81 cell solutions was then sonicated with a Scientific 500 Sonic Dismembrator sonicator using a titanium microprobe for 5 seconds (15% amplitude; 1 second on / 1 second off pulses), and centrifuged again for 5 minutes at 16,000 x g. The supernatant was examined with SDS-PAGE.

2.10 ATPase Stimulation Assay

i) Preparation of Phospholipid Vesicles

500 µL of 50 mg/mL 1,2-dioleoyl-*sn*-glycero-3-[phosphor-*rac*-(1-glycerol)] (DOPG) phospholipids (Avanti Polar Lipids) dissolved in chloroform were transferred to a borosilicate glass test tube using a borosilicate glass pipette. The chloroform was removed by gently streaming argon over the solution, and the phospholipid film was left in a fumehood overnight. The lipid film was resuspended in 2500 µL of 25 mM

Tris pH 7.5, 50 mM KCl by vortexing the glass test tube at room temperature. The phospholipid mixture was then transferred to microcentrifuge tubes and stored at -20°C. Thawed DOPG phospholipids were extruded using 0.1 μM polycarbonate filters with an Avanti Mini-Extruder equipped with Hamilton syringes immediately before use in the ATPase stimulation assay.

ii) Preparation of Malachite Green Working Reagent

The malachite green working reagent was prepared using a previously published protocol (*73*). One volume 4.2% (w/v) ammonium molybdate (Sigma Aldrich) in 4 M HCl was added to three volumes of 0.045% (w/v) Malachite Green (Sigma Aldrich). This solution was stirred for 30-60 minutes and then syringe filtered using a 0.22 μM MF-Millipore membrane. Tween-20 was added to a final concentration of 0.15% (v/v) from a 10% (w/v) stock solution immediately before use in the ATPase assay,

iii) ATPase Stimulation Assay Protocol

Following $MinD_{Ng}$ and $MinE_{Ng}$ purification using nickel affinity chromatography and size exclusion chromatography (size exclusion buffer: 50 mM Tris; 100 mM NaCl; 0.2 mM EDTA; pH=8.5), the protein concentration was determined using a BCA assay. As described below, limits in pipetting volumes for the

pipettes used in these studies often made it necessary to dilute Min protein stock solutions, which necessitated the use of a second BCA assay.

Following protein concentration determination, three 200 μL reaction mixtures were created in separate microcentrifuge tubes. In the first reaction mixture, reaction buffer (250 mM Tris HCl; 500 mM KCl; pH=8.0), $MinD_{Ng}$, ATP (100 mM; Fermentas Life Sciences), DOPG phospholipids (10 mg/mL), $MgCl_2$ (100 mM), and $MinE_{Ng}$ were added in this sequence to give a reaction mixture consisting of 2.7 μM $MinD_{Ng}$, 0.06 μM $MinE_{Ng}$, 5 mM $MgCl_2$, 1 mM ATP, 0.5 mg/mL ATP, 65.75 mM Tris, 79 mM NaCl, 52.5 mM KCl with pH = 8.20. A control reaction mixture omitting $MinD_{Ng}$ was also made with an equivalent volume of size exclusion buffer being added in its place. An additional control was also made that contained no $MinE_{Ng}$ or $MinD_{Ng}$, with size exclusion buffer making up the volume difference. Other control reactions were also occasionally run, where one element of the total reaction mixture was removed, and an equivalent volume of buffer was added. This ensured that the phospholipids, $MgCl_2$, or ATP were not contributing to the observed rate of ATP hydrolysis.

Following addition of $MinE_{Ng}$ to the reaction mixtures, 40 μL aliquots of the reaction mixtures were removed at 13 minute intervals, transferred to new microcentrifuge tubes, and centrifuged for 5 minutes at 16,000 x g with an Eppendorf 5415 D tabletop centrifuge. For the data presented in this thesis, 40 μL aliquots were removed at 2, 15, 28, and 41 minutes following addition of $MinE_{Ng}$ to reaction mixtures; centrifugation for these aliquots was begun at 4, 17, 30, and 43 minutes following addition of $MinE_{Ng}$ to the reaction mixtures. Following centrifugation, 15 μL from the supernatant was added to separate wells of a polystyrene 96 well plate (Fisher)

containing 70 μL malachite green working solution. The colour formation reaction was allowed to proceed for 15 minutes, at which point the absorbance at 620 nm was measured using a Molecular Devices SpectraMax Plus 96 well plate reader. Data was plotted using Microsoft Excel and the line of best fit was determined using the least squares method of regression.

2.11 Protein Concentration Determination

For all experiments presented in the results section, protein concentrations were determined using the commercially available bicinchoninic acid (BCA) assay (Pierce Biotech) (*74;75*). On some occasions the Bradford assay (Bio-Rad) (*76*) was also used to confirm the results of the BCA assay. For both the BCA assay and the Bio-Rad assay, bovine serum albumin (BSA; Invitrogen) was used as a standard. To avoid confusion throughout this subsection, the separate 500 μL protein fractions obtained following size exclusion chromatography are termed protein stock solutions, and the aliquots removed from each protein stock solution to permit determination of the protein stock solution concentration are termed protein test solutions.

The protocol used for the BCA assay was essentially that described by Pierce Biotech. 50 μL of 100 μg/mL, 200 μg/mL, 300 μg/mL, 500 μg/mL, and 800 μg/mL BSA standards (occasionally 1000 μg/mL and 1500 μg/mL BSA standards were also used, depending upon the expected protein concentration determined from the absorbance values from size exclusion chromatography), and 50 μL of blank solutions corresponding to the buffer solutions of both the BCA standards. 50 μL of each protein

stock solution was removed and transferred into a separate microcentrifuge tube, creating the aforementioned protein test solutions; this process was repeated so that two protein test solutions of 50 μL existed for each protein stock solution. Addition of 50 parts of BCA Reagent A (200 mM sodium carbonate, 120 mM sodium bicarbonate, 30 mM bicinchoninic acid, 10 mM sodium tartrate, in 0.1 M sodium hydroxide) to 1 part BCA Reagent B (4% cupric sulphate) created the BCA working reagent, of which, 1 mL was added to each individual 50 μL protein test solution, standard, or blank solution. The microcentrifuge tubes were vortexed, then centrifuged briefly using a VWR galaxy table top centrifuge, and incubated at 37°C for ~40 minutes. Following incubation, all solutions were allowed to cool to room temperature, and the corrected absorbance values of all protein test solutions at 562 nm were measured using an Ultraspec 2100 pro UV/vis spectrometer. Determination of the linear relationship between blank-corrected absorbance and protein standard concentration using software loaded on the Ultraspec 2100 Pro permitted determination of the protein test solution concentration, which was assumed to be identical to the protein stock solution concentration.

The protocol used for the Bio-Rad assay was that described by the manufacturers (Bio-Rad). Briefly, 100 μL of 200 μg/mL, 300 μg/mL, 500 μg/mL, and 800 μg/mL BSA, 100 μL of blank solutions corresponding to the buffer solutions of both the BSA standards and protein solutions, and two replicates of 100 μL for each protein stock solution, were added to individual 5mL polypropylene test tubes. 5 mL Bio-Rad solution (1 part Dye Reagent Concentrate diluted with 4 parts ddH_2O and filtered using a Whatman #1 filter) were added to each individual test tube, and the

tubes were allowed to incubate at room temperature for 10 minutes. Blank-corrected absorbance values were measured with the Ultraspec Pro 2100 UV/vis spectrometer and concentration values determined as in the BCA assay protocol.

2.12 Sodium Dodecyl Sulphate – Polyacrylamide Gel Electrophoresis (SDS-PAGE)

SDS-PAGE was used to determine the approximate purity of protein samples, following a similar protocol to Sambrook *et al.* (*77*). Samples were diluted with an equal volume of 2X SDS-PAGE loading buffer (100 mM Tris pH 6.8, 20% (v/v) glycerol, 4% (w/v) SDS, 0.02% (w/v) bromophenol blue) and heated to 100°C for 5 – 10 minutes. Following heating, 12.5 µL of each sample was loaded onto a pre-cast polyacrylamide gel (Biorad) with a 5% stacking phase and a 15% resolving phase, situated in a Mini-PROTEAN Electrophoresis Cell (Biorad) containing 1 L of SDS-PAGE running buffer (3.03% (w/v) Tris-HCl,14.4% (w/v) glycine, 1% (w/v) SDS pH = 6.5-7.0). 2 µL of Fisher EZ-Run or Invitrogen Benchmark protein markers was applied to allow determination of the approximate molecular weight of each protein. Gels were run at 180 mV for 42 minutes and stained in Coomassie blue stain (50% methanol, 40% ddH_2O, 10% acetic acid, 0.1% (w/v) Coomassie brilliant blue) for ~1 hour with gentle rocking, followed by destaining with destain solution (50% ddH_2O, 40% methanol, 10% acetic acid) for ~1 hour with gentle rocking.

2.13 Preparation and Examination of Microscopy Slides

BL21(DE3) cells transformed with a desired plasmid were grown and overexpressed in M9 medium following an identical protocol as that described in section 2.5. Following three hours of induction with IPTG, a 1 mL aliquot was removed from growing BL21(DE3) cells overexpressing a desired Min protein. The 1 mL aliquot was diluted with ddH_2O until the OD_{600} value reached ~ 0.3, and 20 μL of this diluted cell solution was applied to a glass slide (1 mm thickness; Fisher Premium) which was then passed continuously over the base of a flame until all water was removed from the cell solution. One drop of low viscosity immersion oil (Fisher) was applied to the fixed cells and a glass cover slip (#1 thickness; Fisher) was placed over top of the immersion oil and fixed using commercial nail polish.

Prepared microscope slides were examined using a Zeiss Axiophot phase contrast microscope with 100 x magnification. Cell morphology photos were captured using Image Pro Plus Version 6.0 with an Olympus DP70 camera. Background photos were used to correct for abnormalities in the camera picture capture system, but no other modifications to the photographs were made.

2.14 NMR Spectroscopy

Uniformly ^{15}N-labeled $MinE_{Ng}$ L22D and $MinE_{Ng}$ TSD proteins were purified with nickel affinity chromatography and size exclusion chromatography (size exclusion

buffer: 25 mM Tris; 50 mM NaCl; 200 μM EDTA, 200 μM benzamidine; 0.02% NaN_3; pH = 7.4). 450 μL of each purified protein sample was added to 50 μL of D_2O in a glass 7" NMR sample tube. ^1H-^{15}N HSQC spectra were recorded at 25°C on a Varian Inova 500 Spectrometer, processed with NMRPipe (*78*), and analyzed with NMRView (*79*). $MinE_{Ng}$ L22D concentrations ranged from 0.05 mM to 0.18 mM, and $MinE_{Ng}$ TSD concentrations ranged from 0.1 mM to 0.4 mM. All HSQC spectra were reproduced at least once.

2.15 Circular Dichroism Spectroscopy

Following purification of WT $MinE_{Ng}$, $MinE_{Ng}$ L22D and $MinE_{Ng}$ R21A using nickel affinity chromatography and size exclusion chromatography with diluted size exclusion buffer (12.5 mM Tris; 25 mM NaCl; 50 μM EDTA; pH=8.5), CD spectra were recorded on a Jasco J-810 circular dichroism spetropolarimeter with a 1 nm path length quartz cell at 25°C. Spectral scans were recorded with 8 accumulations from 250 nm – 19 5nm with a 0.2 nm pitch at 20 nm/min, response time of 8 seconds and bandwidth of 1.0 nm. Background subtraction was applied to the recorded protein spectra using a blank spectrum of the buffer. The mean residue ellipticity (MRE) was calculated using the following equation:

$$\langle \Theta \rangle_{MRE} = \frac{\theta}{n \times c \times l}$$

where θ is the sample ellipticity (millidegrees), n is the number of protein residues (95 residues in examined Min proteins), c is the protein concentration (dmol/cm^3) and l is the path length (cm).

Chapter 3: Results

3.1 Solubility Studies of WT $MinE_{Ng}$

Examination of the interaction between $MinE_{Ng}$ and $MinD_{Ng}$ necessitated buffer conditions which would optimally solubilise both proteins. Progress in improving WT $MinE_{Ng}$ solubility was made by Ramos (*80*), who showed that WT $MinE_{Ng}$ was optimally soluble in a high pH buffer consisting of 50 mM Tris, and 250 mM NaCl. Unfortunately, even under these conditions, $MinE_{Ng}$ reached its solubility limit at ~150 μM, and often precipitated when left overnight at room temperature or 4°C. As a consequence of this low solubility, frequent purification of $MinE_{Ng}$ was necessary, and NMR experiments which could aid in studying the MinE-MinD interaction were limited. An incomplete factorial design (IFD) method was therefore used to attempt to improve solubility conditions for $MinE_{Ng}$ WT.

IFD is based on the concept that one can efficiently determine solubility conditions by semi-random sampling of various experimental conditions. Rather than testing a single variable in the experimental system, IFD examines multiple variables simultaneously, ensuring that each possible combination is sampled. This allows more efficient evaluation of the main factors, as well as potentially correlated factors, which affect solubility (*81*).

SamBa software was used to generate an IFD matrix of solution conditions to examine the effect of the type of salt, the salt concentration, pH, and additives, on WT $MinE_{Ng}$ solubility. These various solution conditions (see Appendix A.2) served as

lysis buffers for cells overexpressing WT $MinE_{Ng}$, and after cell lysis the soluble fractions were examined with SDS-PAGE to determine the amount of solubilised WT $MinE_{Ng}$. As shown in Figure 3.1, numerous solution conditions were observed to give rise to relatively high concentrations of soluble WT $MinE_{Ng}$. Nearly all shared the commonality of either possessing a pH of $\geq$8, or containing the detergent CHAPS. The only exception was buffer 60 (250mM NaCl, 0.5M Sucrose, 100mM Tris HCl, pH = 7.5) which solubilized $MinE_{Ng}$, but did not contain CHAPS or high pH conditions.

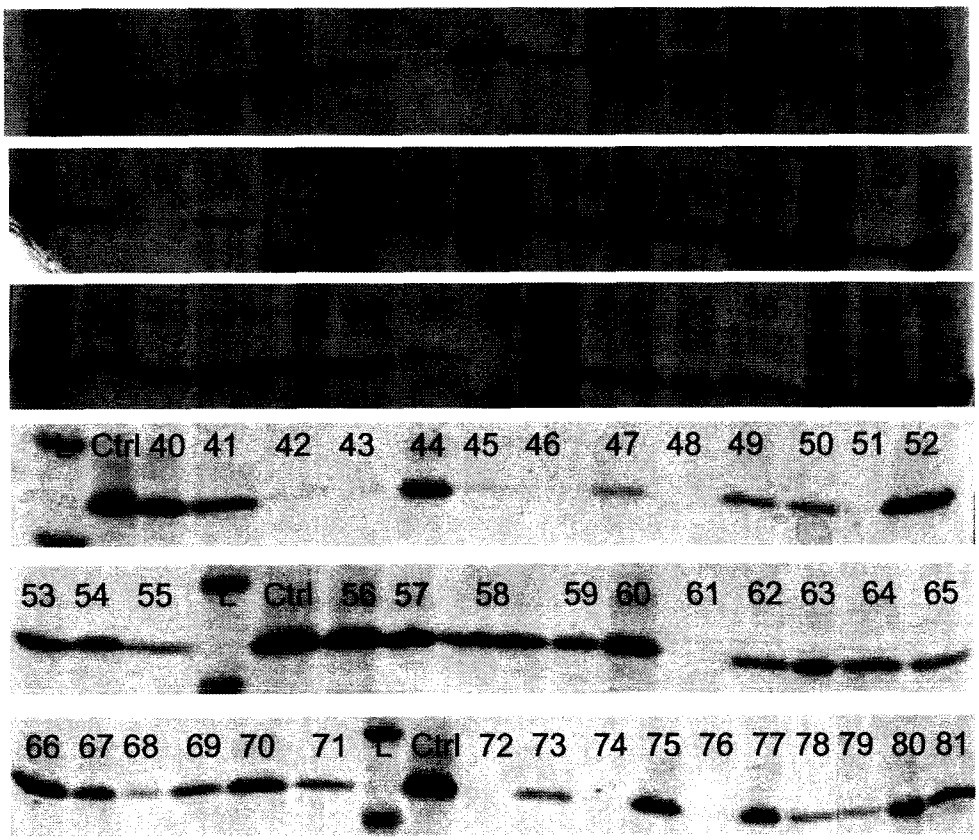

Figure 3.1: Solubility Study of WT MinE$_{Ng}$. *Each number on the gel corresponds to the solution conditions described in Appendix A.2. The indicated solution was used as the lysis buffer for bacteria containing overexpressed WT MinE$_{Ng}$; Coomassie-stained SDS-PAGE gel analysis was performed upon the soluble fraction to estimate the amount of WT MinE$_{Ng}$ that had been solubilized under each condition. The amount of MinE$_{Ng}$ in each solution was compared to a positive control known to completely solubilize WT MinE$_{Ng}$ (Ctrl: 1% SDS, 2 M Urea, 2 mM β-mercaptoethanol, 2.5% glycerol, 15 mM Tris, pH = 7.5. Solution conditions which solubilised WT MinE$_{Ng}$ similarly to that of the positive control are indicated in red.*

In order to determine whether CHAPS could be useful for the isolation of higher concentrations of functional MinE$_{Ng}$, purifications were peformed using buffer 38 (250 mM Na_2SO_4, 20 mM CHAPS, 100 mM NaH_2PO_4, pH = 6.5) as lysis buffer. Unfortunately, as shown in Figure 3.2, size exclusion chromatography of this sample showed a large portion eluting at the void volume, indicating that MinE$_{Ng}$ had formed a water-soluble aggregate with molecular weight > 100 kDa. Similar results were also

obtained when $MinE_{Ng}$ was purified in buffer 23 (125 mM KSCN, 1 mM CHAPS, 100 mM NaH_2PO_4, pH=7.0), and buffer 60. These results demonstrated that while CHAPS was able to increase the solubility of $MinE_{Ng}$, it also caused extensive aggregation, making it unsuitable for our studies.

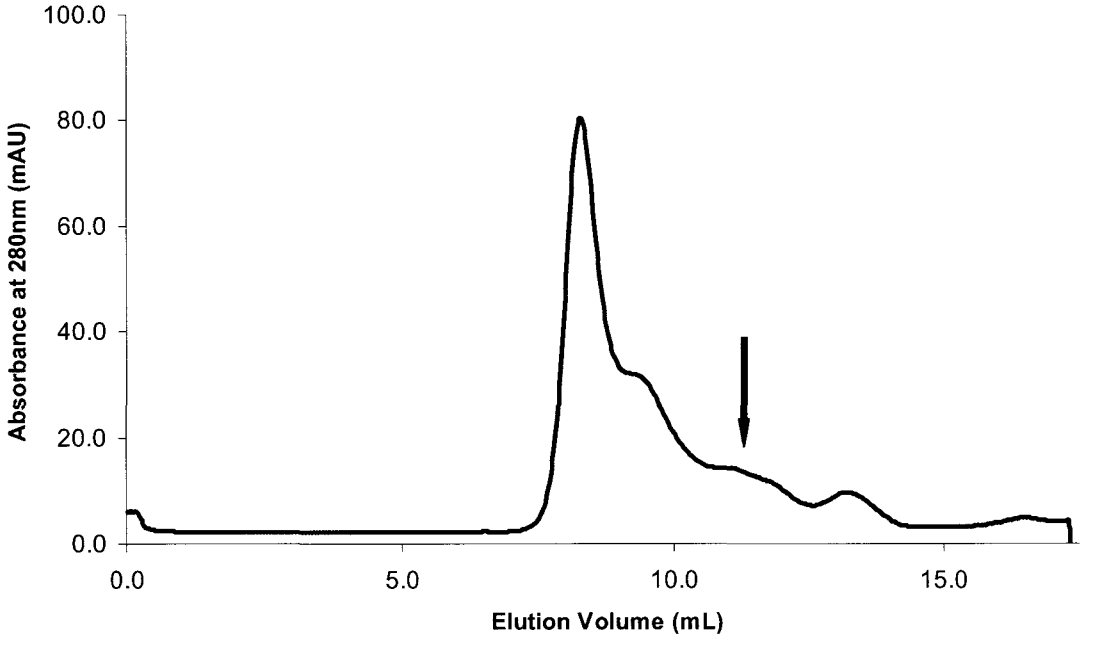

Figure 3.2: WT $MinE_{Ng}$ Purification with CHAPS Buffer Results in Formation of Soluble Aggregates. *Following nickel affinity purification of WT $MinE_{Ng}$ using CHAPS buffer (250 mM Na_2SO_4, 20mM CHAPS, 100mM NaH_2PO_4, pH = 6.5), WT $MinE_{Ng}$ was injected onto a GE Superdex 75 column equilibrated with CHAPS buffer. Only a small fraction of the purified WT $MinE_{Ng}$ eluted at the elution volume corresponding to the dimeric form (red arrow); the predominant fraction came out at the column void volume, signifying aggregation. Similar profiles were observed for buffer 23 and buffer 60.*

As CHAPS buffer conditions generated soluble aggregates of WT $MinE_{Ng}$ that were not useful for structural studies, and alternative additives or salts that could

improve solubility were not discovered, the original buffer conditions previously determined for structural studies of WT $MinE_{Ng}$ were used in this thesis. However, during the course of these studies it became apparent that by maintaining a low concentration of $MinE_{Ng}$ (<70 uM), and altering the original buffer conditions to include 100uM EDTA, precipitation could be prevented, allowing $MinE_{Ng}$ to remain in a functional form for more than three days.

3.2 Site Directed Mutagenesis of WT $MinE_{Ng}$

To attempt to identify the $MinE_{Ng}$ residues responsible for interaction with $MinD_{Ng}$, site directed mutagenesis was used to alter WT $MinE_{Ng}$ such that a library of $MinE_{Ng}$ mutants, differing from WT $MinE_{Ng}$ in the identity of one amino acid, was created (see Table 2.1). To minimize the extent of structural perturbation arising from the amino acid substitution, hydrophobic and charged amino acids were mutated to alanine, with the exception of Ala15 and Asp67, which were mutated, respectively, to aspartic acid and leucine because previous research (*82;83*) suggested that these mutations could result in a change in ability of $MinE_{Ng}$ to interact with $MinD_{Ng}$. Twenty-one $MinE_{Ng}$ mutants were created using site directed mutagenesis, which, when combined with the existing mutants (*84*), gave a total of 24 mutant $MinE_{Ng}$ proteins to examine.

3.3 Development of ATPase Assay

To probe the interaction of WT and mutant $MinE_{Ng}$ with $MinD_{Ng}$, the ability of $MinE_{Ng}$ to stimulate $MinD_{Ng}$'s ATPase activity was examined. Cleavage of ATP results in the release of phosphate, therefore measuring the rate of release of phosphate provided a measure of the $MinD_{Ng}$ ATPase activity. Methods using radioactivity, coupled enzyme reactions, and dye-based phosphate detection have been used to monitor ATP hydrolysis by MinD (*85-92*). The apparent simplicity, sensitivity, and accuracy of a dye based analytical method prompted the choice of this method to examine the ATPase activity of $MinD_{Ng}$, and hence the ability of $MinE_{Ng}$ mutants to stimulate $MinD_{Ng}$'s ATPase activity.

In this approach, the malachite green dye reacts quantitatively with inorganic phosphate and hexamolybdate, causing a shift in the maximum absorbance from ~440 nm to ~620nm (*64*). This gives rise to a linear relationship between absorbance and the amount of phosphate in solution, permitting determination of the phosphate concentration with a simple photometric measurement. As shown in Figure 3.3, this linear relationship was demonstrated with potassium phosphate, which was later used as a standard curve.

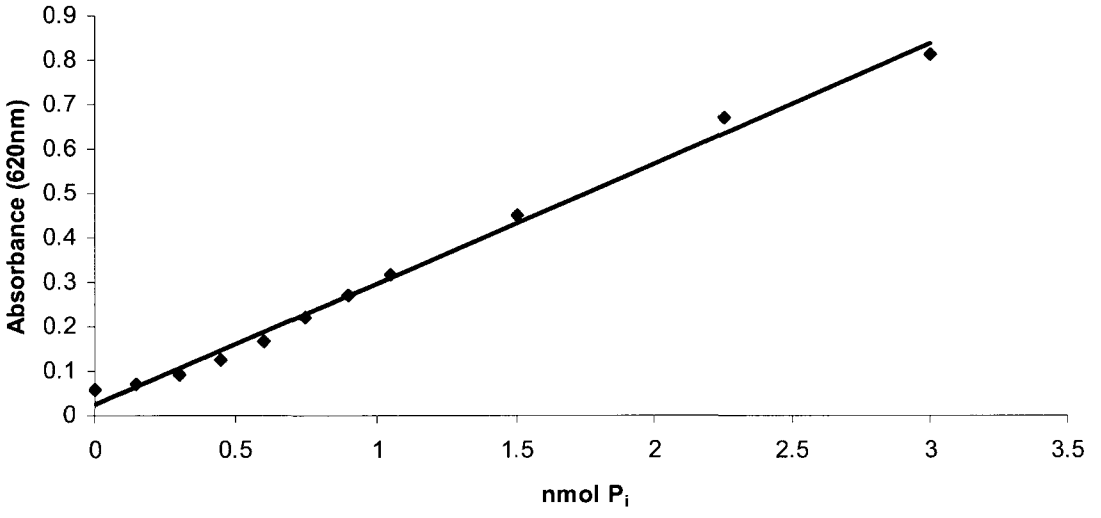

Figure 3.3: Inorganic Phosphate Standard Curve for the Malachite Green Method. *Solutions with varying concentrations of inorganic phosphate were made by diluting KH_2PO_4 with size exclusion buffer (50 mM Tris; 100 mM NaCl; 0.2 mM EDTA; pH = 8.5). 15 µL of each solution was added to 70 µL of malachite green working solution and absorbance values at 620 nm were measured following 15 minutes of incubation. The linear relationship between potassium phosphate and absorbance at 620 nm was determined to be: $y = 2.707x + 0.0262$; $R^2 = 0.9928$.*

Initial attempts to examine the stimulatory effect of $MinE_{Ng}$ upon $MinD_{Ng}$'s ATPase activity used protein samples that had gone through a single round of purification on a nickel affinity column. Stimulation of $MinD_{Ng}$ ATPase activity by $MinE_{Ng}$ was immediately apparent (see Figure 3.4 A); however, it also became apparent that reaction mixtures (buffer, $MinD_{Ng}$, $MinE_{Ng}$, ATP, phospholipid, Mg^{2+}) made with these protein samples often resulted in precipitation of the malachite green - phosphomolybdate complex. This gave rise to anomalous light scattering that prevented accurate phosphate concentration from being determined. As shown in Figure 3.4 B, this prevented reproducible reaction rates from being determined.

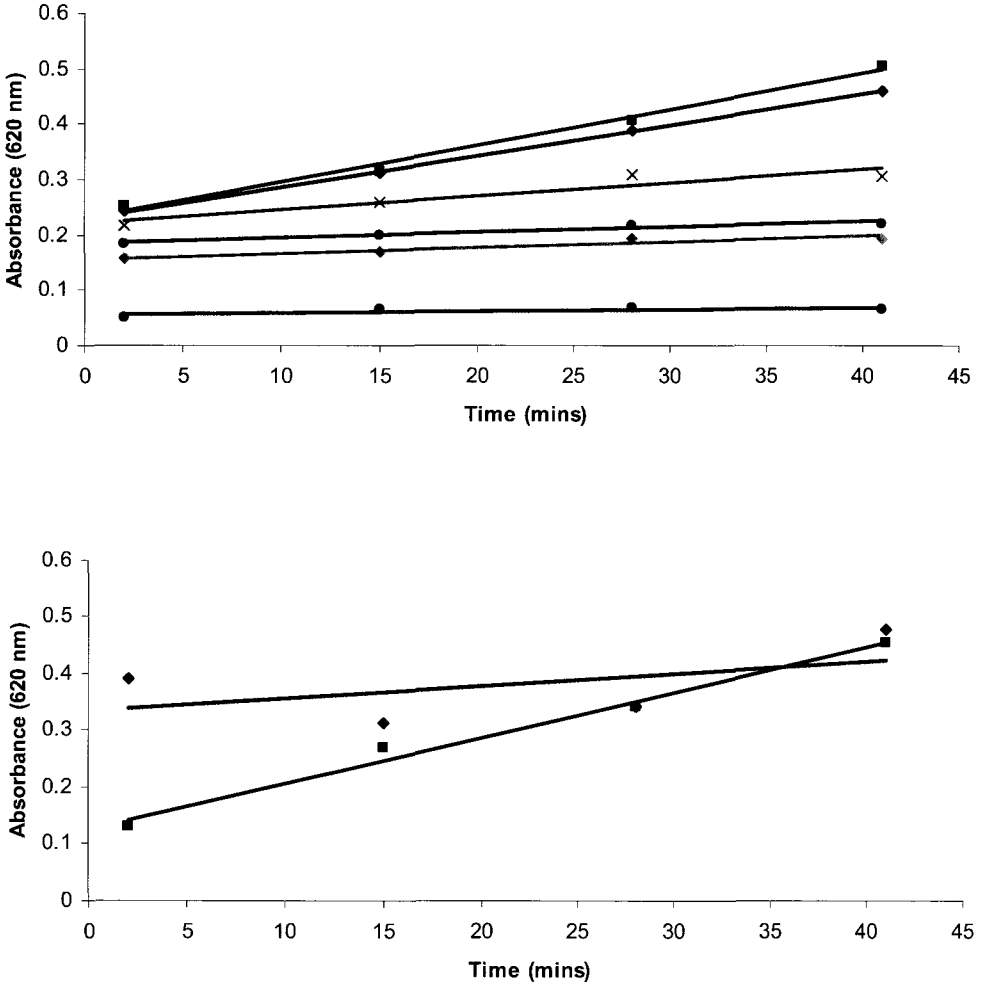

Figure 3.4: Initial Attempts at Malachite Green-Based ATPase Assay. *Following purification of WT $MinE_{Ng}$ and WT $MinD_{Ng}$ with nickel affinity chromatography, ATPase reaction mixtures containing $MinD_{Ng}$, $MinE_{Ng}$, phospholipids, Mg^{2+}, ATP, and reaction buffer were created.* ***A)*** *Reaction mixtures without ATP (dark green line), without protein (grey line), and without $MinD_{Ng}$ (maroon line) show no change in phosphate concentrations over time. When $MinD_{Ng}$ was present without $MinE_{Ng}$ (turquoise line and yellow line), or with $MinE_{Ng}$ (pink line and dark blue line) the concentration of phosphate increased linearly with time.* ***B)*** *Example of anomalous light scattering from sporadic formation of dye precipitates giving rise to poor reproducibility between duplicate reactions (see text). Reaction mixtures contained WT $MinD_{Ng}$, WT $MinE_{Ng}$, and all other necessary components.*

Systematic examination of the various components of the $MinE_{Ng}$ and $MinD_{Ng}$ reaction buffers demonstrated that EDTA and imidazole were the likely cause of precipitation of the malachite green-phosphomolybdate complex. Therefore all protein samples were subsequently subjected to buffer exchange using a desalting column prior to use in the ATPase assay. The concentration of the detergent, Tween-20, was also increased five fold to reduce the potential for precipitation.

Although these modifications greatly improved the assay, there remained considerable variation in the ability of WT $MinE_{Ng}$ to stimulate $MinD_{Ng}$ ATPase activity. Given the tendency for both proteins to precipitate during storage, it was hypothesized that aggregation could be the cause for differences in activity. To test this hypothesis, $MinE_{Ng}$ and $MinD_{Ng}$ samples were examined with size exclusion chromatography. As shown in Figure 3.5, the size exclusion chromatography profiles showed a large peak eluting at the void volume for both $MinD_{Ng}$ and $MinE_{Ng}$, in addition to the expected peaks corresponding to the monomeric $MinD_{Ng}$ and dimeric $MinE_{Ng}$.

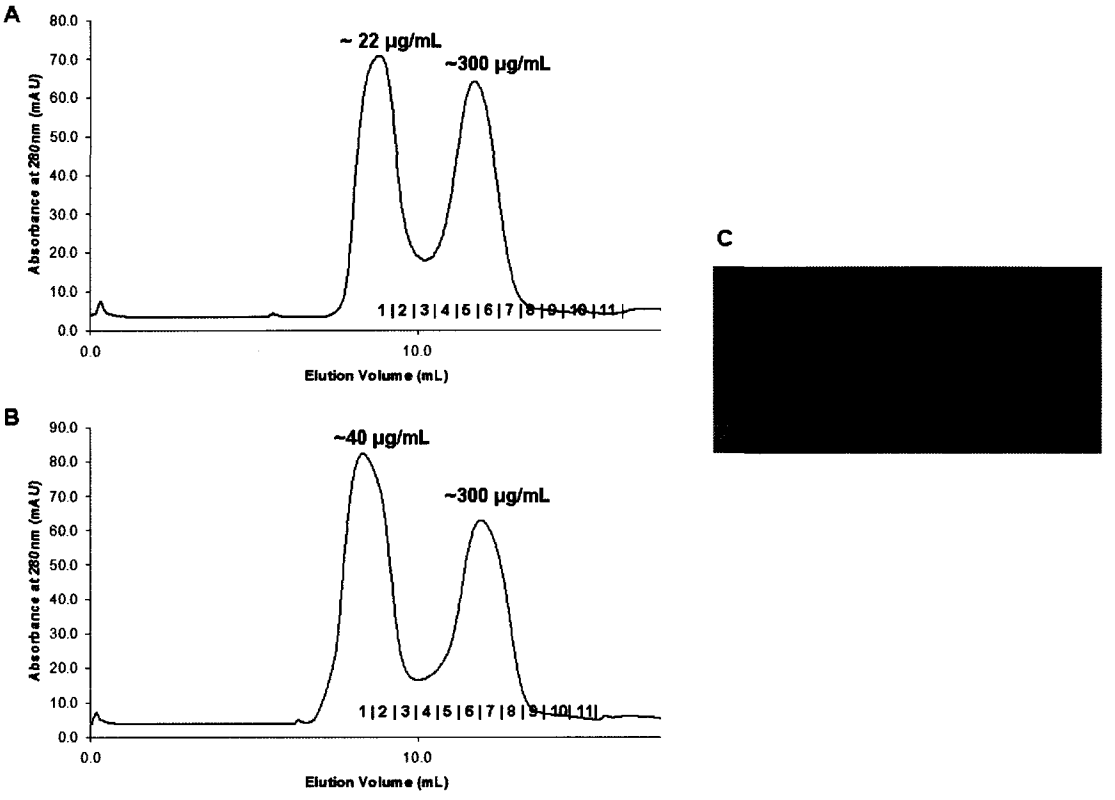

Figure 3.5: Size Exclusion and SDS PAGE of Nickel Affinity Chromatography Purified $MinE_{Ng}$ and $MinD_{Ng}$. *Following nickel affinity chromatography purification, 1500uL of $MinD_{Ng}$ (**A**), and 1500uL of $MinE_{Ng}$ (**B**) were injected onto the GE Superdex 75 column on an AKTA FPLC and indicated fractions analyzed by SDS PAGE (**C**). Lane labels refer to the protein and the particular fraction under examination (i.e. D7 = the 7th fraction from the $MinD_{Ng}$ size exclusion profile). Note the high level of purity for both $MinD_{Ng}$ and $MinE_{Ng}$ samples following size exclusion analysis.*

BCA and Bradford assays of the void volume fraction showed that the concentration of protein was significantly lower than in the $MinE_{Ng}$ or $MinD_{Ng}$ peaks (~30ug/mL compared to ~300ug/mL; see Figure 3.5). In addition, SDS-PAGE analysis of these fractions indicated that the void-volume peak contained little protein compared to fractions collected from the later-eluting peak (Figure 3.5 C). Some insight into the identity of the void volume peak was provided by measuring the ratio of absorbance values at 260nm versus 280nm. For fractions from the void volume peak,

260nm/280nm values were greater than 1.2, suggesting that most of the absorbing species was actually nucleic acid. In contrast, fractions from the other major peak had values close to 1.0, as would be expected for a pure protein sample. As a consequence of these findings, size exclusion chromatography was performed for all subsequent samples, allowing separation of $MinE_{Ng}$ or $MinD_{Ng}$ from the contaminating nucleic acid, with fractions most separated from the DNA peak being used. To obtain sufficient quantities of $MinE_{Ng}$ for the ATPase assay, it was necessary to load larger volumes than recommended by the column manufacturer. Although the resolution was affected, it was still possible to remove the major contaminants using this approach.

An additional source of assay variability that was also evaluated was the phospholipid vesicle component of the reaction buffer. Since *E. coli* PLs are primarily composed of phosphatidylethanolamine (PE) (~57%), and lipid vesicles containing more than 60% PE have a tendency to aggregate , it was possible that large multilamellar vesicles (LMVs) were being formed which would hide a significant amount of PL beneath the outer layer (*93;94*). As a certain concentration range of PL vesicles are necessary for MinD ATPase activity, we were concerned that the actual amount of bilayer surface available for $MinD_{Ng}$ binding might be insufficient. To assess this possibility, the effect of sonication of vesicles prior to use in the $MinD_{Ng}$ ATPase assay was tested. As shown in Figure 3.6, higher activity was observed with pre-sonicated lipids, suggesting that the original vesicle preparation did contain LMV structures.

The difficulty in preventing the formation of LMVs during vesicle preparation, which led to different apparent membrane concentrations from one preparation to

another prompted the use of 1,2-dioleoyl-*sn*-glycero-3-[phosphor-*rac*-(1-glycerol)] (DOPG), since it had previously been shown to support MinD activity (*95;96*). Due to the significantly lower phase transition temperature, this lipid was much easier to handle and reproducibly give rise to LUV preparations, even without the use of sonication. Consequently, all subsequent assays were performed with this lipid, which, in conjunction with the modifications described above, allowed reproducible results to be obtained.

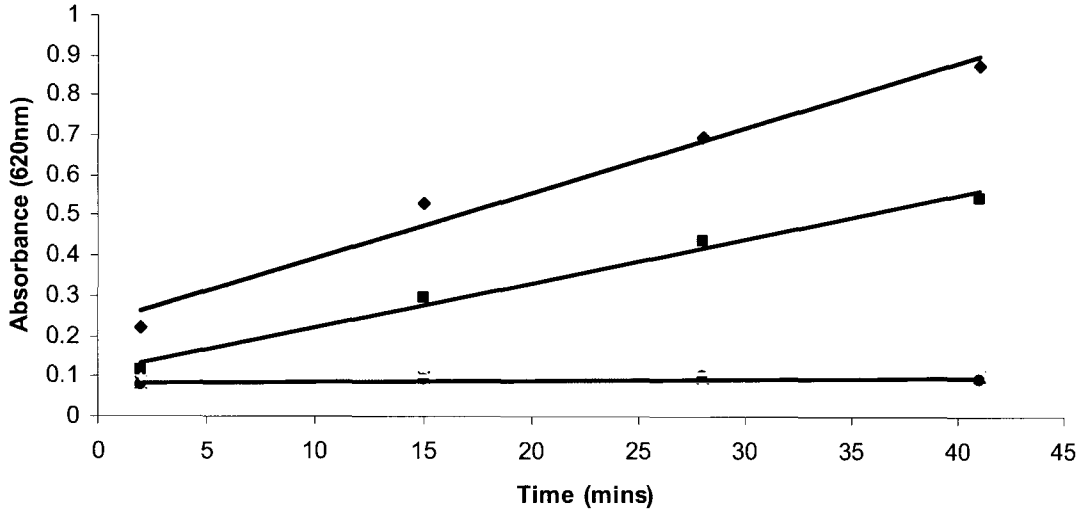

Figure 3.6: Sonication of E. coli Phospholipids Alters Level of Stimulation of $MinD_{Ng}$ ATPase Activity. *Reaction mixtures containing WT $MinD_{Ng}$, WT $MinE_{Ng}$, ATP, E. coli PLs, Mg^{2+}, and reaction buffer were examined for the rate of release of phosphate using the malachite green method. Reaction mixtures using pre-sonicated E. coli PLs (blue line), exhibited showed a higher reaction rate than did non-sonicated E. coli PLs (pink line). Yellow and maroon lines show that when E. coli PLs or Mg^{2+} were not added to the reaction mixture, no stimulation of MinD ATPase activity was observed.*

3.4 Purification of WT and Mutant $MinE_{Ng}$ and $MinD_{Ng}$

Metal-ion affinity chromatography was used to purify WT $MinE_{Ng}$, WT $MinD_{Ng}$, and all $MinE_{Ng}$ mutants shown in Table 2.1, along with $MinE_{Ng}$ E46A, $MinE_{Ng}$ L22D, and $MinE_{Ng}$ A18D. C-terminal hexahistidine tags on all proteins allowed formation of coordinate bonds between the hexahistidine residues and the Ni(II) bound to the nitriloacetic acid chelator, which permitted isolation of the desired Min proteins from other proteins in the cell lysate. The results of typical nickel affinity purifications of WT $MinE_{Ng}$ and $MinD_{Ng}$, examined through SDS-PAGE, are shown in the Coomassie stained gels in Figure 3.7 A. and B. Nickel affinity chromatography resulted in isolation of the desired protein with >95% protein purity. Purification of the 24 mutants generally gave an identical result to the example shown in Figure 3.7, with the exception of E67L, E46A, L22D, D20A, and F8A, which are discussed below.

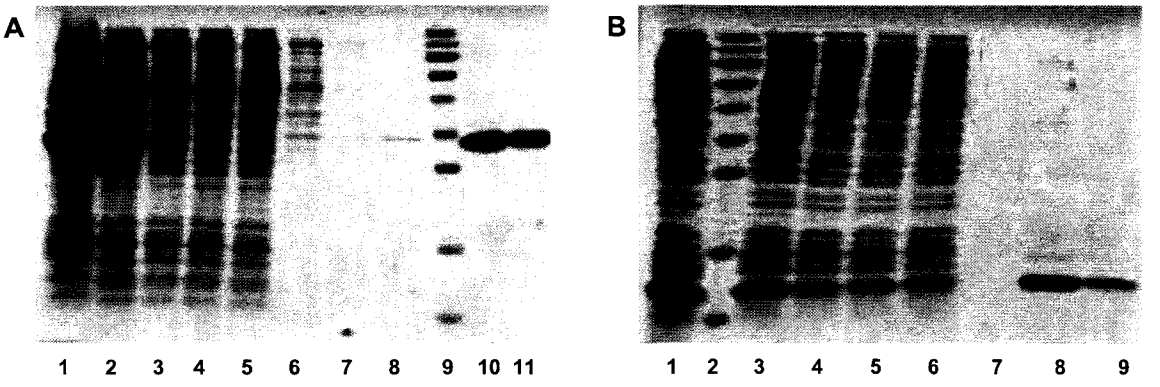

Figure 3.7: SDS-PAGE Gel Analysis of Fractions from Nickel Affinity Chromatography Purifications. *Coomasie stained SDS-PAGE gel of 25uL aliquots removed at various points in the purification.* ***A)*** *Lanes 1 and 2 correspond to the crude cell lysate and supernatant, respectively; lanes 3-5 and lanes 6-8 correspond to fractions taken from the flow through and wash, respectively; lanes 10 and 11 correspond to the eluted $MinD_{Ng}$ protein.* ***B)*** *Lanes 1 and 3 correspond to the crude cell lysate and supernatant fractions; lanes 4-6 and lane 7 correspond to the flow through and wash fractions, respectively; lanes 8-9 show the eluted $MinE_{Ng}$ protein.*

Following metal-ion affinity chromatography, all proteins were further purified using size exclusion chromatography. In most cases chromatography profiles of mutant $MinE_{Ng}$ proteins were the same as that for the WT protein. However, as shown in Figure 3.8, E67L and L22D eluted from the column at smaller elution volumes (E67L = 11.2mL +/- 0.1mL; L22D = 11.7mL +/- 0.3mL) than WT $MinE_{Ng}$ (12.0mL +/- 0.1mL). This suggested that these mutants possess a larger hydrodynamic radius than WT $MinE_{Ng}$, likely due to structural perturbation. Differences were also noted in the solubility for different mutants, with F8A and E46A showing a > 10-fold higher absorbance in the size exclusion profile compared to the WT protein (Figure 3.8). In contrast, D20A showed an approximately 2 fold lower absorbance reflecting the lower solubility observed for this mutant.

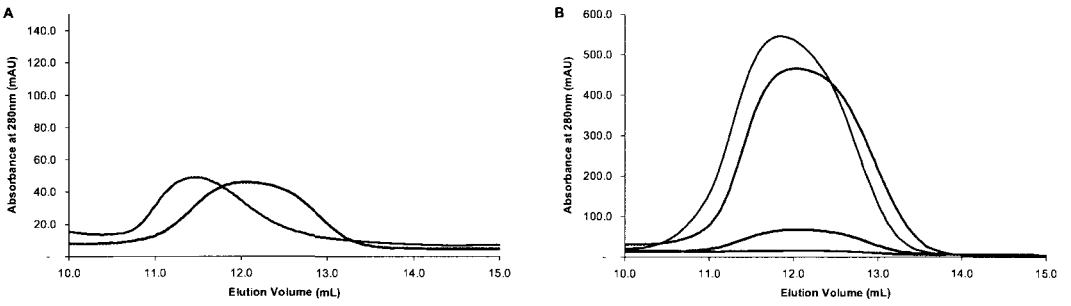

Figure 3.8: Size Exclusion Chromatography Profiles Illustrate Abnormalities in Elution Volume and Solubility. A) *$MinE_{Ng}$ E67L (yellow line) and L22D (pink) are shifted to a lower elution volume relative to WT $MinE_{Ng}$ (blue).* ***B)*** *$MinE_{Ng}$ F8A (turquoise) and E46A (green) show higher solubility than WT $MinE_{Ng}$ (blue), while D20A (red) is less soluble.*

3.5 Identification of Critical MinE Residues Required for Stimulation of MinD Activity

Once the $MinD_{Ng}$ ATPase assay had been optimized as described above, $MinE_{Ng}$ mutants were examined for their ability to stimulate $MinD_{Ng}$'s ATPase activity, using equimolar concentrations of $MinE_{Ng}$ and $MinD_{Ng}$ (2.7 μM) thought to reflect their concentrations *in vivo*. As shown in Figure 3.9, in the absence of $MinE_{Ng}$, $MinD_{Ng}$ hydrolyzed ATP in the presence of phospholipids at a relatively low rate of 4.7+/-2.27 nmol P_i/mg MinD/min. In agreement with previous observations, $MinE_{Ng}$ amplified this activity ~10-fold to give a specific activity of 50.8 +/- 3.13 nmol P_i/mg MinD/min. This is similar to the 10-fold stimulation of MinD ATPase activity observed for the *E. coli* homologues (~2.5 nmol Pi/mg MinD/min with no MinE; ~20 nmol Pi/mg MinD/min with MinE) (*97;98*)., which further confirms previous observations that the *E. coli* and *N. gonorrhoeae* Min proteins are functionally similar.

The assay was also done for a number of the mutants to identify functionally important residues in $MinE_{Ng}$. As shown in Figure 3.9, L22D and A18D showed a reduced ability to stimulate $MinD_{Ng}$ ATPase activity, which agreed with previous observations showing a non-functional state for these mutants (*99-101*). In contrast, all other mutants tested showed WT-like activity.

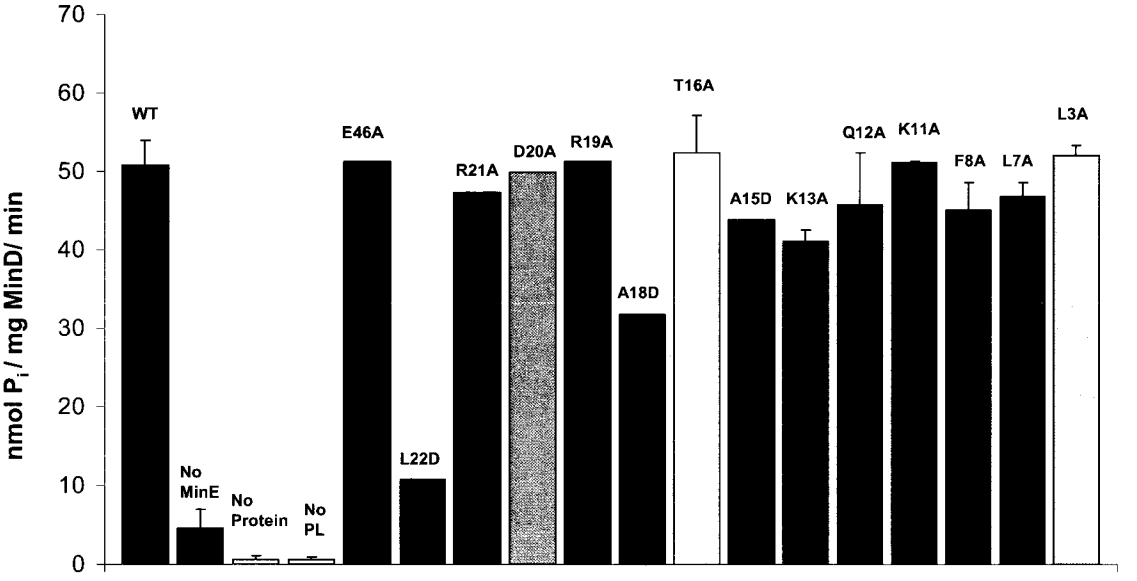

Figure 3.9: ATPase Assay Indicates that $MinE_{Ng}$ L22D and $MinE_{Ng}$ A18D Have a Reduced Ability to Stimulate $MinD_{Ng}$ ATPase Activity. *Various $MinE_{Ng}$ mutants were examined for their ability to stimulate $MinD_{Ng}$'s ATPase activity, using equimolar concentrations of $MinE_{Ng}$ and $MinD_{Ng}$ (2.7uM) in reaction mixtures containing all components required for activity (reaction buffer, Mg^{2+}, ATP, PLs).*

During the course of the analysis, unexpected results arose for the $MinE_{Ng}$ mutant R19A, which was expected to be less efficient than the WT protein, based on results obtained by Hu and Lutkenhaus with *E. coli* homologues (*102*) which showed that it exhibited a reduced ability to stimulate $MinD_{Ec}$ ATPase activity. The possibility remained that this reduction might not be detected if a significantly large concentration of $MinE_{Ng}$ R19A was available to stimulate $MinD_{Ng}$. To examine this possibility,

ATPase assays were performed at a range of $MinE_{Ng}$ concentrations to determine the concentration of $MinE_{Ng}$ that would give rise to a more sensitive response to functionally disruptive MinE mutations. As illustrated in Figure 3.10, lowering the concentration of WT $MinE_{Ng}$ from 2.7 μM to 0.15 μM did not decrease the level of stimulation of $MinD_{Ng}$ ATPase by WT $MinE_{Ng}$. Smaller levels of stimulation were only obtained when the concentration of WT $MinE_{Ng}$ was 0.1 μM or lower. As concentrations of WT $MinE_{Ng}$ around the inflection point (between 0 and 0.1 μM MinE) were most sensitive to changes in the ability of $MinE_{Ng}$ to bind $MinD_{Ng}$ and stimulate its ATPase activity, subsequent assays were performed using 0.06 μM $MinE_{Ng}$.

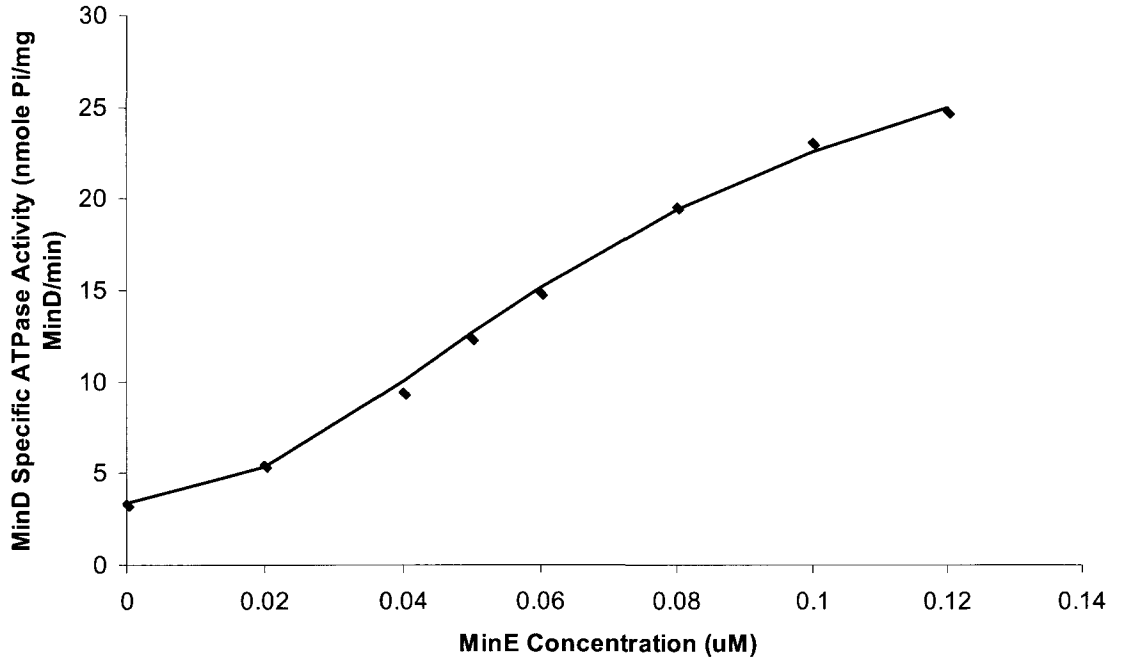

Figure 3.10: Stimulation of $MinD_{Ng}$ Specific ATPase Activity Varies with WT $MinE_{Ng}$ Concentration. *The $MinD_{Ng}$ specific ATPase activity was examined in reaction mixtures containing 2.7uM MinD, DOPG phospholipids, ATP, Mg^{2+}, reaction buffer, and variable concentrations of WT $MinE_{Ng}$. The $MinE_{Ng}$-dependent change in activity could be fit with the Hill equation with $K_{0.5}$=0.7uM, V_{max}=50nmol P_i/mg MinD/min) and a hill coefficient (h) of 2, shown by the blue line.*

The results from the new analysis with lower $MinE_{Ng}$ concentrations are shown in Figure 3.11. With these modified conditions, WT $MinE_{Ng}$ was shown to stimulate $MinD_{Ng}$ ATPase activity ~ 7-fold. As previous observations in this thesis indicated, $MinE_{Ng}$ L22D and A18D were unable to stimulate $MinD_{Ng}$ ATPase activity. However, $MinE_{Ng}$ R21A also showed significantly reduced activity, suggesting the importance of residue Arg21 for the interaction. R19A also showed a difference in ATPase stimulation activity, although the effect was much smaller for this mutant. No other mutants showed any difference in activity relative to WT $MinE_{Ng}$, suggesting that the

other areas of the anti-MinCD domain were not directly involved in the interaction with $MinD_{Ng}$.

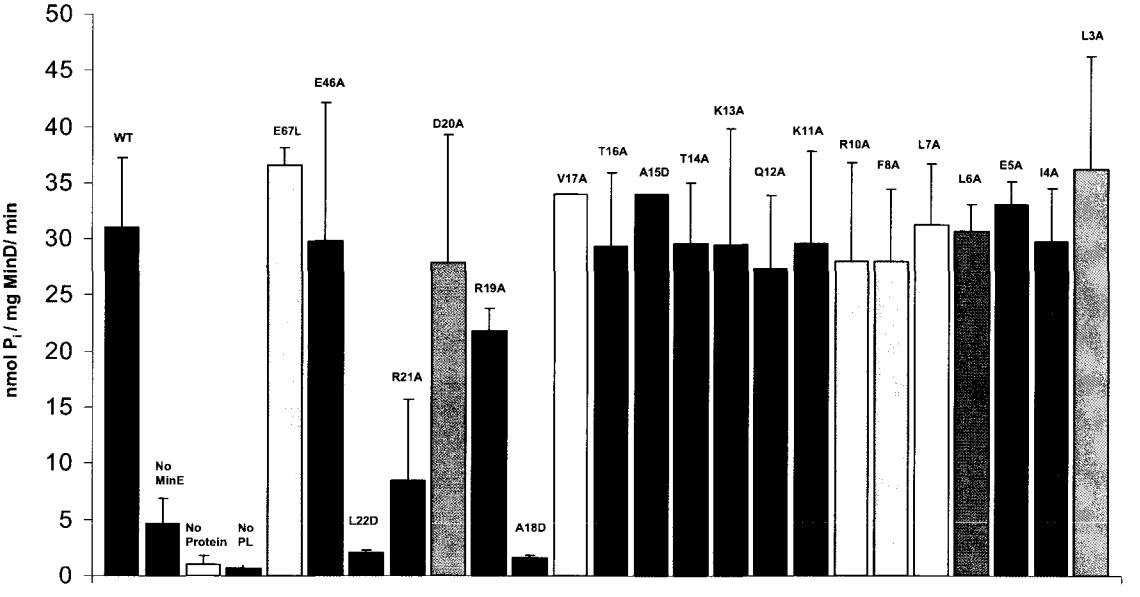

Figure 3.11: $MinD_{Ng}$ ATPase Stimulation by WT and Mutant $MinE_{Ng}$ Under Non-Saturating Conditions. *The $MinD_{Ng}$ specific ATPase activity was monitored in complete reaction mixtures containing 2.7 μM $MinD_{Ng}$, 0.06 μM $MinE_{Ng}$.*

Two $MinE_{Ng}$ samples with a mutation in the TSD were also tested in this assay: E46A, which had been shown to be important for the topological specificity function of MinE (*103;104*), and E67L, which had previously been shown to be unable to stimulate $MinD_{Ng}$ ATPase activity (*105*). As shown in Figure 3.11, my observations strongly suggest that both mutants are able to stimulate $MinD_{Ng}$ ATPase activity to a similar level as WT $MinE_{Ng}$, indicating that these parts of the TSD do not seem to be involved in stimulation of ATPase activity.

3.6 Preliminary Results from In Vivo Assay of $MinE_{Ng}$ Function

In order to determine the effect of these mutations *in vivo*, attempts were made to develop an *in vivo* assay based on the knowledge that overexpression of functional $MinE_{Ng}$ mutants in bacterial cells containing a complete chromosomal copy of the Min proteins results in minicells and short filamentous cell morphology (*106-108*). For this purpose, plasmids containing WT or mutant $MinE_{Ng}$ were transformed into *E. coli* BL21(DE3) cells, expression was induced with IPTG, and the resulting cell morphology was examined with phase contrast microscopy.

As shown in Figure 3.12, E. *coli* BL21(DE3) cells without transformed $MinE_{Ng}$ plasmid exhibit a regular rod-shaped morphology. Following overexpression, similar morphologies were observed for *E. coli* BL21(DE3) cells containing $MinE_{Ng}$ L22D and A18D plasmids, indicating that these mutants are not active *in vivo*. However, overexpression of WT $MinE_{Ng}$ or any $MinE_{Ng}$ mutant that had exhibited full activity *in vitro* disrupted symmetric cell division, which was evident from the observation of both minicells and elongated cells, similar to previous observations (*109-111*). These results corroborated our *in vitro* findings, and again highlighted the importance of residues L22 and A18 for stimulation of $MinD_{Ng}$ ATPase activity.

Although the in vivo results obtained showed nice agreement with the in vitro results, during the course of the mutant screen it became apparent that reproducibility was difficult to obtain. Unfortunately, time constraints did not allow the source of this variability to be identified, and also prevented the acquisition of similar data for

mutants E67L, E46A, and R21A . For these reasons, all of the in vivo data presented in this thesis must be considered to be preliminary at this stage.

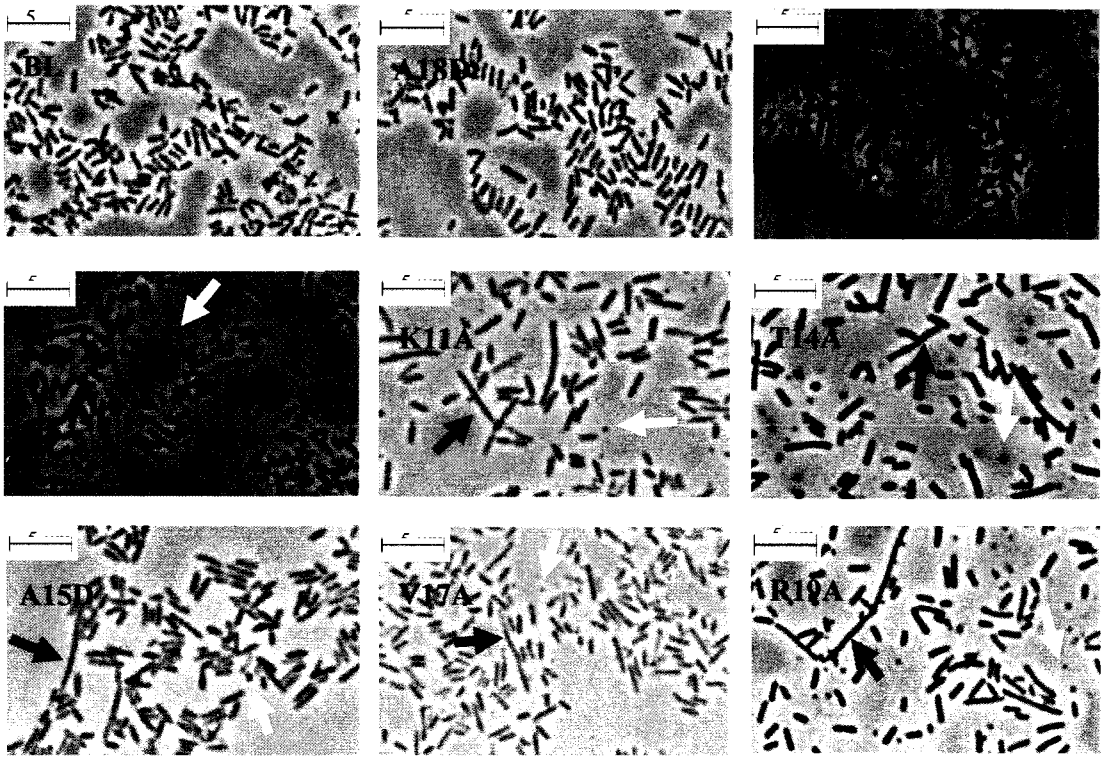

Figure 3.12: Preliminary Results from in vivo Assay of $MinE_{Ng}$ Function. *Phase contrast microscopy of E. coli BL21(DE3) overexpressing WT or the indicated $MinE_{Ng}$ mutant. Samples showing elongated cells (indicated by red arrow) and minicells (indicated with yellow arrow) indicative of disruption of symmetric cell division were observed. $MinE_{Ng}$ expression levels were confirmed to be similar for all samples by Coomassie-stained SDS-PAGE gel analysis (data not shown).*

3.7 Conformational Studies of $MinE_{Ng}$ L22D and R21A

One possible explanation for the absence of activity observed for $MinE_{Ng}$ L22D, R21A, and A18D was that these mutations induced structural perturbations in a way that prevented interactions with $MinD_{Ng}$. In the case of $MinE_{Ng}$ A18D, previous experiments using circular dichroism (CD) spectroscopy and nuclear magnetic resonance (NMR) spectroscopy had shown that the structure was not affected by this mutation (*112*). However, no structural information was available for $MinE_{Ng}$ R21A; therefore we were interested in studying the structural properties of this mutant.

During purification it was apparent that $MinE_{Ng}$ R21A had poor solubility compared to the WT protein, which consequently limited spectroscopic studies of $MinE_{Ng}$ R21A's conformation to circular dichroism experiments. A preliminary CD spectrum for this mutant (Fig. 3.13A) shows a difference in the shape and intensity compared to the WT protein, suggesting that this mutation gives rise to a small conformational difference. To gain more insight into the nature of this change, the thermal stability of this protein was evaluated by monitoring the ellipticity at 222 nm while the temperature of the sample was raised by 2°C/min up to 95°C. As shown in Figure 3.13B, there was a rapid decrease in ellipticity in the temperature range 60°C-95°C, with the melting transition temperature being ~80°C. This cooperative loss of secondary structure is characteristic of a folded protein, indicating that this mutant retained a significant amount of tertiary structure. However, the thermal stability of the WT protein appeared to be even greater than this value, since its ellipticity change occurred at a higher temperature, and did not appear to reach a plateau expected for a

completely unfolded state. This suggests that the actual melting temperature for the WT protein was higher than 75°C, indicating a very stable protein. Overall, these results suggest that substitution of alanine for arginine in this position has a destabilizing effect on the structure, which may at least partially explain the effect on MinE activity. Similar results were also obtained for L22D (data not shown), confirming the previously described structural perturbation (*113*).

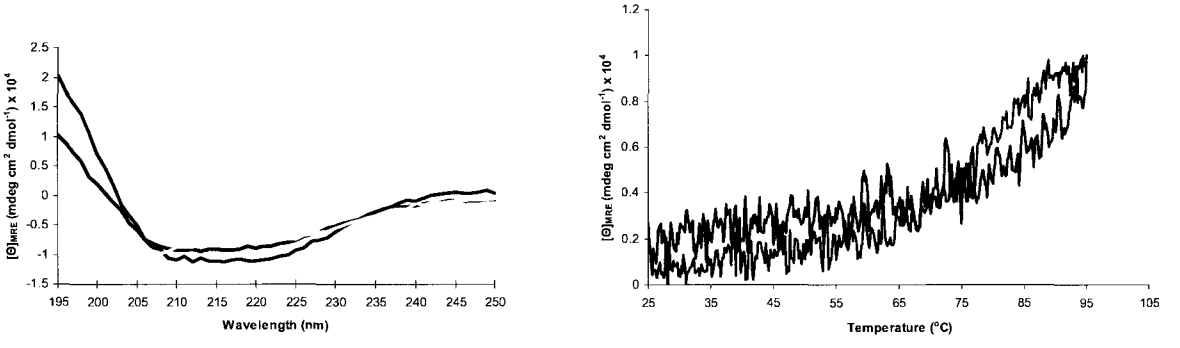

Figure 3.13: Circular Dichroism Data Suggests that MinE R21A is Structurally Perturbed. A) *CD spectra of 4.0 μM R21A (pink), WT (blue), or L22D (yellow) $MinE_{Ng}$ samples.* ***B)*** *The ellipticity of 4.0 μM R21A (pink) and WT (blue) $MinE_{Ng}$ monitored at 222 nm as the temperature was raised by 2°C/min to probe thermal stability.*

Previous work in the Goto laboratory showed that the $MinE_{Ng}$ L22D mutant had CD and NMR properties that were significantly different from the WT $MinE_{Ng}$ protein, suggesting a significant structural perturbation (*114*). In addition, the NMR spectrum of the $MinE_{Ng}$ L22D mutant indicated that one portion of the L22D mutant was in a flexible unfolded form, whereas another significant portion adopted a structure that was distinct from any part of the WT $MinE_{Ng}$ structure. Given our findings that the $MinE_{Ng}$ L22D mutant was unable to stimulate $MinD_{Ng}$ ATPase activity *in vitro*, we sought to

gain further structural insight into this mutant. For this purpose, an ^{15}N-labeled sample of an N-terminally truncated $MinE_{Ng}$ protein containing residues 31-89 corresponding to the TSD was prepared ("MinE TSD"). ^{1}H-^{15}N HSQC NMR spectra were recorded for the $MinE_{Ng}$ L22D and $MinE_{Ng}$ TSD samples under identical conditions. This type of spectrum correlates the amide proton chemical shift with the chemical shift of the attached nitrogen atom, providing atomic level information of the local chemical environment for each amide proton and serving as a "fingerprint" spectrum for the protein. As shown in Figure 3.14, a significant number of peaks in the TSD spectrum (red), were superimposable with peaks from the folded part of L22D, suggesting that the observable L22D amide protons existed in a nearly identical chemical environment as the observable TSD amide protons. This demonstrates that the part of L22D that remains structured has the same fold as the isolated TSD.

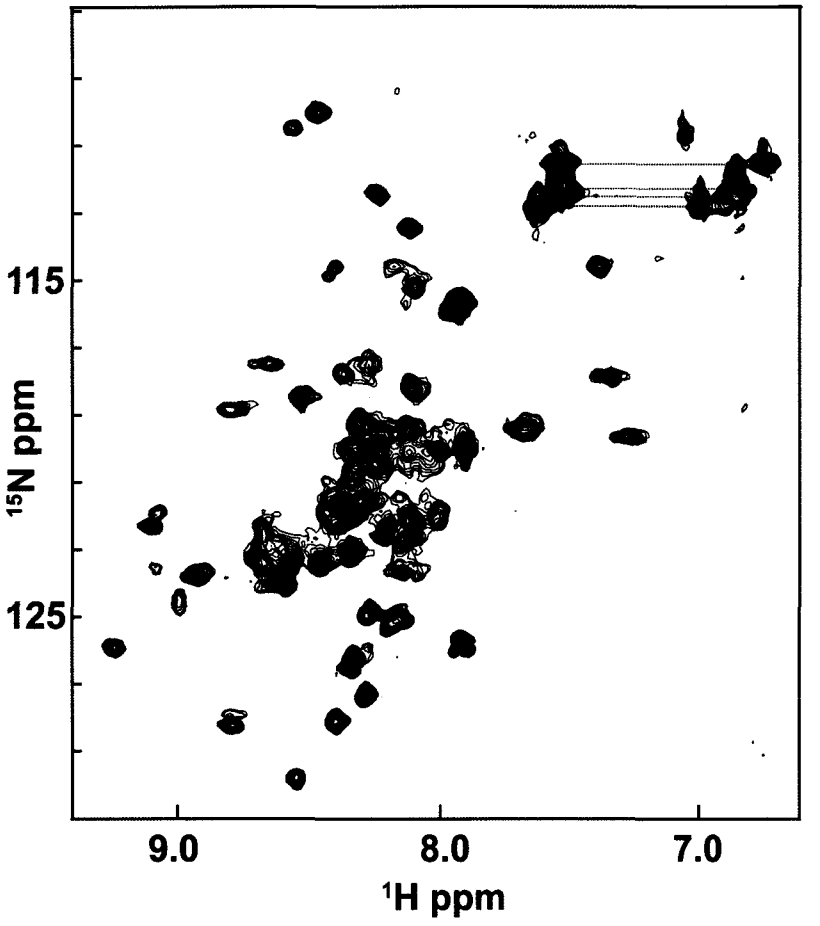

Figure 3.14: *^{1}H-^{15}N HSQC spectrum of $MinE_{Ng}$ TSD (red) superimposed on the L22D spectrum (black).*

3.8 Stimulation of $MinD_{Ng}$ ATPase Activity by $MinE_{Ng}$ Anti-MinCD Domain Peptides

To further examine the role of the TSD in anti-MinCD activity, a synthetic peptide consisting of only the first 22 residues of WT $MinE_{Ng}$ ($MinE_{Ng}^{1-22}$) was also tested for activity in the $MinD_{Ng}$ ATPase assay. As shown in Figure 3.15, the synthetic peptide stimulated $MinD_{Ng}$ ATPase activity to a similar level as WT $MinE_{Ng}$. This was a noteworthy result, since not only did it provide strong evidence that no part of

$MinE_{Ng}$ beyond residue 22 was required for ATPase stimulation, but it also suggested that the dimeric state of $MinE_{Ng}$ was not necessary for anti-MinCD activity. In addition, I also discovered that a peptide containing only the first 17 residues of $MinE_{Ng}$ ($MinE_{Ng}^{1-17}$) did not stimulate $MinD_{Ng}$ activity, even when used at higher concentrations, confirming that residues preceding Ala18 are not important for stimulation of $MinD_{Ng}$ ATPase activity.

The high activity obtained with $MinE_{Ng}^{1-22}$ raised the possibility that the residues mutated in the two functionally compromised mutants that also showed significant structural perturbations from the WT protein, namely L22D and R21A, may nonetheless be directly involved in interactions with MinD. To determine whether this was the case, peptides containing these mutations ($MinE_{Ng}^{1-22(L22D)}$, and $MinE_{Ng}^{1-22(R21A)}$) were also assayed. As shown by the preliminary results in Figure 3.15, $MinE_{Ng}^{1-22(L22D)}$ did not stimulate $MinD_{Ng}$ ATPase activity, even when used at higher concentrations, suggesting that residue Leu22 directly participates in anti-MinCD activity. In addition, $MinE_{Ng}^{1-22(R21A)}$ exhibited a concentration dependent ability to stimulate $MinD_{Ng}$ ATPase activity, similar to the behavior of the full-length $MinE_{Ng}$ R21A mutant. Specifically, the $MinE_{Ng}^{1-22(R21A)}$ concentration had to be greater than 0.06uM for stimulation of $MinD_{Ng}$ ATPase activity to be observed. Therefore Arg21 also seems to be directly involved in stimulation of $MinD_{Ng}$ ATPase activity.

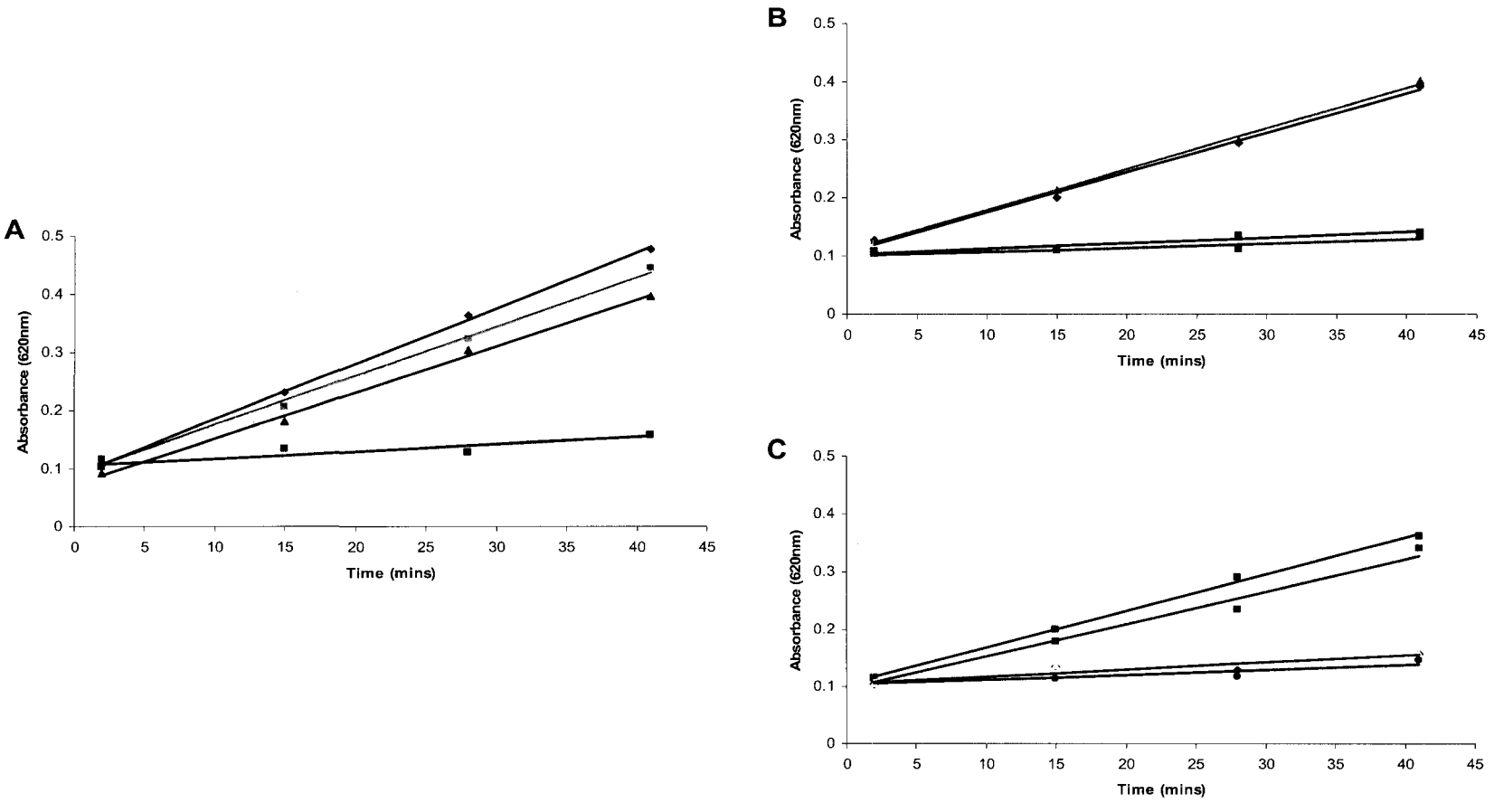

Figure 3.15: Stimulation of $MinD_{Ng}$ ATPase Activity by Anti-MinCD Domain Peptides. *Results from the malachite green assay for phosphate taken from $MinD_{Ng}$ reactions at various time points, as monitored by aborbance at 620 nm. Best-fit lines obtained from linear regression are also shown. For all graphs the ATPase activity of 2.7 μM $MinD_{Ng}$ in the absence of $MinE_{Ng}$ is shown in blue, and in the presence of 0.06 μM WT $MinE_{Ng}$ in pink. Activity profiles are shown for* **A)** *0.06 μM $MinE_{Ng}^{1-22}$ (grey and red), B) 2.7 μM $MinE_{Ng}^{1-17}$ (orange) C) 2.7 μM $MinE_{Ng}^{1-22(L22D)}$ (maroon) and 0.06 μM $MinE_{Ng}^{1-22(R21A)}$ (yellow) and 2.7 μM $MinE_{Ng}^{1-22(R21A)}$ (green).*

3.9 Results Summary

To study the interaction between $MinE_{Ng}$ and $MinD_{Ng}$, various $MinE_{Ng}$ mutant proteins were created through site directed mutagenesis and then purified with nickel affinity chromatography followed by size exclusion chromatography. An *in vitro* ATPase assay was developed to examine the extent to which each mutant could stimulate $MinD_{Ng}$ ATPase activity, as this served as a measure of the MinE-MinD interaction. An *in vivo* assay was also developed which confirmed the findings from the ATPase assay. Examination of all mutants with the developed ATPase assay revealed a number of important findings:

1) Residues Leu22 and Ala18 are crucial residues, which, when mutated in the full length WT $MinE_{Ng}$ protein to aspartic acid, result in non functional $MinE_{Ng}$ mutants. Residue Arg21 is an important residue, which, when mutated in the full length WT $MinE_{Ng}$ protein to alanine, results in a mutant which is functional at 2.7uM but not at 0.06uM.

2) Residues Asp67 and Asp46 are non-crucial residues, which, when mutated in the full length WT $MinE_{Ng}$ protein to leucine and alanine, respectively, result in functional $MinE_{Ng}$ mutants.

4) A 22 residue peptide corresponding to the first 22 residues of the N-terminal region of WT $MinE_{Ng}$ ($MinE_{Ng}^{1-22}$) is able to stimulate $MinD_{Ng}$ ATPase activity to a similar

extent as WT $MinE_{Ng}$. In contrast, a 17 residue peptide corresponding to the first 17 residues of the N-terminal region of WT $MinE_{Ng}$ is unable to stimulate $MinD_{Ng}$ ATPase activity.

5) $MinE_{Ng}^{1\text{-}22(L22D)}$ is unable to stimulate MinD ATPase activity while, $MinE_{Ng}^{1\text{-}22(R21A)}$, is only able to stimulate $MinD_{Ng}$ ATPase activity when present at higher concentrations.

It was also shown that:

6) CD spectroscopy and thermal stability studies suggest that the structure of R21A is perturbed relative to the WT protein.

7) The local chemical environment of the observable $MinE_{Ng}$ L22D amide protons resembles the local chemical environment of observable $MinE_{Ng}$ TSD amide protons as determined by NMR spectroscopy.

Chapter 4: Discussion

Symmetric cell division in gram negative bacteria requires that MinE suppresses the inhibitory activity of MinCD at midcell, but not at the cell poles. To accomplish this, MinE transiently binds MinD, which results in the displacement of MinC, the stimulation of MinD's ATPase activity, and the induction of MinD oscillation between the cell poles such that the time averaged concentration of MinCD is lowest at midcell. The anti-MinCD domain of MinE has been implicated as the component of MinE which binds to MinD. However, the precise MinE residues necessary for the MinE-MinD interaction are unknown, and the mechanism of the interaction is unclear. Further, structural information from the Goto laboratory suggested that some of the MinE residues previously implicated in the MinE-MinD interaction were structural in nature. To gain insight into this interaction, this investigation studied the anti-MinCD domain and two TSD mutants, $MinE_{Ng}$ E46A and E67L, through *in vitro* and *in vivo* techniques.

4.1 Specific Activity of MinD from N. gonorrhoeae

In agreement with previous research on the *E. coli* Min proteins (*115;116*), my findings show that MinD from *N. gonorrhoeae* exhibits a low level of basal ATPase activity that is stimulated ~10-fold by MinE. This similarity further confirms previous observations that the *E. coli* and *N. gonorrhoeae* Min proteins are functionally similar.

However, one interesting difference between the *N. gonorrhoeae* Min protein data and previous studies with the *E. coli* proteins was that the specific activity values were ~ 2.5-fold higher for the *N. gonorrhoeae* proteins. Although structural differences between the homologues may account for this difference, the high sequence conservation and the similar degree of MinD ATPase stimulation suggested that these differences should not be very large. Instead it is more likely that the different lipid systems used to measure MinD ATPase activity was the more significant source for these differences, since my study used the anionic DOPG lipid, while other groups had used a total lipid extract from *E. coli* that would be rich in phosphatidylethanolamine. The dissociation constant of ATP bound $MinD_{Ec}$ with *E. coli* phospholipids has been estimated as 4.8 μM, whereas with DOPG it was 1.4 μM, reflecting a preferential interaction with anionic phospholipids (*117*). Consequently, our *in vitro* assay would be expected to give rise to 2-3-fold more bound MinD than the equivalent system using *E. coli* phospholipids. This could explain the ~ 3x greater specific ATPase activity obtained in our study. This analysis provides the first direct demonstration that MinD ATPase activity can be modulated through a change of phospholipid composition, and supports the hypothesis that MinD preferentially interacts with anionic phospholipids.

When investigating the ideal MinD:MinE molar ratios to assay MinE function it was found that only when the molar ratio of MinD to MinE exceeded 20:1 did lower specific activities appear. Similar experiments performed with the *E. coli* Min proteins and *E. coli* phospholipids showed saturation of MinD ATPase activity for MinD:MinE molar ratios of ~5:1. Although not the same as the ratio determined in our system, the fact that it is also not 1:1 suggests that MinE is either capable of simultaneously

stimulating more than one molecule of MinD, or that only a fraction of MinD is available for stimulation of ATPase activity. In either scenario, the polymeric structures known to be adopted by MinD when bound to the lipid bilayer may be the underlying source of this effect, particularly since the nature of the polymer is known to depend on the lipid type (*118-120*). My observations would also be consistent with MinE-stimulated fraying at the ends of polymeric MinD structures observed by electron microscopy, suggesting that only the terminal regions of MinD superstructures may be available for interactions that stimulate MinD activity (*121;122*).

Given the sigmoidal dependence of MinD activity with MinE concentration, it was possible to fit this profile to the Hill equation. This allowed us to determine the Hill coefficient for this system, which was found to be 2, suggesting that the interaction of one MinE molecule led to more favorable interactions with at least one other MinE molecule. This fits well with the known tendency for MinE to dimerize, the affinity of which was measured at 0.6 uM for the E. coli protein (*123*). In our system the MinE concentration giving rise to half-maximal activity ($K_{0.5}$) was found to be ~0.06 uM, which is an order of magnitude lower than this dissociation constant. Nonetheless, differences in *N. gonorrhoeae* and *E. coli* MinE sequences compounded with the different conditions being tested could account for a difference in dimerization strength of this magnitude. If this is the case then it is likely that the decrease in MinD stimulation activity being observed at lower MinE concentrations in our experiments reflects a change in the dimerization state of MinE

4.2 $MinE^{1-22}$ is Sufficient to Stimulate MinD ATPase Activity

While previous *in vivo* experiments have shown that the expression of $MinE^{1-22}$ is sufficient to disrupt the MinCD complex (*124*), prior to the current work it had never been demonstrated that this peptide could stimulate MinD ATPase activity at levels comparable to WT MinE. My results suggest that MinE residues 23-32 are not necessary for the anti-MinCD activity, counter to the hypothesis forwarded by Pichoff *et al.* (*125*) and also implies that the key MinE residues for the MinE-MinD interaction are located exclusively in the anti-MinCD domain, suggesting a total functional and structural independence of the first 22 residues of MinE.

However, the observation that $MinE^{1-22}$ is sufficient to stimulate MinD ATPase activity did not completely eliminate the possibility that residues in the TSD might play a functional, though indirect, role in the MinE-MinD interaction. In fact, it has been observed that $MinE^{32-88}$ partially interferes with the MinD-MinC interaction in a yeast three hybrid system and that $MinE^{1-88}$ is more effective than $MinE^{1-31}$ in disrupting the MinC-MinD interaction in a yeast three-hybrid system (*126*). In addition $MinE^{1-88}$ K19A was capable of interfering with the MinC-MinD interaction in a yeast three hybrid system, but $MinE^{1-31}$ K19A did not interact MinD in a two hybrid system (*127*). These results raise the possibility that the binding interaction between MinD and the TSD could result in a conformational change of the anti-MinCD domain from an inactive to active conformation and removal of residues 23-88 might have mimicked this conformational change, thus permitting the anti-MinCD domain to enter into an

active conformation. The nature of this hypothetical conformational transition and its role in topological specificity function is not yet possible to determine, but our demonstration that the topological specificity mutant MinE E46A was still capable of stimulating MinD ATPase activity suggests that the formation of E-rings and stimulation of MinD ATPase activity are separate phenomena. However, *E. coli* mutants showing no anti-MinCD activity also do not form E-rings (e.g. L22R, A18T, I25A) (*128*), suggesting a role for anti-MinCD activity in E-ring formation.

4.3 Structural and Functional Impact of R21A and L22D

This is the first study to identify Arg21 as a functionally important residue for MinE. However, purification of $MinE_{Ng}$ R21A was hindered by poor solubility, likely due to the lower stability of this protein compared to the WT $MinE_{Ng}$, as presented in my thermal denaturation studies. This observation is also similar to previous results with the double mutant R21A/D20A of $MinE_{Ec}$, since this mutant was found to be unstable *in vivo*. Our NMR structure shows that this residue is at the end of a β-strand in the dimeric interface in close proximity to Glu83 in the adjacent subunit (unpublished data), suggesting that the loss of this interaction has a destabilizing effect on the dimer.

The fact that the R21A mutant appears to affect the MinE structure raised the possibility that the lower activity reflected this conformational change. However, our results with the $MinE^{1-22}$ WT and R21A peptides suggest that the structure of this region in the full-length protein may not be important for the interaction. Previous

NMR studies with the *E. coli* homologue of $MinE^{1-22}$ showed that the peptide was largely unstructured at this site (*129*) . Therefore, it is likely that R21 plays a direct role in binding and/or activating MinD, and is one of the residues at the protein-protein interface.

In the case of L22D, the structural effects of the mutation appear to be more severe, with a notable difference in CD spectra of WT $MinE_{Ng}$ and L22D, and a thermal denaturation temperature significantly lower than that of WT (data not shown, but see (*130*)). In the full-length $MinE_{Ng}$ structure this residue is located at the dimeric interface, in a region of the protein that is not accessible to solvent. Consequently it is not surprising that introduction of a negative charge disrupts the structure and decreases its stability. However, the cooperative melting transition obtained for this mutant indicates that some part of the protein is still folded in spite of the drastic change introduced to its sequence.

In the case of L22D the solubility of the mutant was sufficient to allow its ^{1}H-^{15}N HSQC spectrum to be recorded, providing additional insight into the nature of the structural perturbation shown by CD. As previously noted (*131*), this spectrum indicates that a large part of the protein is unfolded, but that some region does appear to be structured. Of greatest interest is the new data showing that almost all peaks obtained from the WT TSD HSQC spectrum (Figure 3.15, red) coincided with a peak from the L22D spectrum (black), indicating that the chemical environments of the corresponding amide protons are identical. Given that the isolated topological specificity domain from *E. coli* is known to adopt a stable dimeric fold (Figure 1.5) these results suggest that the part of the sequence corresponding to the TSD in L22D

must adopt the same structure as the isolated TSD. According to this scenario, residues 23-31 would be displaced from the center of the β-sheet while residues 72-81 would form the central part of the new dimeric interface as seen in the TSD structure determined by King *et al.* (*132*). Meanwhile the anti-MinCD residues would project out into the solvent as unfolded polypeptides, since N-terminal helix binding site on the β-sheet would be disrupted by this change.

The significant structural change caused by the L22D mutation would make it appear likely that the loss of anti-MinCD activity was due to the disruption of a biologically important structure. This would be supported by the location of L22 in the full-length MinE structure, since this residue would not be accessible for interactions, being buried in the hydrophobic interior of the dimer. However, somewhat unexpectedly we found that the $MinE^{1-22}$ L22D peptide was also completely inactive, even when higher concentrations of peptide were used. This suggests that L22 could in fact be one of the residues that is directly involved in MinD binding, although this would require a significant structural change. One other possibility that must be considered is that L22 is only adjacent to the binding site, and that introduction of an aspartic acid at this location introduces unfavourable contacts between MinD and the peptide. In order to resolve these possibilities, it will be necessary to investigate the impact of less drastic changes to the amino acid sequence at this site (e.g. L22A) in the future.

4.4 Preliminary In vivo Results Agree with In vitro Results

The knowledge that MinE L22D and A18D had previously been discovered to be non-functional mutants using *in vivo* systems (*133*) supported the biological relevance of our findings. However, the conditions used in our *in vitro* ATPase assay differed significantly from biological conditions: the ratio of $MinD_{Ec}$ to $MinE_{Ec}$ in an *E. coli* cell is 1.4:1 (*134*), whereas the $MinD_{Ng}$:$MinE_{Ng}$ ratio in our assay was 45:1; and the *E. coli* phospholipid bilayer is composed of a mixture of PE, PG, and CL phospholipids, whereas our system contained only a variant of PG phospholipids.

To confirm that our *in vitro* results were biologically relevant, we developed an *in vivo* system based on the observation that overexpression of functional WT $MinE_{Ng}$ in *E. coli* cells results in the formation of minicells and filamentous cell morphology (*135*). As expected, there was general agreement between our *in vivo* and *in vitro* results for the tested MinE mutants. Unfortunately, these results were difficult to reproduce, and though they were reproduced at least once, anomalous results were obtained. For instance, reproducible data was not obtained for $MinE_{Ng}$ R21A. In the future, a better *in vivo* system, using ΔminCDE cells, must be developed to confirm these preliminary *in vivo* findings.

4.5 Implications for Theories Describing the MinE-MinD Interaction

The results presented in this thesis imply that many of the current theories describing the MinE-MinD interaction require significant alteration to account for these new findings.

i) Implications for the Soj/SpoOj Hypothesis

MinD is a member of a subgroup of ATPases which are involved in diverse functions, but bear the similarity of possessing a deviant Walker A motif, which is characterized by a signature lysine (Figure 4.1) (*136;137*). Another member of this ATPase subgroup is Soj, which shows a number of functional similarities to MinD: Soj oscillates on or between nucleoids only when in the presence of DNA and a partner protein, SpoOj; the binding of Soj to DNA is ATP dependent; Soj assembles into nucleoprotein filaments when in the presence of ATP, and DNA; and the structure of Soj strongly resembles the structure of MinD, insofar as a dimer and monomer can be compared (*138*).

Walker A Motif	G X X X X G K T/S
Deviant Walker A Motif	X **K** G G X X K T/S

Figure 4.1: Comparison of the Walker A Motif with the Deviant Walker A Motif found in MinD. *The Walker A motif is considered to be a nucleotide binding motif, which is present as a loop around the bound nucleotide, binding to the phosphate oxygen atoms using the lysine and threonine/serine residues (139). The deviant Walker A motif bears a signature lysine residue (bold), which is hypothesized to play a role in stabilizing negative charges arising during nucleotide hydrolysis (140).*

The many observed functional similarities between MinD and Soj, as well as the observation that the alignment of the N-termini of SpoOj and MinE shows sequence homology, led to the proposal by Leonard *et al.* that MinE amplifies MinD ATPase activity through the same "conserved mechanism of nucleotide hydrolysis activation" which exists in the SpoOj/Soj system (*141*). Specifically, it was observed that SpoOj R10A was unable to activate Soj, indicating the crucial importance of the Arg10 SpoOj residue in this interaction. Alignment of SpoOj and MinE suggested that residues Arg21 or Arg19 should play an equivalent role in MinE.

However, our results showed that neither the R19A nor the R21A mutation of MinE corresponded with complete abrogation of the ability to stimulate MinD ATPase activity. Further, our results showed that all other mutations of positively charged residues in the N-terminus of MinE (K13A, K11A, R10A) did not affect the ability of MinE to stimulate MinD ATPase activity, suggesting that MinE and SpoOj activate their respective partner proteins through different mechanisms.

Leonard *et al.* also observed that a peptide corresponding to the first 20 residues of SpoOj stimulated Soj ATPase activity 92% less than the full SpoOj protein. If MinE shared a similar mechanism of nucleotide hydrolysis activation, then a similar result would be expected. However, our results showed that $MinE_{Ng}^{1-22}$ activated $MinD_{Ng}$ ATPase activity to the same extent as WT MinE, providing more evidence that the method of MinD activation by MinE differs from the method of Soj activation by SpoOj.

ii) Implications for the Arginine Finger Hypothesis

Lutkenhaus and Sundaramoorthy have proposed that the role of MinE may be similar to the role of the GTPase activating protein in stimulating GTP hydrolysis in small G proteins, whereby MinE enhances MinD catalysis by donating an arginine residue to the active site to stabilize the negative charge of ATP during hydrolysis (*142*).

As indicated above, the data presented in this study shows that positively charged residues of MinE are unlikely to play a crucial role in stimulating MinD ATPase activity, as MinE R21A, R19A, K13A, K11A, and R10A are all capable of stimulating MinD ATPase activity. It is therefore unlikely that the arginine finger hypothesis is correct; however, redundant functional roles of two closely situated positive charges could reconcile the observations from our study with the arginine finger hypothesis. For example, if MinD could accommodate MinE residues R21, D20, and R19 into its active site, and only one positively charged residue was necessary to

stabilize ATP hydrolysis, then mutation of either R21 or R19 would not have an effect upon the ability of MinE to stimulate MinD ATPase activity. Rather, a double R21 and R19 mutation would be necessary for stimulation of MinD ATPase activity to be abrogated. Further, our evidence tends to suggest that MinE residues L22 and A18 are the key residues in the MinE-MinD interaction, but it is possible that mutations to these residues might only be altering the structure around the true catalytic site centred on R19-R21.

iii) Implications for the MinD Competition Hypothesis

Ma *et al.* have hypothesised that MinE competes with MinD residue K11, the "signature" lysine of the deviant Walker A motif, for binding with other residues in MinD (*143*). According to this hypothesis, the interaction between MinE residues and MinD residues D152 or S148 disrupts their electrostatic interaction with K11, leading to a conformational change of MinD which results in the stimulation of MinD activity. However, for the reasons described above, this hypothesis is also unlikely. Our data indicates that hydrophobic residues L22 and A18 are the key residues for the MinE-MinD interaction. Nonetheless, this does not rule out the importance of the various interactions surrounding K11. The MinD competition hypothesis could be partially correct, in which electrostatic interactions between K11 and positively charged residues play an important role in the stimulation of MinD ATPase activity. I speculate that rather than MinE first disrupting the internal electrostatic interactions in the MinD protein centered around residue K11, a conformational change in MinD caused by MinE binding could lead to the disruption of these electrostatic interactions.

iv) Implications for the Coiled-Coil Hypothesis

King *et al.* have proposed that MinE residues 1-35 exist in an α-helix conformation, based on the observation that $MinE^{1-22}$ is predicted to be a nascent helix, the $MinE^{6-35}$ sequence is predicted to have a high propensity to form a coiled coil (*144*), and the N-terminal residues 31-35 form a helix in the solved structure of the $MinE_{Ec}$ TSD (*145*). Mutagenesis studies by King *et al.* using yeast two and three hybrid assays suggested that residue I25, L22, and A18 were necessary for the MinE-MinD interaction, and that these residues cluster to one side of a hypothetical helix that could be formed by this part of MinE (*146*). Based on these observations, *King et al.* proposed that an interaction between this helical surface and a complementary site on a MinD α-helix results in the formation of a coiled coil structure, triggering a conformational change in MinD that amplifies MinD ATPase activity (*147*).

The solved structure of MinE E46A would appear to invalidate this theory, as residues 23-28 exist in a β-strand which are structurally important. However, a slight modification of the coiled-coil theory could account for the structural importance of residues 23-28 while reconciling the functionally important residues found in our study. As $MinE^{1-22}$ has been shown to have some propensity for helix formation, an interaction between MinE and MinD could shift the $MinE^{1-22}$ equilibrium towards an α-helix conformation, permitting the formation of a coiled coil between the newly formed MinE α-helix and a MinD α-helix. The precise MinE-MinD interaction leading to this coiled-coil structure is difficult to predict, but would involve residues A18, L22 and R21, which are conveniently located on one side of this hypothetical α-helix.

An alternative way in which the coiled-coil hypothesis could be accommodated would involve a significant conformational change involving residues 23-28. Our observations concerning the structure of MinE L22D suggest that in this mutant these residues are not located at the dimeric interface, which is instead comprised of β-strands corresponding to residues 73-81. It is possible that an interaction with MinD could occur which would trigger a conformational change from the structure shown in Figure 1.4 to that adopted by L22D containing the TSD structure. This would allow residues 23-28 to also contribute to the α-helix as originally proposed by King and coworkers. This would suggest that a MinE peptide that included these residues would provide greater stimulation of MinD ATPase activity than that observed with $MinE^{1-22}$. Future studies with longer MinE peptides are planned to investigate this possibility.

v) Implications for Dimerization of the anti-MinCD Domain

It has long been uncertain whether the context of the anti-MinCD domain may be important for the stimulation of MinD ATPase activity. Pichoff *et al.* showed that full length MinE was better at suppressing MinCD division inhibition than was $MinE^{1-32}$, which was shown to be a monomer (*148*), suggesting that dimerization of the N terminal is important for the MinE-MinD interaction. Zhang *et al.* showed that MinE heterodimers consisting of MinE WT and $MinE^{22-88}$ were incapable of preventing MinCD division inhibition; strongly suggesting that dimerization of the anti-minCD domain plays a role in the MinE-MinD interaction (*149*). Finally, in the purportedly similar Soj/SpoOj system, SpoOj (the purported MinE equivalent) is proposed to

undergo DNA dependent dimerization of its N-terminal, which would suggest that MinE should undergo a similar dimerization of its N-terminal.

In light of the observations by Pichoff *et al.* that $MinE^{1-32}$ is a monomer, my observation that $MinE^{1-22}$ was able to stimulate MinD ATPase activity to the same extent as WT MinE suggests that dimerization of the N-terminal of MinE is not necessary for stimulation of MinD ATPase activity. How this data can be reconciled with the data presented by Zhang *et al.* with inactive MinE heterodimers is difficult to envisage, as the two results seem to directly conflict. However, the elimination of one N-terminal helix in a MinE dimer would be expected to expose a hydrophobic patch on the b-sheet where this helix normally docks, giving rise to aggregation or lipid-binding behavior that inactivates this heterodimer. In this case then the heterodimer could not be expected to behave like a monomeric anti-MinCD domain. Since this type of complication is not a concern for my studies with the peptide, the most attractive conclusion is that MinE dimerization does not seem to be important for stimulation of MinD activity.

vi) Summary of Implications for Theories Describing the MinE-MinD Interaction

To summarize, the data presented in this thesis has important implications for theories describing the MinE-MinD interaction. It suggests that all of the currently extant theories describing MinE-MinD interaction require significant modification. The Soj/SpoOj hypothesis, arginine finger hypothesis and MinD competition hypothesis contrast sharply with the data presented in this thesis, and only the coiled-coil

hypothesis can realistically be reconciled with this data. Finally, the data presented in this thesis also appears to resolve the longstanding question of whether dimerization of the MinE N-terminal is necessary to stimulate MinD ATPase activity: dimerization is not necessary.

Claims to Original Research

1. Delineated region of MinE that is important for stimulation of MinD ATPase activity.

2. Provided evidence that $MinE^{1-22}$ is a functionally autonomous domain of MinE.

3. Showed that dimerization does not appear to be a prerequisite for MinE stimulation of MinD ATPase activity.

4. Demonstrated that the structure of MinE L22D resembles the structure of MinE TSD.

5. Provided evidence that MinD ATPase activity may be modulated by a change in phosphoplipid composition.

References

1. Lutkenhaus, J. (2007) *Annu. Rev. Biochem. 76*, 539-562.
2. Adler, H. I., Fisher, W. D., Cohen, A., and Hardigree, A. A. (1967) *Proc. Natl. Acad. Sci. U. S. A 57*, 321-326.
3. Bi, E. F. and Lutkenhaus, J. (1991) *Nature 354*, 161-164.
4. Lutkenhaus, J. and Addinall, S. G. (1997) *Annu. Rev. Biochem. 66*, 93-116.
5. Weiss, D. S. (2004) *Mol. Microbiol. 54*, 588-597.
6. Woldringh, C. L., Mulder, E., Huls, P. G., and Vischer, N. (1991) *Res. Microbiol. 142*, 309-320.
7. Sun, Q., Yu, X. C., and Margolin, W. (1998) *Mol. Microbiol. 29*, 491-503.
8. Wu, L. J. and Errington, J. (2004) *Cell 117*, 915-925.
9. Bernhardt, T. G. and de Boer, P. A. (2005) *Mol. Cell 18*, 555-564.
10. Wu, L. J., Ishikawa, S., Kawai, Y., Oshima, T., Ogasawara, N., and Errington, J. (2009) *EMBO J. 28*, 1940-1952.
11. de Boer, P. A., Crossley, R. E., and Rothfield, L. I. (1988) *J. Bacteriol. 170*, 2106-2112.
12. de Boer, P. A., Crossley, R. E., and Rothfield, L. I. (1989) *Cell 56*, 641-649.
13. de Boer, P. A., Crossley, R. E., and Rothfield, L. I. (1992) *J. Bacteriol. 174*, 63-70.
14. de Boer, P. A., Crossley, R. E., and Rothfield, L. I. (1989) *Cell 56*, 641-649.
15. Sun, Q., Yu, X. C., and Margolin, W. (1998) *Mol. Microbiol. 29*, 491-503.
16. de Boer, P. A., Crossley, R. E., and Rothfield, L. I. (1989) *Cell 56*, 641-649.
17. Pichoff, S. and Lutkenhaus, J. (2001) *J. Bacteriol. 183*, 6630-6635.
18. Bi, E. F. and Lutkenhaus, J. (1991) *Nature 354*, 161-164.
19. de Boer, P. A., Crossley, R. E., and Rothfield, L. I. (1989) *Cell 56*, 641-649.

20. Raskin, D. M. and de Boer, P. A. (1999) *Proc. Natl. Acad. Sci. U. S. A 96*, 4971-4976.

21. Rowland, S. L., Fu, X., Sayed, M. A., Zhang, Y., Cook, W. R., and Rothfield, L. I. (2000) *J. Bacteriol. 182*, 613-619.

22. Hu, Z. and Lutkenhaus, J. (1999) *Mol. Microbiol. 34*, 82-90.

23. Raskin, D. M. and de Boer, P. A. (1999) *J. Bacteriol. 181*, 6419-6424.

24. Raskin, D. M. and de Boer, P. A. (1999) *Proc. Natl. Acad. Sci. U. S. A 96*, 4971-4976.

25. Raskin, D. M. and de Boer, P. A. (1999) *Proc. Natl. Acad. Sci. U. S. A 96*, 4971-4976.

26. Raskin, D. M. and de Boer, P. A. (1999) *Proc. Natl. Acad. Sci. U. S. A 96*, 4971-4976.

27. Corbin, B. D., Yu, X. C., and Margolin, W. (2002) *EMBO J. 21*, 1998-2008.

28. Eng, N. F., Szeto, J., Acharya, S., Tessier, D., and Dillon, J. A. (2006) *Res. Microbiol. 157*, 333-344.

29. Ramirez-Arcos, S., Szeto, J., Dillon, J. A., and Margolin, W. (2002) *Mol. Microbiol. 46*, 493-504.

30. Szeto, J., Acharya, S., Eng, N. F., and Dillon, J. A. (2004) *J. Bacteriol. 186*, 7175-7185.

31. Papadopoulos, J. S. and Agarwala, R. (2007) *Bioinformatics. 23*, 1073-1079.

32. Waterhouse, A. M., Procter, J. B., Martin, D. M., Clamp, M., and Barton, G. J. (2009) *Bioinformatics. 25*, 1189-1191.

33. Hu, Z., Gogol, E. P., and Lutkenhaus, J. (2002) *Proc. Natl. Acad. Sci. U. S. A 99*, 6761-6766.

34. Hu, Z. and Lutkenhaus, J. (2003) *Mol. Microbiol. 47*, 345-355.

35. Szeto, T. H., Rowland, S. L., Habrukowich, C. L., and King, G. F. (2003) *J. Biol. Chem. 278*, 40050-40056.

36. Hu, Z. and Lutkenhaus, J. (2001) *Mol. Cell 7*, 1337-1343.

37. Lackner, L. L., Raskin, D. M., and de Boer, P. A. (2003) *J. Bacteriol. 185*, 735-749.

38. Hu, Z., Saez, C., and Lutkenhaus, J. (2003) *J. Bacteriol. 185*, 196-203.

39. Ma, L., King, G. F., and Rothfield, L. (2004) *Mol. Microbiol. 54*, 99-108.

40. Ma, L., King, G. F., and Rothfield, L. (2004) *Mol. Microbiol. 54*, 99-108.

41. Ramirez-Arcos, S., Szeto, J., Dillon, J. A., and Margolin, W. (2002) *Mol. Microbiol. 46*, 493-504.

42. Shih, Y. L., Le, T., and Rothfield, L. (2003) *Proc. Natl. Acad. Sci. U. S. A 100*, 7865-7870.

43. Hale, C. A., Meinhardt, H., and de Boer, P. A. (2001) *EMBO J. 20*, 1563-1572.

44. Fu, X., Shih, Y. L., Zhang, Y., and Rothfield, L. I. (2001) *Proc. Natl. Acad. Sci. U. S. A 98*, 980-985.

45. Margolin, W. (2001) *Curr. Biol. 11*, R395-R398.

46. Shih, Y. L., Le, T., and Rothfield, L. (2003) *Proc. Natl. Acad. Sci. U. S. A 100*, 7865-7870.

47. Shih, Y. L., Fu, X., King, G. F., Le, T., and Rothfield, L. (2002) *EMBO J. 21*, 3347-3357.

48. Zhao, C. R., de Boer, P. A., and Rothfield, L. I. (1995) *Proc. Natl. Acad. Sci. U. S. A 92*, 4313-4317.

49. Pichoff, S., Vollrath, B., Touriol, C., and Bouche, J. P. (1995) *Mol. Microbiol. 18*, 321-329.

50. Zhao, C. R., de Boer, P. A., and Rothfield, L. I. (1995) *Proc. Natl. Acad. Sci. U. S. A 92*, 4313-4317.

51. Pichoff, S., Vollrath, B., Touriol, C., and Bouche, J. P. (1995) *Mol. Microbiol. 18*, 321-329.

52. Zhao, C. R., de Boer, P. A., and Rothfield, L. I. (1995) *Proc. Natl. Acad. Sci. U. S. A 92*, 4313-4317.

53. Pichoff, S., Vollrath, B., Touriol, C., and Bouche, J. P. (1995) *Mol. Microbiol. 18*, 321-329.

54. Hu, Z. and Lutkenhaus, J. (2001) *Mol. Cell 7*, 1337-1343.

55. Ma, L. Y., King, G., and Rothfield, L. (2003) *J. Bacteriol. 185*, 4948-4955.

56. Eng, N. F., Szeto, J., Acharya, S., Tessier, D., and Dillon, J. A. (2006) *Res. Microbiol. 157*, 333-344.

57. King, G. F., Shih, Y. L., Maciejewski, M. W., Bains, N. P., Pan, B., Rowland, S. L., Mullen, G. P., and Rothfield, L. I. (2000) *Nat. Struct. Biol. 7*, 1013-1017.

58. King, G. F., Rowland, S. L., Pan, B., Mackay, J. P., Mullen, G. P., and Rothfield, L. I. (1999) *Mol. Microbiol. 31*, 1161-1169.

59. Ramos, D., Ducat, T., Cheng, J., Eng, N. F., Dillon, J. A., and Goto, N. K. (2006) *Biochemistry 45*, 4593-4601.

60. King, G. F., Shih, Y. L., Maciejewski, M. W., Bains, N. P., Pan, B., Rowland, S. L., Mullen, G. P., and Rothfield, L. I. (2000) *Nat. Struct. Biol. 7*, 1013-1017.

61. Hu, Z. and Lutkenhaus, J. (2001) *Mol. Cell 7*, 1337-1343.

62. Ma, L. Y., King, G., and Rothfield, L. (2003) *J. Bacteriol. 185*, 4948-4955.

63. Eng, N. F., Szeto, J., Acharya, S., Tessier, D., and Dillon, J. A. (2006) *Res. Microbiol. 157*, 333-344.

64. Soyenkoff, B. (1947) *J. Biol. Chem. 168*, 447-457.

65. Pettersson, L., Anderson, I., and Ohman, L.-O. (1985) *Acta. Chem. Scand. 39*, 53-58.

66. Voet, D. and Voet, J. G. (2004) *Biochemistry* John Wiley & Sons, Inc..

67. Ramos, D., Ducat, T., Cheng, J., Eng, N. F., Dillon, J. A., and Goto, N. K. (2006) *Biochemistry 45*, 4593-4601.

68. Ford, K. G., Whitmarsh, A. J., and Hornby, D. P. (1994) *Methods Mol. Biol. 30*, 185-197.

69. Bertani, G. (1951) *J. Bacteriol. 62*, 293-300.

70. Ausubel, F. M., Brent, R., Kingston, R. E., Moore, D. D., Seidman, J. G., Smith, J. A., and Struhl, K. (2001) *Current Protocols in Molecular Biology* John Wiley & Sons, Inc..

71. Sambrook, J., Fritsch, E. F., and Maniatis, T. (1989) *Molecular Cloning: A Laboratory Manual* Cold Spring Harbor Laboratory, Cold Spring Harbor, N.Y.

72. Ducat, T., Declerck, N., Gostan, T., Kochoyan, M., and Demene, H. (2006) *J. Biomol. NMR 34*, 137-151.

73. Harder, K. W., Owen, P., Wong, L. K., Aebersold, R., Clark-Lewis, I., and Jirik, F. R. (1994) *Biochem. J. 298 (Pt 2)*, 395-401.

74. Wiechelman, K. J., Braun, R. D., and Fitzpatrick, J. D. (1988) *Anal. Biochem. 175*, 231-237.

75. Smith, P. K., Krohn, R. I., Hermanson, G. T., Mallia, A. K., Gartner, F. H., Provenzano, M. D., Fujimoto, E. K., Goeke, N. M., Olson, B. J., and Klenk, D. C. (1985) *Anal. Biochem. 150*, 76-85.

76. Bradford, M. M. (1976) *Anal. Biochem. 72*, 248-254.

77. Sambrook, J., Fritsch, E. F., and Maniatis, T. (1989) *Molecular Cloning: A Laboratory Manual,* Cold Spring Harbor Laboratory, Cold Spring Harbor, N.Y.

78. Delaglio, F., Grzesiek, S., Vuister, G. W., Zhu, G., Pfeifer, J., and Bax, A. (1995) *J. Biomol. NMR 6*, 277-293.

79. Johnson, B. and Blevins, R. (1994) *J Biomol NMR 4*, 603-614.

80. Ramos, D. Conformation Studies of Cell Division Regulator MinE by Nuclear Magnetic Resonance and Circular Dichroism Spetroscopy. 2006. Ottawa Carleton Chemistry Institute.

Ref Type: Thesis/Dissertation

81. Carter, C. W., Jr. and Carter, C. W. (1979) *J Biol. Chem. 254*, 12219-12223.

82. Ma, L. Y., King, G., and Rothfield, L. (2003) *J. Bacteriol. 185*, 4948-4955.

83. Eng, N. F., Szeto, J., Acharya, S., Tessier, D., and Dillon, J. A. (2006) *Res. Microbiol. 157*, 333-344.

84. Ramos, D., Ducat, T., Cheng, J., Eng, N. F., Dillon, J. A., and Goto, N. K. (2006) *Biochemistry 45*, 4593-4601.

85. Hu, Z. and Lutkenhaus, J. (2003) *Mol. Microbiol. 47*, 345-355.

86. Hu, Z. and Lutkenhaus, J. (2001) *Mol. Cell 7*, 1337-1343.

87. Eng, N. F., Szeto, J., Acharya, S., Tessier, D., and Dillon, J. A. (2006) *Res. Microbiol. 157*, 333-344.

88. Szeto, J., Eng, N. F., Acharya, S., Rigden, M. D., and Dillon, J. A. (2005) *Res. Microbiol. 156*, 17-29.

89. Szeto, J., Acharya, S., Eng, N. F., and Dillon, J. A. (2004) *J. Bacteriol. 186*, 7175-7185.

90. Lackner, L. L., Raskin, D. M., and de Boer, P. A. (2003) *J. Bacteriol. 185*, 735-749.

91. Zhou, H., Schulze, R., Cox, S., Saez, C., Hu, Z., and Lutkenhaus, J. (2005) *J. Bacteriol. 187*, 629-638.

92. Loose, M., Fischer-Friedrich, E., Ries, J., Kruse, K., and Schwille, P. (2008) *Science 320*, 789-792.

93. Chernomordik, L. V. and Kozlov, M. M. (2003) *Annu. Rev. Biochem. 72*, 175-207.

94. Avanti Polar Lipids. Preparation of Liposomes. 2009.
Ref Type: Generic

95. Eng, N. F., Szeto, J., Acharya, S., Tessier, D., and Dillon, J. A. (2006) *Res. Microbiol. 157*, 333-344.

96. Szeto, J., Acharya, S., Eng, N. F., and Dillon, J. A. (2004) *J. Bacteriol. 186*, 7175-7185.

97. Hu, Z. and Lutkenhaus, J. (2001) *Mol. Cell 7*, 1337-1343.

98. Lackner, L. L., Raskin, D. M., and de Boer, P. A. (2003) *J. Bacteriol. 185*, 735-749.

99. Ma, L. Y., King, G., and Rothfield, L. (2003) *J. Bacteriol. 185*, 4948-4955.

100. Eng, N. F., Szeto, J., Acharya, S., Tessier, D., and Dillon, J. A. (2006) *Res. Microbiol. 157*, 333-344.

101. Hu, Z. and Lutkenhaus, J. (2001) *Mol. Cell 7*, 1337-1343.

102. Hu, Z. and Lutkenhaus, J. (2001) *Mol. Cell 7*, 1337-1343.

103. King, G. F., Shih, Y. L., Maciejewski, M. W., Bains, N. P., Pan, B., Rowland, S. L., Mullen, G. P., and Rothfield, L. I. (2000) *Nat. Struct. Biol. 7*, 1013-1017.

104. Shih, Y. L., Fu, X., King, G. F., Le, T., and Rothfield, L. (2002) *EMBO J. 21*, 3347-3357.

105. Eng, N. F., Szeto, J., Acharya, S., Tessier, D., and Dillon, J. A. (2006) *Res. Microbiol. 157*, 333-344.

106. Zhao, C. R., de Boer, P. A., and Rothfield, L. I. (1995) *Proc. Natl. Acad. Sci. U. S. A 92*, 4313-4317.

107. de Boer, P. A., Crossley, R. E., and Rothfield, L. I. (1989) *Cell 56*, 641-649.

108. Ramirez-Arcos, S., Szeto, J., Dillon, J. A., and Margolin, W. (2002) *Mol. Microbiol. 46*, 493-504.

109. Zhao, C. R., de Boer, P. A., and Rothfield, L. I. (1995) *Proc. Natl. Acad. Sci. U. S. A 92*, 4313-4317.

110. de Boer, P. A., Crossley, R. E., and Rothfield, L. I. (1989) *Cell 56*, 641-649.

111. Ramirez-Arcos, S., Szeto, J., Dillon, J. A., and Margolin, W. (2002) *Mol. Microbiol. 46*, 493-504.

112. Ramos, D., Ducat, T., Cheng, J., Eng, N. F., Dillon, J. A., and Goto, N. K. (2006) *Biochemistry 45*, 4593-4601.

113. Ramos, D., Ducat, T., Cheng, J., Eng, N. F., Dillon, J. A., and Goto, N. K. (2006) *Biochemistry 45*, 4593-4601.

114. Ramos, D., Ducat, T., Cheng, J., Eng, N. F., Dillon, J. A., and Goto, N. K. (2006) *Biochemistry 45*, 4593-4601.

115. Hu, Z. and Lutkenhaus, J. (2001) *Mol. Cell 7*, 1337-1343.

116. Lackner, L. L., Raskin, D. M., and de Boer, P. A. (2003) *J. Bacteriol. 185*, 735-749.

117. Mileykovskaya, E., Fishov, I., Fu, X., Corbin, B. D., Margolin, W., and Dowhan, W. (2003) *J Biol. Chem. 278*, 22193-22198.

118. Shih, Y. L., Le, T., and Rothfield, L. (2003) *Proc. Natl. Acad. Sci. U. S. A 100*, 7865-7870.

119. Hu, Z., Gogol, E. P., and Lutkenhaus, J. (2002) *Proc. Natl. Acad. Sci. U. S. A 99*, 6761-6766.

120. Suefuji, K., Valluzzi, R., and RayChaudhuri, D. (2002) *Proc. Natl. Acad. Sci. U. S. A 99*, 16776-16781.

121. Suefuji, K., Valluzzi, R., and RayChaudhuri, D. (2002) *Proc. Natl. Acad. Sci. U. S. A 99*, 16776-16781.

122. Hu, Z., Gogol, E. P., and Lutkenhaus, J. (2002) *Proc. Natl. Acad. Sci. U. S. A 99*, 6761-6766.

123. Zhang, Y., Rowland, S., King, G., Braswell, E., and Rothfield, L. (1998) *Mol. Microbiol. 30*, 265-273.

124. Zhao, C. R., de Boer, P. A., and Rothfield, L. I. (1995) *Proc. Natl. Acad. Sci. U. S. A 92*, 4313-4317.

125. Pichoff, S., Vollrath, B., Touriol, C., and Bouche, J. P. (1995) *Mol. Microbiol. 18*, 321-329.

126. Ma, L. Y., King, G., and Rothfield, L. (2003) *J. Bacteriol. 185*, 4948-4955.

127. Ma, L. Y., King, G., and Rothfield, L. (2003) *J. Bacteriol. 185*, 4948-4955.

128. Ma, L. Y., King, G., and Rothfield, L. (2003) *J. Bacteriol. 185*, 4948-4955.

129. King, G. F., Rowland, S. L., Pan, B., Mackay, J. P., Mullen, G. P., and Rothfield, L. I. (1999) *Mol. Microbiol. 31*, 1161-1169.

130. Ramos, D., Ducat, T., Cheng, J., Eng, N. F., Dillon, J. A., and Goto, N. K. (2006) *Biochemistry 45*, 4593-4601.

131. Ramos, D., Ducat, T., Cheng, J., Eng, N. F., Dillon, J. A., and Goto, N. K. (2006) *Biochemistry 45*, 4593-4601.

132. King, G. F., Shih, Y. L., Maciejewski, M. W., Bains, N. P., Pan, B., Rowland, S. L., Mullen, G. P., and Rothfield, L. I. (2000) *Nat. Struct. Biol. 7*, 1013-1017.

133. Eng, N. F., Szeto, J., Acharya, S., Tessier, D., and Dillon, J. A. (2006) *Res. Microbiol. 157*, 333-344.

134. Shih, Y. L., Fu, X., King, G. F., Le, T., and Rothfield, L. (2002) *EMBO J. 21*, 3347-3357.

135. Ramirez-Arcos, S., Szeto, J., Dillon, J. A., and Margolin, W. (2002) *Mol. Microbiol. 46*, 493-504.

136. Lutkenhaus, J. and Sundaramoorthy, M. (2003) *Mol. Microbiol. 48*, 295-303.

137. Ramakrishnan, C., Dani, V. S., and Ramasarma, T. (2002) *Protein Eng 15*, 783-798.

138. Leonard, T. A., Butler, P. J., and Lowe, J. (2005) *EMBO J 24*, 270-282.

139. Ramakrishnan, C., Dani, V. S., and Ramasarma, T. (2002) *Protein Eng 15*, 783-798.

140. Lutkenhaus, J. and Sundaramoorthy, M. (2003) *Mol. Microbiol. 48*, 295-303.

141. Leonard, T. A., Butler, P. J., and Lowe, J. (2005) *EMBO J 24*, 270-282.

142. Lutkenhaus, J. and Sundaramoorthy, M. (2003) *Mol. Microbiol. 48*, 295-303.

143. Ma, L., King, G. F., and Rothfield, L. (2004) *Mol. Microbiol. 54*, 99-108.

144. King, G. F., Rowland, S. L., Pan, B., Mackay, J. P., Mullen, G. P., and Rothfield, L. I. (1999) *Mol. Microbiol. 31*, 1161-1169.

145. King, G. F., Shih, Y. L., Maciejewski, M. W., Bains, N. P., Pan, B., Rowland, S. L., Mullen, G. P., and Rothfield, L. I. (2000) *Nat. Struct. Biol. 7*, 1013-1017.

146. Ma, L. Y., King, G., and Rothfield, L. (2003) *J. Bacteriol. 185*, 4948-4955.

147. King, G. F., Rowland, S. L., Pan, B., Mackay, J. P., Mullen, G. P., and Rothfield, L. I. (1999) *Mol. Microbiol. 31*, 1161-1169.

148. Pichoff, S., Vollrath, B., Touriol, C., and Bouche, J. P. (1995) *Mol. Microbiol. 18*, 321-329.

149. Zhang, Y., Rowland, S., King, G., Braswell, E., and Rothfield, L. (1998) *Mol. Microbiol. 30*, 265-273.

Appendix

A.1 Temperature Cycling Program Used in Eppendorf Mastercycler Personal

CNTRL TUBE
LID = 105°C
NOWAIT = AUTO

1 T= 95°C	2min
2 T= 95°C	1min
3 T= 60-67°C (see Table 2.1)	1min
4 T= 68°C	12min
5 GOTO 2	
6 T= 68°C	10min
7 Hold at 4°C	Enter

A.2 Buffer Conditions Used for Solubility Study of WT $MinE_{Ng}$

Solution #	pH	Salt	Additive
1	6	50mM Na_2SO_4	1M Sucrose
2	7	250mM Na_2SO_4	0.25M Sucrose
3	7.5	500mM Na_2SO_4	1M Sucrose
4	4.5	500mM Na_2SO_4	1% Glycerol
5	4.5	-----	0.5M Sucrose
6	4.5	500mM KSCN	50mM CHAPS
7	6	-----	10% Glycerol
8	6	500mM Na_2SO_4	1mM CHAPS
9	5.5	500mM NaCl	0.25M Sucrose
10	7.5	250mM KSCN	10mM CHAPS
11	6.5	250mM KSCN	50mM CHAPS
12	8.5	-----	0.25M Sucrose
13	8	50mM Na_2SO_4	0.25M Sucrose
14	8.5	50mM Na_2SO_4	1mM CHAPS
15	5.5	-----	1M Sucrose
16	4.5	250mM KSCN	1mM CHAPS
17	4.5	250mM NaCl	1M Sucrose
18	7.5	250mM Na_2SO_4	0.25M Sucrose
19	8.5	500mM NaCl	10mM CHAPS
20	5	250mM Na_2SO_4	1% Glycerol
21	8	-----	5% Glycerol
22	6.5	-----	1mM CHAPS
23	7	250mM KSCN	1mM CHAPS
24	8	50mM KSCN	10mM CHAPS
25	5.5	50mM KSCN	0.5M Sucrose
26	8	-----	1% Glycerol
27	8.5	500mM KSCN	5% Glycerol
28	6	-----	50mM CHAPS
29	6.5	50 mM NaCl	1% Glycerol
30	6.5	500mM Na_2SO_4	10% Glycerol
31	8	50mM NaCl	10% Glycerol
32	7	-----	1% Glycerol
33	5.5	-----	50mM CHAPS
34	7	500mM Na_2SO_4	5% Glycerol
35	6	50mM KSCN	0.25M Sucrose
36	5	50mM KSCN	50mM CHAPS
37	6.5	50mM NaCl	10mM CHAPS

38	8	250mM Na_2SO_4	50mM CHAPS
39	7.5	50mM Na_2SO_4	50mM CHAPS
40	7.5	-----	10% Glycerol
41	6.5	250mM KSCN	0.25M Sucrose
42	5	500mM KSCN	0.25M Sucrose
43	5	50mM Na_2SO_4	0.5M Sucrose
44	8.5	50mM KSCN	1% Glycerol
45	5.5	-----	10mM CHAPS
46	4.5	50mM KSCN	5% Glycerol
47	5	500mM NaCl	10% Glycerol
48	4.5	-----	10mM CHAPS
49	5.5	250mM Na_2SO_4	5% Glycerol
50	6	250mM NaCl	5% Glycerol
51	5	50mM NaCl	1mM CHAPS
52	8.5	250mM NaCl	50mM CHAPS
53	7	250mM NaCl	1M Sucrose
54	8	250mM NaCl	0.5M Sucrose
55	6.5	-----	1M Sucrose
56	8.5	50mM Na_2SO_4	1M Sucrose
57	8.5	-----	0.5M Sucrose
58	6	500mM Na_2SO_4	10mM CHAPS
59	7.5	50mM NaCl	5% Glycerol
60	7.5	250mM NaCl	0.5M Sucrose
61	5.5	50mM NaCl	1mM CHAPS
62	7	-----	0.5M Sucrose
63	7.5	-----	1mM CHAPS
64	6.5	500mM Na_2SO_4	0.5M Sucrose
65	6	500mM NaCl	0.5M Sucrose
66	7	50mM KSCN	10mM CHAPS
67	8.5	250mM Na_2SO_4	10% Glycerol
68	5.5	250mM KSCN	10% Glycerol
69	6	250mM KSCN	1% Glycerol
70	5	250mM Na_2SO_4	10mM CHAPS
71	6.5	500mM NaCl	5% Glycerol
72	4.5	-----	0.25M Sucrose
73	7	500mM NaCl	10% Glycerol
74	5	-----	5% Glycerol
75	8	500mM KSCN	1M Sucrose
76	4.5	50mM Na_2SO_4	10% Glycerol
77	7.5	500mM KSCN	1% Glycerol
78	5.5	500mM NaCl	1% Glycerol
79	5	-----	1M Sucrose
80	8	500mM KSCN	1mM CHAPS
81	7	50mM NaCl	50mM CHAPS

For solution conditions with pH = 4.5, 5, and 5.5, 100mM sodium acetate was used as buffer. For solution conditions with pH = 6, 6.5, and 7, 100mM sodium phosphate was used as buffer. For solution conditions with pH = 7.5, 8, and 8.5, 100mM Tris-HCl was used as buffer.

A.3 Raw Data from ATPase Assay

The raw data obtained from ATPase assays for WT MinE (dark blue line), MinE E67L (red line), MinE E46A (orange line), MinE L22D (light yellow line), MinE R21A (dark red line), MinE D20A (black line), MinE R19A (sky blue line), MinE A18D (tan line), MinE V17A (turquoise line), MinE T16A (plum line), MinE A15D (yellow line), MinE T14A (bright green line), MinE K13A (light green line), Q12A (lime line), K11A (light orange line), R10A (gold line), F8A (lavender line), L6A (dark yellow line), E5A(dark grey line), I4A (violet line), L3A (indigo line), and $MinE^{1-22}$ (bright green line) are presented below. As well, the raw data for ATPase assays with reactions without MinE (pink line), and without ATP, phospholipids, or magnesium (all black lines) are presented.

i) ATPase Assay Examining $MinE_{Ng}$ Mutants (2.7uM MinD; 2.7uM MinE)

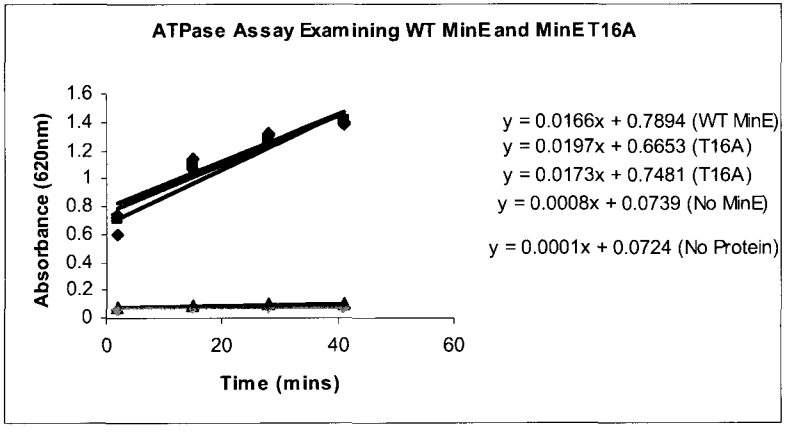

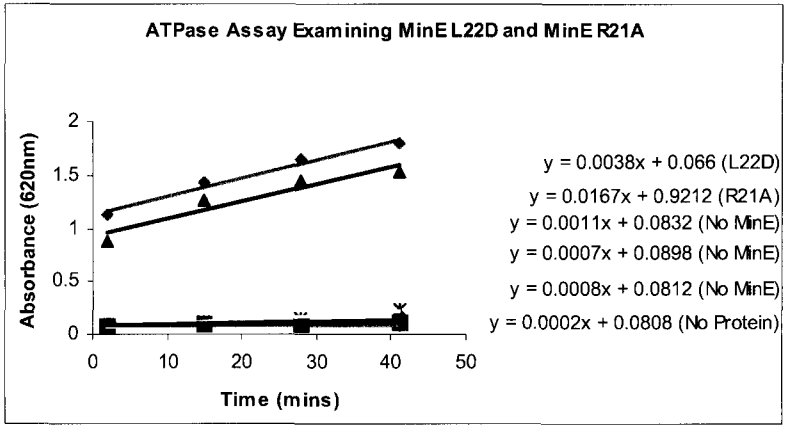

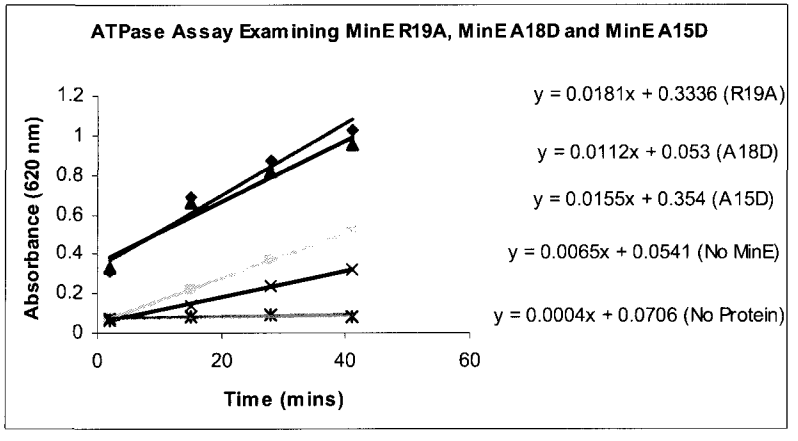
ATPase Assay Examining MinE R19A, MinE A18D and MinE A15D
Absorbance (620 nm)
Time (mins)
y = 0.0181x + 0.3336 (R19A)
y = 0.0112x + 0.053 (A18D)
y = 0.0155x + 0.354 (A15D)
y = 0.0065x + 0.0541 (No MinE)
y = 0.0004x + 0.0706 (No Protein)

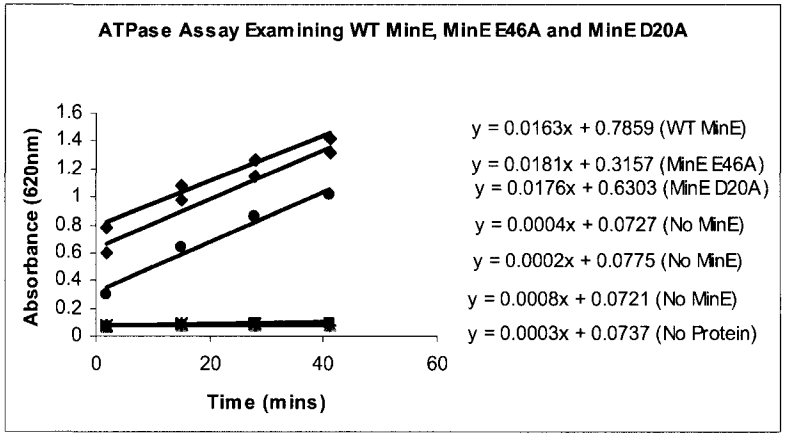
ATPase Assay Examining WT MinE, MinE E46A and MinE D20A
Absorbance (620nm)
Time (mins)
y = 0.0163x + 0.7859 (WT MinE)
y = 0.0181x + 0.3157 (MinE E46A)
y = 0.0176x + 0.6303 (MinE D20A)
y = 0.0004x + 0.0727 (No MinE)
y = 0.0002x + 0.0775 (No MinE)
y = 0.0008x + 0.0721 (No MinE)
y = 0.0003x + 0.0737 (No Protein)

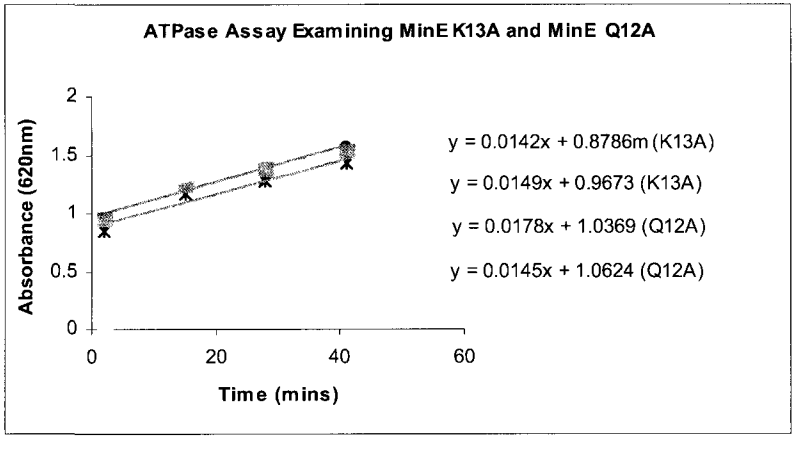
ATPase Assay Examining MinE K13A and MinE Q12A
Absorbance (620nm)
Time (mins)
y = 0.0142x + 0.8786m (K13A)
y = 0.0149x + 0.9673 (K13A)
y = 0.0178x + 1.0369 (Q12A)
y = 0.0145x + 1.0624 (Q12A)

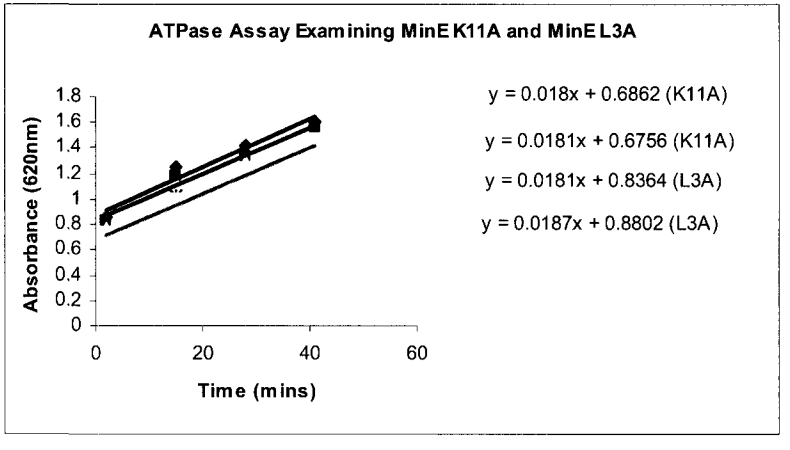
ATPase Assay Examining MinE K11A and MinE L3A
Absorbance (620nm)
Time (mins)
y = 0.018x + 0.6862 (K11A)
y = 0.0181x + 0.6756 (K11A)
y = 0.0181x + 0.8364 (L3A)
y = 0.0187x + 0.8802 (L3A)

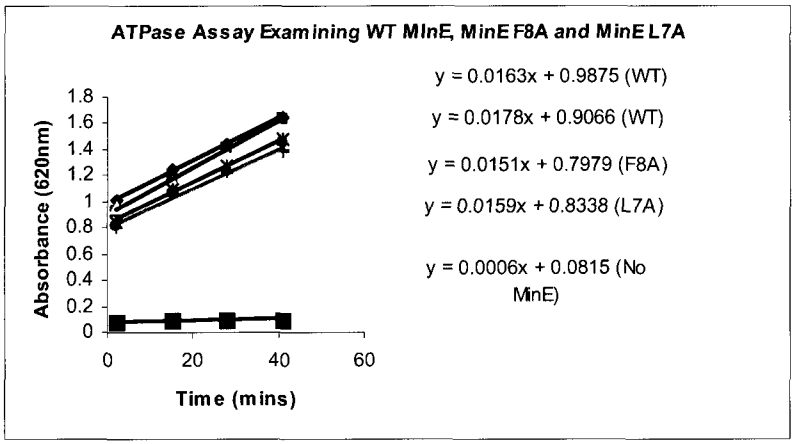

ii) ATPase Assay Examining $MinE_{Ng}$ Mutants (2.7uM MinD; 0.06uM MinE)

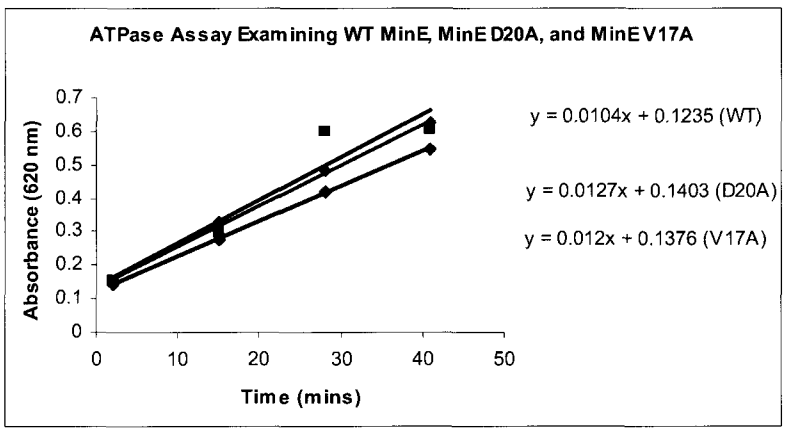

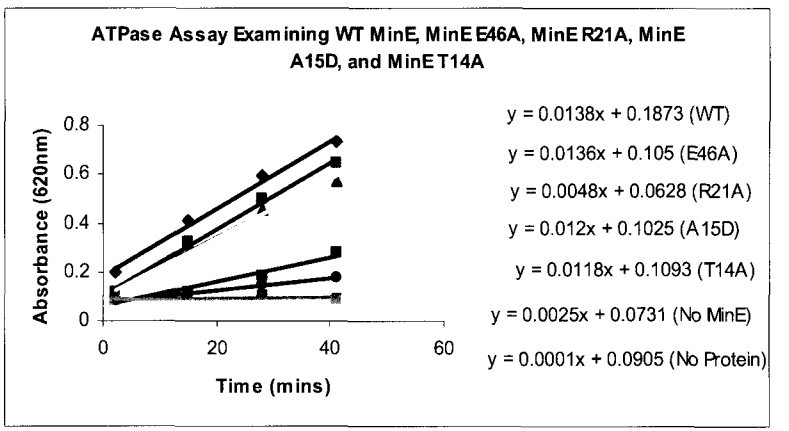

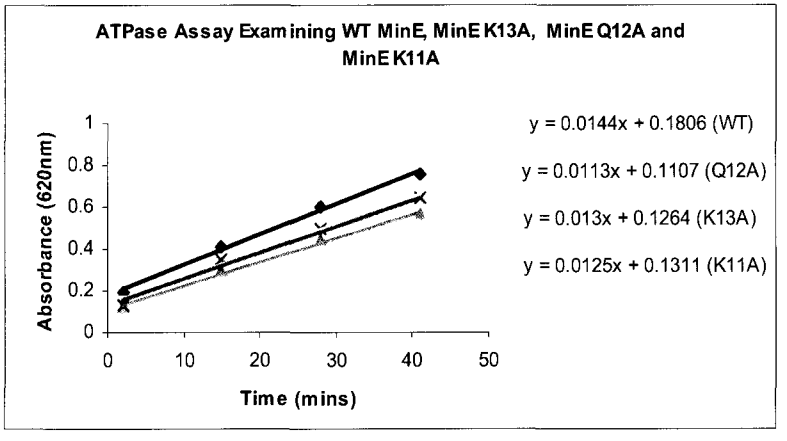
ATPase Assay Examining WT MinE, MinE K13A, MinE Q12A and MinE K11A
Absorbance (620nm)
Time (mins)
y = 0.0144x + 0.1806 (WT)
y = 0.0113x + 0.1107 (Q12A)
y = 0.013x + 0.1264 (K13A)
y = 0.0125x + 0.1311 (K11A)

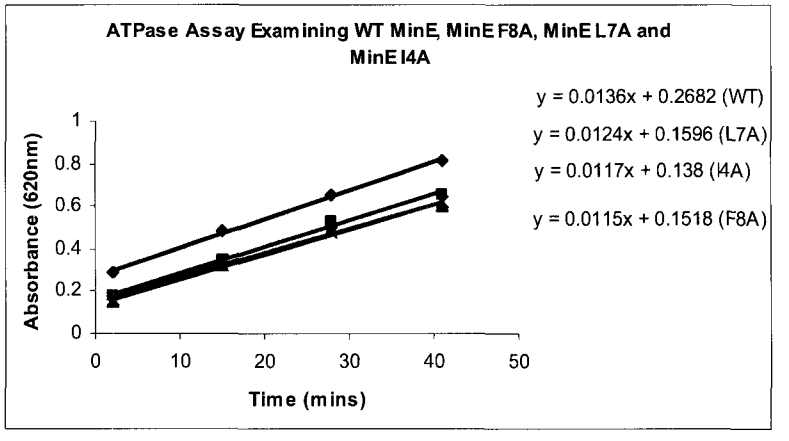
ATPase Assay Examining WT MinE, MinE F8A, MinE L7A and MinE I4A
Absorbance (620nm)
Time (mins)
y = 0.0136x + 0.2682 (WT)
y = 0.0124x + 0.1596 (L7A)
y = 0.0117x + 0.138 (I4A)
y = 0.0115x + 0.1518 (F8A)

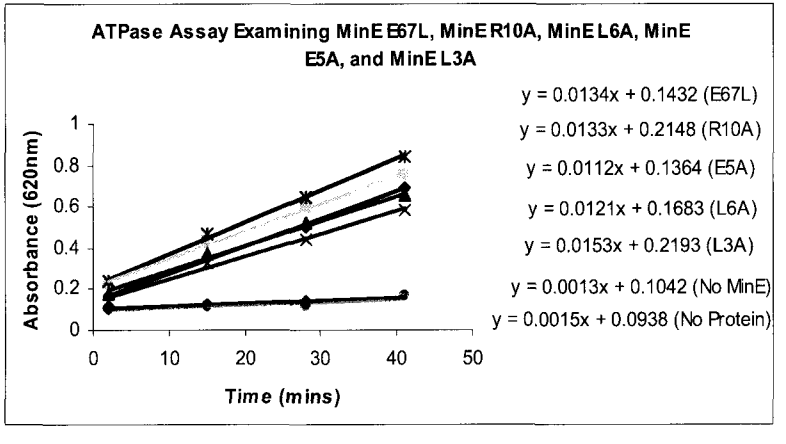
ATPase Assay Examining MinE E67L, MinE R10A, MinE L6A, MinE E5A, and MinE L3A
Absorbance (620nm)
Time (mins)
y = 0.0134x + 0.1432 (E67L)
y = 0.0133x + 0.2148 (R10A)
y = 0.0112x + 0.1364 (E5A)
y = 0.0121x + 0.1683 (L6A)
y = 0.0153x + 0.2193 (L3A)
y = 0.0013x + 0.1042 (No MinE)
y = 0.0015x + 0.0938 (No Protein)

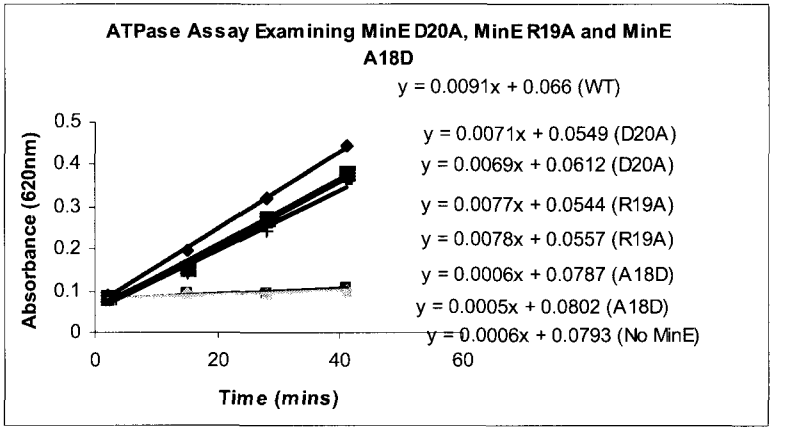
ATPase Assay Examining MinE D20A, MinE R19A and MinE A18D
Absorbance (620nm)
Time (mins)
y = 0.0091x + 0.066 (WT)
y = 0.0071x + 0.0549 (D20A)
y = 0.0069x + 0.0612 (D20A)
y = 0.0077x + 0.0544 (R19A)
y = 0.0078x + 0.0557 (R19A)
y = 0.0006x + 0.0787 (A18D)
y = 0.0005x + 0.0802 (A18D)
y = 0.0006x + 0.0793 (No MinE)

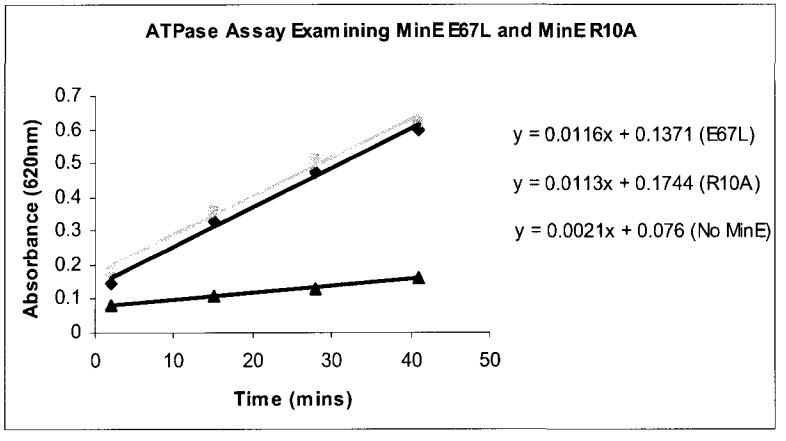
ATPase Assay Examining MinE E67L and MinE R10A
Absorbance (620nm)
Time (mins)
y = 0.0116x + 0.1371 (E67L)
y = 0.0113x + 0.1744 (R10A)
y = 0.0021x + 0.076 (No MinE)

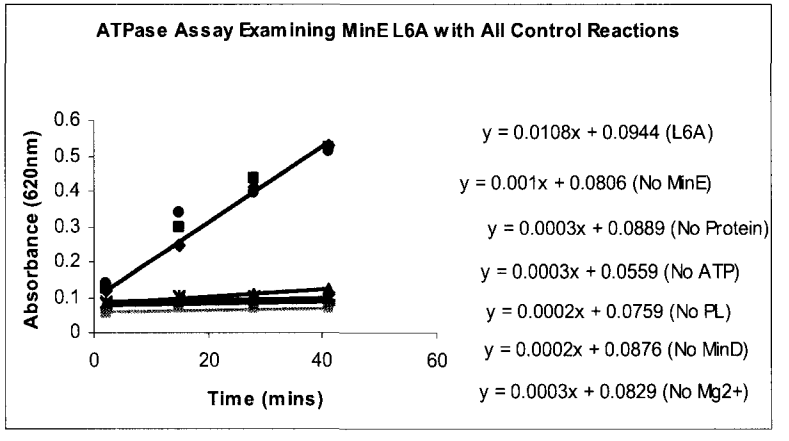
ATPase Assay Examining MinE L6A with All Control Reactions
Absorbance (620nm)
Time (mins)
y = 0.0108x + 0.0944 (L6A)
y = 0.001x + 0.0806 (No MinE)
y = 0.0003x + 0.0889 (No Protein)
y = 0.0003x + 0.0559 (No ATP)
y = 0.0002x + 0.0759 (No PL)
y = 0.0002x + 0.0876 (No MinD)
y = 0.0003x + 0.0829 (No Mg2+)

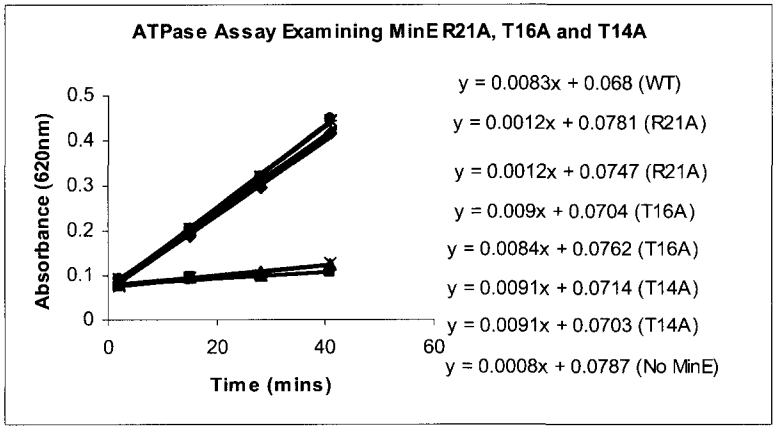
ATPase Assay Examining MinE R21A, T16A and T14A
Absorbance (620nm)
Time (mins)
y = 0.0083x + 0.068 (WT)
y = 0.0012x + 0.0781 (R21A)
y = 0.0012x + 0.0747 (R21A)
y = 0.009x + 0.0704 (T16A)
y = 0.0084x + 0.0762 (T16A)
y = 0.0091x + 0.0714 (T14A)
y = 0.0091x + 0.0703 (T14A)
y = 0.0008x + 0.0787 (No MinE)

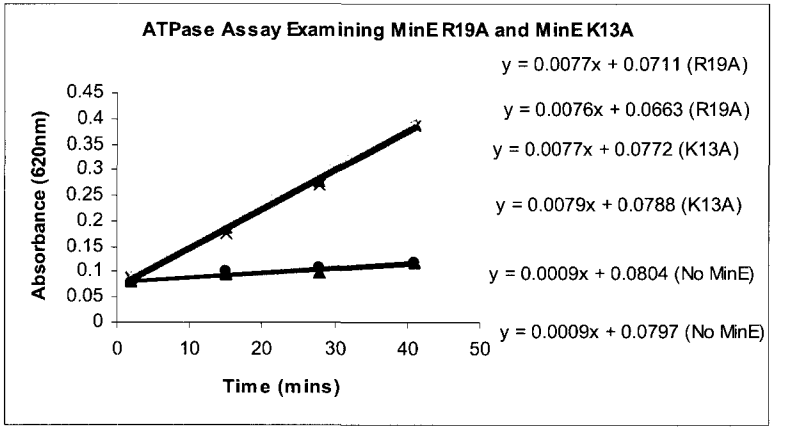
ATPase Assay Examining MinE R19A and MinE K13A
Absorbance (620nm)
Time (mins)
y = 0.0077x + 0.0711 (R19A)
y = 0.0076x + 0.0663 (R19A)
y = 0.0077x + 0.0772 (K13A)
y = 0.0079x + 0.0788 (K13A)
y = 0.0009x + 0.0804 (No MinE)
y = 0.0009x + 0.0797 (No MinE)

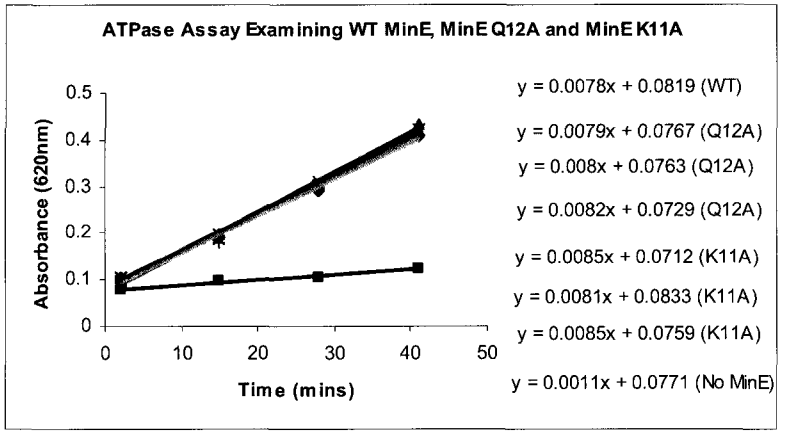
ATPase Assay Examining WT MinE, MinE Q12A and MinE K11A
Absorbance (620nm)
Time (mins)
y = 0.0078x + 0.0819 (WT)
y = 0.0079x + 0.0767 (Q12A)
y = 0.008x + 0.0763 (Q12A)
y = 0.0082x + 0.0729 (Q12A)
y = 0.0085x + 0.0712 (K11A)
y = 0.0081x + 0.0833 (K11A)
y = 0.0085x + 0.0759 (K11A)
y = 0.0011x + 0.0771 (No MinE)

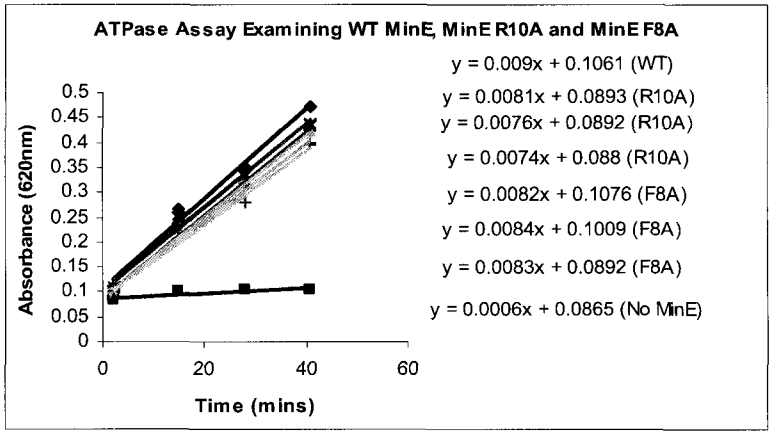
ATPase Assay Examining WT MinE, MinE R10A and MinE F8A
Absorbance (620nm)
Time (mins)
y = 0.009x + 0.1061 (WT)
y = 0.0081x + 0.0893 (R10A)
y = 0.0076x + 0.0892 (R10A)
y = 0.0074x + 0.088 (R10A)
y = 0.0082x + 0.1076 (F8A)
y = 0.0084x + 0.1009 (F8A)
y = 0.0083x + 0.0892 (F8A)
y = 0.0006x + 0.0865 (No MinE)

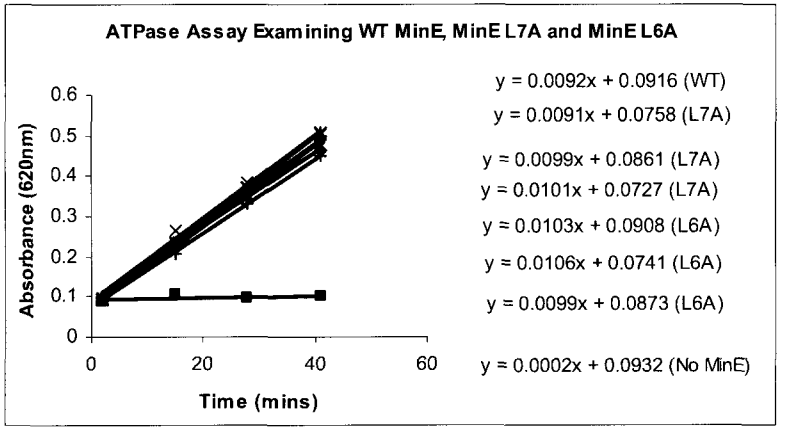
ATPase Assay Examining WT MinE, MinE L7A and MinE L6A
Absorbance (620nm)
Time (mins)
y = 0.0092x + 0.0916 (WT)
y = 0.0091x + 0.0758 (L7A)
y = 0.0099x + 0.0861 (L7A)
y = 0.0101x + 0.0727 (L7A)
y = 0.0103x + 0.0908 (L6A)
y = 0.0106x + 0.0741 (L6A)
y = 0.0099x + 0.0873 (L6A)
y = 0.0002x + 0.0932 (No MinE)

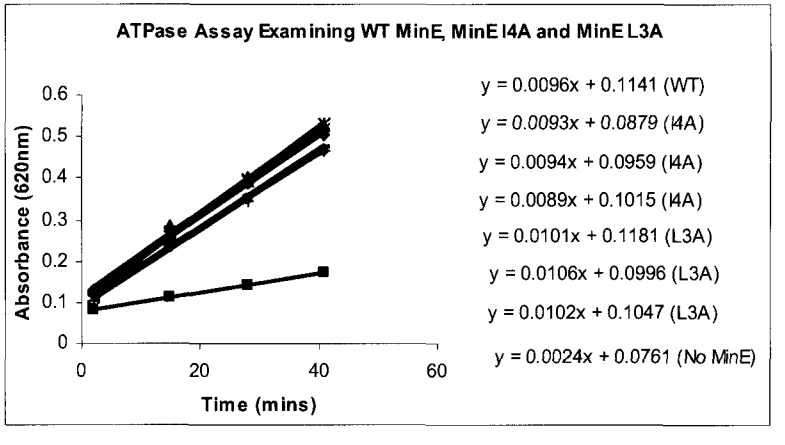
ATPase Assay Examining WT MinE, MinE I4A and MinE L3A
Absorbance (620nm)
Time (mins)
y = 0.0096x + 0.1141 (WT)
y = 0.0093x + 0.0879 (I4A)
y = 0.0094x + 0.0959 (I4A)
y = 0.0089x + 0.1015 (I4A)
y = 0.0101x + 0.1181 (L3A)
y = 0.0106x + 0.0996 (L3A)
y = 0.0102x + 0.1047 (L3A)
y = 0.0024x + 0.0761 (No MinE)

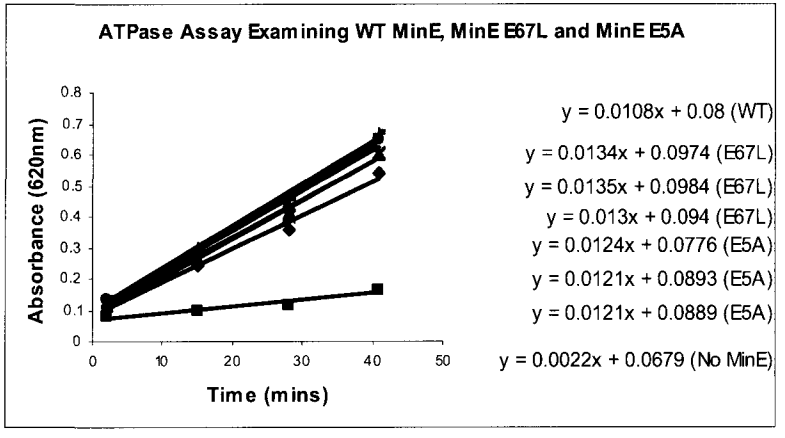

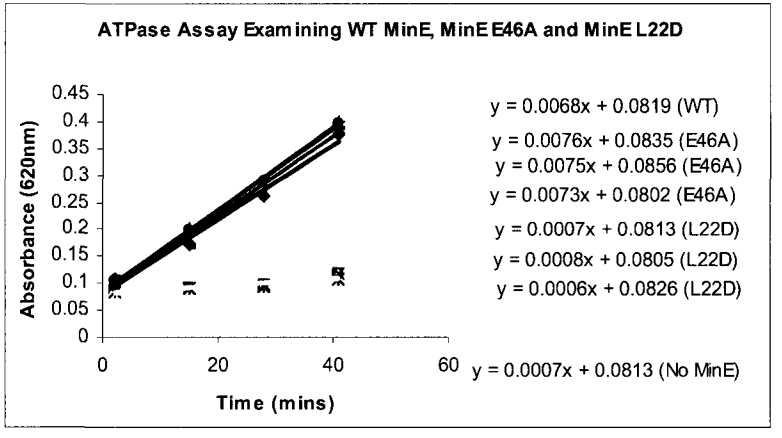

iii) ATPase Assay Examining Synthetic Peptides (2.7uM MinD; variable concentration MinE)

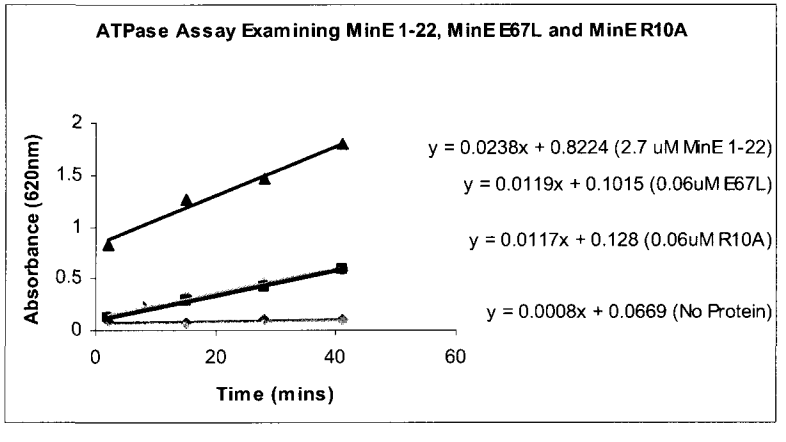

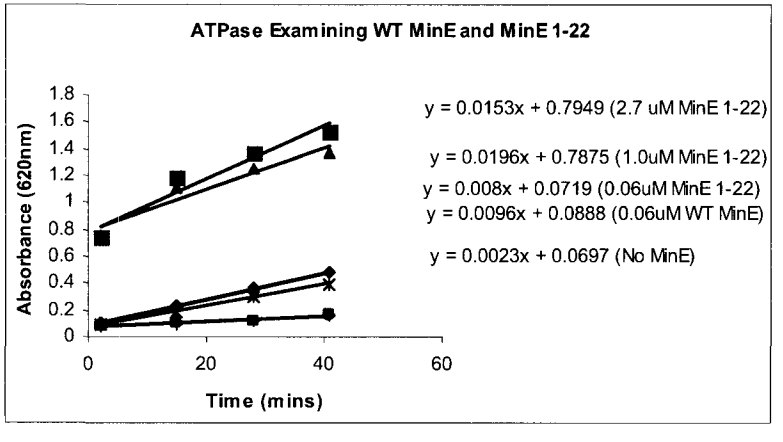

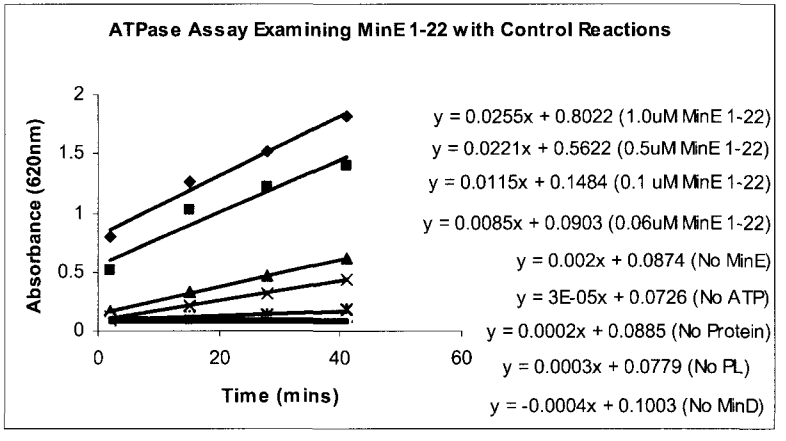
ATPase Assay Examining MinE 1-22 with Control Reactions
Absorbance (620nm)
2
1.5
1
0.5
0
0
20
40
60
Time (mins)
y = 0.0255x + 0.8022 (1.0uM MinE 1-22)
y = 0.0221x + 0.5622 (0.5uM MinE 1-22)
y = 0.0115x + 0.1484 (0.1 uM MinE 1-22)
y = 0.0085x + 0.0903 (0.06uM MinE 1-22)
y = 0.002x + 0.0874 (No MinE)
y = 3E-05x + 0.0726 (No ATP)
y = 0.0002x + 0.0885 (No Protein)
y = 0.0003x + 0.0779 (No PL)
y = -0.0004x + 0.1003 (No MinD)